Title

Mouse Models of Periodic Paralysis in Andersen Tawil Syndrome and Functional Studies of Novel Nav1.4 mutations in Myotonia & Myopathy

Author

Elia, Nathaniel

Publication Date

2020

Peer reviewed|Thesis/dissertation

UNIVERSITY OF CALIFORNIA

Los Angeles

Mouse Models of Periodic Paralysis in Andersen Tawil Syndrome and Functional Studies of Novel Nav1.4 mutations in Myotonia & Myopathy

A dissertation submitted in partial satisfaction of the requirement for the degree of Doctor of Philosophy in Molecular, Cellular, and Integrative Physiology

by

Nathaniel Curtis Elia

2020

ABSTRACT OF THE DISSERTATION

Mouse Models of Periodic Paralysis in Andersen Tawil Syndrome and Functional Studies of Novel Nav1.4 mutations in Myotonia & Myopathy

by

Nathaniel Curtis Elia

Doctor of Philosophy in Molecular, Cellular, and Integrative Physiology

University of California, Los Angeles, 2020

Professor Stephen Caldwell Cannon, Chair

The precise control of skeletal muscle excitation, contraction, and relaxation relies upon a highly choreographed sequence of ionic currents in the sarcolemmal membrane. Mutations of ion channels can lead to deleterious changes of ionic currents that impair muscle fiber excitability and thereby cause either weakness or involuntary after-contractions. The work presented here aims to define the functional consequences for newly identified disease mutations in a sodium channel and to establish the mechanism by which the partial loss of a potassium conductance creates susceptibility to episodic attacks of weakness.

The majority of this work focuses on Andersen-Tawil syndrome, a form of periodic paralysis caused by loss-of-function mutations of the inward rectifying potassium channel Kir2.1. While a genetic basis was established for the disease, it was unknown how this defect creates

susceptibility to episodes weakness, or whether as in other forms of periodic paralysis, the attacks are exacerbated by low or high potassium. To investigate this, we generated two different mouse models of ATS, one genetic and the other pharmacologic, that enabled us to explore the mechanistic relationship between the loss of a potassium conductance and the functional deficits in muscle excitation and contraction. We found that loss of muscle force was consistently induced by a high-K challenge, whereas only in the setting of a severely reduced the inward rectifier current (e.g. 6% remaining) did the muscle also exhibit weakness in a low-K challenge. Simulations of a model fiber provided insights on this divergent K-dependence for eliciting weakness and also identified approaches for manipulating conductances, transporters, or pumps to reduce the likelihood of an episode of paralysis. We tested a variety of agents and found that K_{ATP} channel openers may provide a means for pharmacologic intervention.

The remainder of the work characterizes two newly identified mutations in the voltage-gated sodium channel ($Na_V1.4$). The first is a novel loss-of-function mutation found in recessive congenital myopathy plus fluctuating weakness. The second study identified gain-of-function changes for a $Na_V1.4$ mutation associated with an unusually early onset of myotonia with congenital anomalies, and defined a new syndrome, myotonic myopathy with secondary joint and bone anomalies.

The dissertation of Nathaniel Curtis Elia is approved by

James N. Weiss

Riccardo Olcese

Thomas J. O'Dell

Stephen Caldwell Cannon, Committee Chair

University of California, Los Angeles

2020

Dedicated to

My family, my friends, and my mentors.

TABLE OF CONTENTS

LIST OF FIGURES

LIST OF TABLES

LIST OF SYMBOLS & ABBREVIATIONS

HyperPP – hyperkalemic periodic paralysis

HypoPP – hypokalemic periodic paralysis

ATS – Andersen-Tawil Syndrome

cKO – conditional knockout

FDB – flexor digitorum brevis

IO – interosseous

CMAP – compound muscle action potential

AP – Action Potential

K – Potassium

Na – Sodium

HypoPP – Hypokalemic Periodic Peralysis

HyperPP – Hyperkalemic Periodic Peralysis

I_{kir} – Inward rectifying [K] current

I_{cl} – Cl current

I_{Na} – Na^+ current

9-AC – 9-anthracene carboxilic acid

BMT – Bumetanide

ACKNOWLEDGMENTS

The work presented here was possible only due to the numerous incredible people that have invested their time and energy into my development and growth as both a scientist and an individual.

Firstly, I would like to thank my graduate advisor and mentor Dr. Stephen C. Cannon, who has far exceeded what I thought a good mentor would be. While his ability to accurately recall the details of dozens of papers from the seventies and eighties still astounds me, it is his insatiable hunger to better understand muscle physiology and his ability to think creatively and innovatively, in a field that has existed for decades, that inspires me most. His excitement about skeletal muscle biophysics is not only contagious, but palpable, as I have often joked how I imagine his relaxing weekends likely involve a stack of recently published biophysical papers, differential equations, and a Corona. I would like to thank him for setting an example of creative thinking and problem solving that I have tried to emulate in my own research, as well as an enthusiasm that kept me exited, even when I managed to break every single glass electrode I made for the day. Lastly, I want to acknowledge the guidance and advice Dr. Cannon provided to me during my PhD, even when busy with looming grant deadlines or administrative work. Much of my success is due not only to the independence allowed to me, but also Dr. Cannon's guidance on experimental directions he encouraged me to pursue, or very kindly encouraged me not to.

Furthermore, I would like to acknowledge the impact my lab members have had both on this project and my growth as a scientist. To Fenfen Wu, I owe much of my benchtop expertise. She allowed me to hit the ground running, teaching me many of the protocols our lab uses, and answering many of my questions regarding all too common technical issues. To Marbella Quinonez, I owe much of the project efficiency. Marbella not only handled the mouse colonies,

but also took part in genotyping and experimental assistance. Additionally, her cheerful attitude and encouragement made days in lab pass by much more quickly. To Marino DiFranco I owe my technical expertise. Marino was pivotal in helping me set up or modify the electrophysiological rigs used for many of the experiments mentioned in this dissertation. In addition, his expertise and advice on experiments were invaluable, and his humor was a constant source of laughter in our lab. While not in our lab, I also need to thank Ekaterina Mokhonova for her assistance on my western blot experiments.

I would also like to thank my committee, each of which have provided important perspective and feedback on my project as it has morphed into what is now presented. Dr. James Weiss was pivotal in articulating potential pitfalls and shortcomings of cardiac experiments I initially wanted to include in my project; Dr. Riccardo Olcese was always welcoming and approachable for questions whether biophysics related or not; and Dr. Thomas O'dell was always willing to help, readily offering not only advice, but even physical tissue samples should I have needed it.

While not having a direct impact on this work, I would also like to acknowledge and thank my former undergraduate research mentor Dr. Christoph Lossin. It is to him I owe my entire start in research and interest in muscle biophysics. Dr. Lossin not only invested heavily in me as an undergraduate, he also gave me the training, the encouragement, and the independence to feel confident with electrophysiology. It is because of Dr. Lossin that I first learned of myotonia, and discovered the literature written by my current mentor. I would not be in my current position were it not for the high-risk chance he took to personally teach me, a third-year undergraduate student, the complexities of electrophysiology.

Outside of research I would like to acknowledge my family who I have been extremely lucky to have shape me as an individual and who have by my side throughout this entire process. I would like to thank my parents, Curtis and Diane Elia, who have been excellent examples of what it means to both live and work faithfully and diligently. They are, in my professional scientific opinion, the best parents one could ever have asked for ($P<.0001$, $n=1$). Additionally, I would like to acknowledge my sisters, Nicole and Rachel Elia for keeping me constantly entertained. Thankfully, they have thus far decided not to attempt a PhD, allowing me to achieve and maintain my position as the highest degree holder in the intermediate family, something I plan to now mention to them in every future argument about anything.

While there are too many friends who have impacted me these last four years for me to list, it is some of my close friends from my childhood and undergraduate that played a major role in preparing me for, and encouraging me through, everything I have undergone these last four years. I'd like to thank Steven and Jonathan DeSmidt, who taught me as a kid how to stay up past 1am, something that as has now become all too common, and who are still a constant source of motivational *Avatar the Last Airbender* quotes. Additionally, I would like to thank my close friends in Southern California, namely John Esten and Estevan Pena, for being phenomenal influences, though not always for the better. Our trips to Vegas together provided a wonderful time to escape from the stress of work, and instead a time to stress about the absurd fraction of my graduate student stipend I lost to the blackjack table.

Lastly, I would be remiss to not acknowledge the help I have received from my own colleagues in the PhD program, namely Artin Soroosh and Jonathan Hoang, for not only keeping me sane, fed, and caffeinated, but also for their insightful conversations, perspectives, and experimental advice. I would also like to personally thank Artin Sroosh for his assistance in my

qPCR work and stating that he would not get upset should I drop all the sybr green again right after being told to be very careful with it, a notable rotation experience that will hopefully never be repeated in my career.

Two of the chapters in this body of work are modified reprints of work published by myself and colleagues. They are as follows;

Chapter II is a version of Elia N, Palmio J, Castañeda MS, Shieh PB, Quinonez M, Suominen T, Hanna MG, Männikkö R, Udd B, Cannon SC. (2019) Myasthenic congenital myopathy from recessive mutations at a single residue in Nav1.4.. doi:10.1212/WNL.000000000000718. Author contributions are as follows. NE, MH, RM, BU, and SC designed the study. Clinical Assessment: JP, PS, and TS conducted the clinical assessment. NE, MS C, MQ, and RM recordeded data. NE, JP, PC, MQ, MH, RM, BU, and SC wrote the manuscript.

Chapter III is a version of Elia, N. Nault, T. McMillan, H. Graham, G. Huang, L. Cannon, S (2020) Myotonic Myopathy with Secondary Joint and Skeletal Anomalies From the c.2386C>G, p.L769V Mutation in SCN4A. Author contributions are as follows. NE, SC, GG, and HM designed the study. HM performed the clinical assessment. TN, LH, and GG performed the genetic analysis. NE measured sodium currents and analyzed them with SC. Computer simulations were performed by SC. SC, GG, and HM wrote the paper.

VITA

EDUCATION

2016-2020 Ph.D. Candidate; Molecular, Cellular, and integrative physiology (MCIP)
University of California Los Angeles
Advisor: Stephen C. Cannon

2011-2016 B.S.; Neurobiology, physiology, and behavior (NPB)
University of California Davis

2011-2016 B.A.; Economics
University of California Davis

AWARDS AND FELOWSHIPS RECEIVED

2018 NIH – T32AR065972 - Muscle Cell Biology, Pathophysiology, and Therapeutics Training Program

2017 NIH – T32GM065823 - Training in Molecular, Cellular & Integrative Physiology

2015 Faculty for undergraduate neuroscience travel award

PROFESSIONAL SOCIETIESS

2017-2020 Biophysical Society

2015-2017 Society for Neuroscience

TEACHING EXPERIENCE

2018-2019 UCLA. Teaching Assistant. Course: Life Science 7C; Physiology and Human Biology

RESEARCH EXPERIENCE

2016-2020 UCLA. David Geffen Dept. of Physiology. Graduate Student Researcher.

2012-2016 UCDavis. Davis School of Medicine Dept. of Neurology. Student researcher.

SELECT PRESENTATIONS & ABSTRACTS

1. **N Elia**, E Mokhonova, M Quinonez, S Cannon. A Skeletal Muscle Conditional KCNJ2 Knock-Out Mouse Model for Periodic Paralysis in Andersen-Tawil Syndrome (2019) Biophysical Society Annual Meeting 2019
2. **N Elia**, P Shieh, M Quinonez, S Cannon. NaV1. 4 Loss of Function Changes for Recessively Inherited Myopathy with Fluctuating Weakness (2018) Biophysical Society Annual Meeting 2018
3. **N Elia**, S Dhillon, E Cruz, X Xiong, P Chen, A Smith, D Feldman, S Hirose, T Klassen, C Saunders, and C Lossin. Sodium channel Nav1.2 dysfunction in fetal akinesia deformation sequence Society for Neuroscience Annual Meeting 2016.
4. **Elia N**, Xiong X, Dhillon S, Montalvo A, Chen P, Tang S, Feldman DH, and Lossin C. Modulation of the cardiac sodium channel Nav1.5 by the antiepileptic agent lacosamide. Society for Neuroscience Annual Meeting 2015.

PEER-REVIEWED PUBLICATIONS

1. **Elia N,** Nault T, McMillan HJ, Graham GE, Huang L and Cannon SC (2020) Myotonic Myopathy With Secondary Joint and Skeletal Anomalies From the c.2386C>G, p.L796V Mutation in SCN4A. Front. Neurol. 11:77. doi: 10.3389/fneur.2020.00077
2. **Elia, N.,** Palmio, J., Castañeda, M. S., Shieh, P. B., Quinonez, M., Suominen, T., Hanna, M. G., Männikkö, R., Udd, B., & Cannon, S. C. (2019) Myasthenic congenital myopathy from recessive mutations at a single residue in NaV1.4. Neurology, 92(13), e1405–e1415. doi:10.1212/WNL.0000000000000718

CHAPTER 1

1.1 INTRODUCTION

Andersen-Tawil Syndrome (ATS) is a rare genetic disorder and a unique variant of periodic paralysis, being the only one that presents with a triad of symptoms at variable penetrance including dysmorphia and cardiac arrhythmias in addition to the attacks of skeletal muscle weakness[1,2]. ATS is inherited as an autosomal dominant trait with approximately 30% of probands being classified as de novo[3]. ATS has an estimated prevalence of approximately 1 in 1million, although actual numbers may be higher due to misdiagnosis or lack of symptoms[4].

60% of ATS cases, termed ATS-1, are associated with mutations in the KCNJ2 gene, which codes for the Kir2.1 subunit of an inward rectifying potassium channel expressed in skeletal, cardiac, and smooth muscle, as well as osteoblasts[5,6]. In one Japanese family with ATS, a mutation of KCNJ5 encoding the G-protein activated inward rectifier channel Girk3.4 was identified. Co-expression of mutant Girk3.4 with WT Kir2.1 showed a dominant-negative reduction of the Kir current. The interpretation is that the ATS mutation of Girk3.4 is equivalent to a loss-of-function mutation for Kir2.1. The gene culpable for the remaining ATS patients, defined as having ATS-2[7], is still an area of active investigation. In this Thesis Dissertation, the designation ATS will refer to study of ATS-1 and the study of the Kir2.1 channel.

The Kir2.1 protein is a member of the Kir2.X family of subunits (Kir2.1-2.6) that combine as tetramers to form an inward rectifying potassium channel[8]. In skeletal muscle, both Kir2.1 and Kir2.2 are expressed, generating both homo and heterotetramers responsible for the inward rectified potassium current (I_{Kir}), and are the primary regulators of resting membrane potential[9,10]. Currently over 60 known mutations exist primarily consisting of single nucleotide mutation with four known frameshift deletions, three nonsense mutations, and one insertion[3]. Nearly one half of

the reported KCNJ2 mutations occur at residues known to be important for PIP2–channel interaction, while others are thought to inhibit trafficking, pore formation, or integration into the membrane[10,11]. There is currently no consistent genotype–phenotype relationship, with carriers of the same mutation possessing zero to all three of the phenotypic manifestations of the disease[10].

All currently known ATS mutations of Kir2.1 have a dominant negative loss-of-function, meaning that a single mutated subunit is sufficient to compromise the functionality of the entire channel. Functional studies on a limited number of mutants have shown no detectable current for homomeric channels comprised solely of mutant subunits. When these mutants were coexpressed at a 1:1 ratio with WT, the total current was reduced to 10% to 30% of that generated from WT transcript only[12]. Functional studies in biopsied and cultured myotubes from ATS patients, show a similar defect, with current reduced to 50% as that of WT myotubes[13]

Our current understanding of ATS, and more specifically the characterization of factors that may trigger attacks of periodic paralysis, is limited because the risk of arrhythmia prevents provocative testing as is often used to identify trigger factors in other forms of periodic paralysis. This lack of clarity regarding the trigger factors has a negative impact on patient management, because the first-line intervention for any form of periodic paralysis is lifestyle changes to avoid trigger factors (e.g. K supplementation or dietary restriction). It is currently unknown how to best advise patients with ATS due to the uncertainty regarding whether high or low serum potassium triggers an attack.

While one prior study demonstrated the ability to induce an attack with a provocative high K challenge[1], it is also well documented that spontaneous episodes of periodic paralysis have occurred in patients who are hypo, hyper and even normo-kalemic [1,14,15]. Even with this lack of consistency, many neurologists believe the attacks of periodic paralysis in ATS are provoked by

alterations in extracellular potassium, thus leading to the term “dyskalemic periodic paralysis” as a classification for ATS.

The work presented here aims to better define how the reduction in I_{kir} causes susceptibility to attacks of periodic paralysis and thereby gain insights for possible intervention. To examine this question, we developed a conditional knock out mouse model as well as an ex vivo pharmacologic model. Voltage-clamp studies of isolated fibers and isometric contraction tests of whole muscle were used to better understand the relationship between I_{kir}, extracellular K, and cellular excitability. These experimental observations were coupled with computational modeling of fiber excitability to gain more insights on opportunities for interventions, many of which were tested in preclinical studies.

1.2 MATERIALS AND METHODS

Generation of KCNJ2 cKO mouse model

Model generation

The skeletal muscle specific KCNJ2 cKO mouse was generated through utilizing a cre-lox system on a B6 background. Mice were provided by Mark Neilson (Univ. VT) containing loxP sites flanking the second exon of KCNJ2. To generate a skeletal muscle specific conditional knockout, these mice were crossed with a skeletal muscle expressing Cre line driven by the myosin, light polypeptide 1 promoter (Myl1tm1(cre)Sjb/J) from Jackson labs. The resulting heterozygous mice KCNJ2 (Fl/+, Cre/-), were then backcrossed with the original mice, KCNJ2 (fl/fl) to generate a homozygous conditional knockout of KCNJ2 (fl/fl, cre/-). This continued for 6 generations to create a congenic mouse line.

To assess the tissue specificity of cre driven by the myosin, light polypeptide 1 promoter, (Myl1tm1(cre)Sjb/J) mice were crossed with ROSA26-EGFP reporter mice containing a loxP flanked stop codon prior to an EGFP transcript. Muscle sections were obtained from adult mice (Aged 90-100 days). The soleus, EDL, and heart, were fixed using 1% PFA in PBS overnight. Tissue was then washed and placed in 5% sucrose in PBS overnight and then 20% sucrose in PBS overnight. Tissue was set in OCT, and frozen in liquid nitrogen prior to sectioning. 10 microns thick transverse muscle sections were cut on a cryostat, mounted on a slide and were immediately imaged under a confocal microscope to assess GFP expression by tissue type.

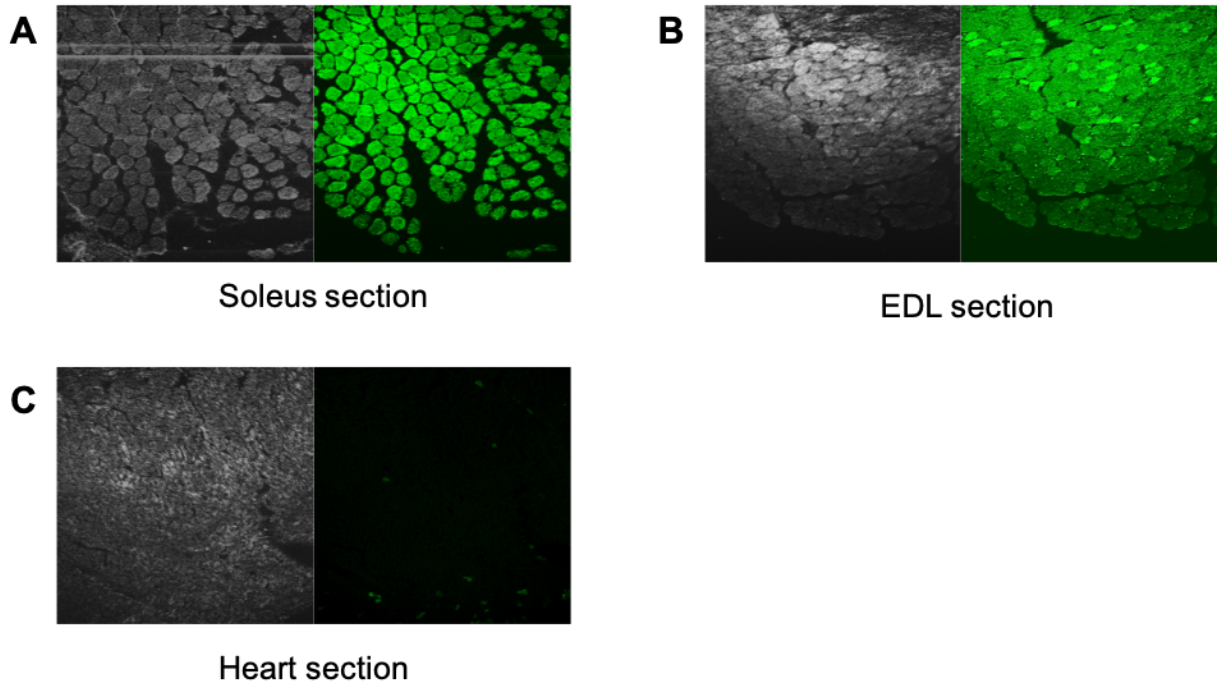

Figure i. The expression of soluble GFP driven by the presence of cre recombinase in a tissue specific manor. (**A**) The soleus muscle of the mouse containing predominantly slow twitch muscle imaged under bright field and florescence shows robust GFP expression in each imaged muscle fiber. (**B**) The Extensor Digitorum Longus (EDL) muscle containing predominantly fast twitch muscle imaged under bright field and florescence shows robust GFP expression in each imaged muscle fiber. (**C**) Cardiac tissue taken from the

ventricle of the murine heart imaged under bright field and florescence shows slight cre expression in multiple cardiac cells.

Images demonstrate robust GFP expression in skeletal muscle from the extensor digitor longus (EDL), a predominantly fast twitch muscle, and soleus, a predominantly slow twitch muscle (figure i). Because of the intense homogeneous staining of essentially all fibers, mice heterozygous for inclusion of Cre were considered sufficient for the skeletal muscle specific knockout of KCNJ2 and were used for our experiments with either homozygous and heterozygous conditional knockouts. Cardiac tissue however also contained some a few GFP positive cardiac myocytes.

genotyping

Genotyping of the genetic mouse models was confirmed from tail-snip DNA using PCR. Separate reactions were conducted to test for the presence of loxP sites and cre independently. The primers to amplify the floxed exon 2 of KCNJ2 were 5' TCCGATGACACTGAGAACCTGGA, 3' TGGATGCTTCCGAGAACCTTGG. Resulting PCR product was run on a 1% agarose gel to discriminate a 600 bp product from the floxed allele containing a pair of loxP sites from the 520 bp WT allele. Het floxed would appear as two distinct bands in a single lane at both sizes. Cre presence was assessed by using two different reverse primers, one recognizing cre 3' GCAAACGGACAGAAGCATTT, and one recognizing the WT 3' CGATCTTAATAGCAGACAGATCG. Forward primer sequence was the same for both 5' CACACTGCTCTTCCAAGTGTC. The PCR reaction products were resolved on a 1% agarose gel to detect the Cre sequence (250 bP) or the WT sequence (200 bp) as a control for template quality. Homozygous cre expression would show only one band between the two lanes, while heterozygous mice would show a single band in each lane of the pair.

Western blot (performed by Ekaterina Mohkovana)

Soleus and FDB muscles were dissected from adult mice aged 90 to 150 days in a cold bicarbonate buffered physiological solution (118 mM NaCl, 4.7 mM KCl, 1.8 mM $MgSO_4$, 2.4 mM CaCl, 1.8 mMNa_2PO_4, 10 mM Glucose) bubbled with 95% O_2, 5% $C0_2$ (pH 7.4). Muscles were then flash frozen in liquid nitrogen prior to homogenization in ice cold Mito buffer (0.2 mM EDTA, 0.25 mM sucrose, 20 mM HEPES) containing a protease/phosphate inhibitor (pierce). Removal of myofibrils, nuclei and mitochondria was accomplished through low speed centrifugation, and isolation of the membrane fraction through high speed centrifugation. Protein concentration estimation was preformed using protein assay kit (GE healthcare). 200 ∝g of each sample was loaded into the wells of a 7.5% PAAG gel and run at 20 mA with transfer onto a nitrocellulose membrane ran at 350 mA for 1.5 hours. The membrane was blocked in 5% milk-PBS-T and incubated overnight before staining with a primary antibody a-Kir2.1 1:3000 (NeuroMab, Davis, clone N112B/14) and DHPRa1s 1:2000 (Thermo Scientific MA3-920). Secondary staining was rabbit anit-mouse-HRP (signma, A9044) 1:10000 for one hour. Western blot signal was developed using Radiance plus substrate (azure biosytems) and imaged on the Azure C300 imaging system (azure Biosystems).

qPCR.

The abundance of KCNJ2 transcript was determined by qPCR. Whole soleus, flexor digitorum brevis (FDB) , and interosseus (IO) muscles were dissected from WT, homozygous KCNJ2 cKO (fl/fl, cre/-), heterozygous KCNJ2 cKO (fl/+, cre/-), and control (fl/fl, -/-) mice and flash frozen in liquid nitrogen. Whole muscle blocks were mechanically homogenized using ice

cold RLT using a dounce homogenizer, and total RNA was extracted and purified using the Qiagen RNeasy Fibrous Tissue Mini Kit. RNA was quantified using a nanodrop and equal amounts of purified RNA (1ug per RT reaction) were converted to cDNA using iscript reverse transcription supermix (bio-rad)

qPCR measurements were carried out on the Bio-Rad CFX384 using SYBR Green-based PCR (Applied Biosystems). Reactions were completed in technical triplicates with primers specific for KCNJ2, KCNJ12, GAPDH and β-actin. Comparative quantification was conducted using $\Delta\Delta C_t$ normalizing to the average between GAPDH and β-actin and calibrated to the abundance of WT transcript of the gene.

Primers were

KCNJ2 5’ TCTCGGAAGCATCCATCTCT,

3’ TCGGTGAAGACACACCAAAA

KCNJ12 5’ TTCATGGCAGCCTTTCTCTT

3’ GGGCACTCTTCAGTCACACA

GAPDH 5’ GTGTTTCCTCGTCCCGTAGA

3’ AATCTCCACTTTGCCACTGC

β-actin 5’ TGGCACCACACCTTCTACAA,

3’ CTGGGGTGTTGAAGGTCTCA.

Two Electrode Voltage clamp

skeletal muscle isolation

Homozygous and heterozygous KCNJ2 cKO mice, as well at WT mice aged 90 to 150 days old were anesthetized with isoflurane sacrificed using cervical dislocation. The hind limbs of the

mice were rapidly removed and submerged in ice-cold, oxygenated (95% O_2, 5% CO_2) bicarbonate buffered physiological solution (118 mM NaCl, 4.7 mM KCl, 1.8 mM $MgSO_4$, 2.4 mM CaCl, 1.8 mMNa_2PO_4, 10 mM Glucose, pH 7.4,). The flexor digitorum brevis (FDB) and interosseus (IO) muscles were dissected from both the right and left hind limb of the mouse and placed in a dish of Tyrode supplemented with collagenase. Muscle was then placed in an incubator at 37 degrees centigrade for 50 minutes before being removed and placed in 5mL fresh Tyrode solution. Digested muscles were mechanically dissociated using trituration with fire polished glass pipettes to isolate individual fibers. Remaining tendons and visually undissociated muscle were discarded and 100uL of remaining solution was pipetted onto each glass bottom pitri dishes. Ice-cold Tyrode was added to fully cover the glass in the dish and cells were allowed to sit at room temperature for one to three hours to adhere to the glass before recording. Once adhered, muscle fibers were placed on an inverted microscope and perfused with fresh Tyrode using a gravity profusion system flushing out cells that had not adequately adhered to the dish.

Cells were chosen for experiments based upon the visual health of the cell dictated through observations of clear and distinct Z lines, smooth membranes, and size, using cells around 600 microns long and 50 microns wide. As an additional test of fiber quality, the waveform of the action potential (AP) was assessed under current. Acceptable fibers had a low holding current (< 10 nA) to maintain V_{rest} = -80 mV, an AP peak ≥ +30 mV, and an AP duration < 8 msec.

Microelectrode and Bath conditions

Microelectrodes were pulled from borosilicate glass to a tip resistance of 10-15 Mohm using the Sutter P1000 microelectrode puller and filled with an internal solution containing 50 mM EGTA, a calcium chelator, to prevent contractions. The internal solution consisted of (in mM) 150

KOH, 50 EGTA, 5 Mg_2Cl, 20 MOPS, 5 Tris-ATP, NaOH, 5 Tris-Cre, 5 GLUT, 50 ASP). Three different external solutions were used for fiber recordings, all containing 100µM 9-anthracene carboxilic acid (9-AC) to prevent chloride current. The solutions are as follows:

Tyrode: 140 mM NaCl, 4 mM KCl, 1 mM $MgSO_4$, 2 mM CaCl, 10 mM HEPES, 10 mM Glucose, 100µM 9-AC, pH 7.4

100[K^+]: 50 mM NaCl, 100 mM KCl, 2 mM $CaCl_2$, 1 mM $MgCl_2$, 10 mM HEPES, 100µM 9-AC, pH 7.4

100[K^+] + 1 mM Ba^{2+}:

50 mM NaCl, 100 mM KCl, 2 mM $CaCl_2$, 1 mM $MgCl_2$, 100µM 9-AC 10 mM HEPES, 100µM 9-AC 1 mM Ba^{2+}, pH 7.4

Cells were initially placed in Tyrode solution until health of the cell was established. The bath solution was then exchanged to a symmetrical K solution (100[K^+]), to enhance the detection of large I_{Kir} currents at negative voltages. Lastly, the bath solution was exchanged to a symmetrical K solution containing 1 mM Ba^{2+}, a highly specific blocker of I_{kir} current, allowing us to measure the background leak current of the cell.

Two-Electrode Voltage-Clamp

Upon impaling the cells with both electrodes, the holding potential was adjusted to -90mV in current clamp mode and 0.5 msec current pulses were applied to induce action potentials to further assess the health of cell. For cells with healthy action potentials, current injection was removed, and the external solution was slowly exchanged to a symmetrical K solution to prevent a contraction. At the end of the solution exchange, the membrane potential of the fiber was between -5 mV and 2 mV. The amplifier was then switched to voltage clamp mode, with a holding potential

of 0 mV. Cells were subjected to voltage steps of 10 mV between -160 to +80 mV for 100 ms, both in the presence and absence of 1 mM Ba^{2+}. Because there is slight rundown of I_{Kir} during a voltage step, probably as a consequence of potassium depletion in the T-tubule, the current amplitude at each voltage was measured as the average current for the final 20ms of the 100ms pulse. Background currents in barium were digitally subtracted from the total current recordings to calculate the barium-sensitive I_{Kir} current used for analysis.

Ex vivo contraction testing

Muscle isolation

Isometric force was recorded from the soleus muscle of mice aged 90 to 170 days. Mice were anesthetized with isoflurane and sacrificed using cervical dislocation. The hind legs of the mice were removed and placed into an ice-cold bicarbonate buffered physiological solution (118 mM NaCl, 4.7 mM KCl, 1.8 mM $MgSO_4$, 2.4 mM CaCl, 1.8 mMNa_2PO_4, 10mM Glucose) bubbled in 95% O_2, 5% CO_2 (pH 7.5). The gastrocnemius was removed to reveal the tendons connecting the soleus on the fibula and the inserts via the tuber calcanei. Sutures containing a washer for anchoring were then tied around both tendons prior to excising the muscle and suspending between a force transducer and a fixed post.

Bath conditions

The muscle was immersed in a tissue bath heated to 37 degrees centigrade and continuously bubbled with 95% O_2 and 5% CO_2. Three primary solutions were utilized for these experiments, and these were occasionally fortified with pharmaceutical interventions or barium. The solutions were in (mM):

4.7[K^+]: 118 NaCl, 4.7 KCl, 1.8 $MgSO_4$, 2.4 CaCl, 1.8 Na_2PO_4, 10 Glucose

2[K^+]: 120 NaCl, 2 KCl, 1.18 $MgSO_4$, 2.54 $CaCl_2$, 1.18mM NaH_2PO_4, 10 Glucose

10[K^+]: 112 NaCl, 10 KCl, 1.18 $MgSO_4$, 2.54 $CaCl_2$, 1.18 NaH2PO_4, 10 Glucose

Baseline tetanic isometric force was established in 4.7nmM [K^+] bicarbonate buffered physiological solution. For provocative potassium sensitivity experiments, the bath solution was exchanged to one containing 2 mM [K^+] or 10 mM [K^+].

Stimulus protocol

Tetanic stimulation for a fused contraction (0.5 msec 80 mA pulses, at 100 Hz for 400 msec; Aurora 701C) was applied every 2 min using wire field electrodes perpendicular to the muscle. The rest length of the muscle (L_0) was adjusted to obtain the largest amplitude isometric contraction, and the baseline force was established as thirty minutes of stable force production in 4.7mM [K^+], prior to provocative potassium challenge. For pharmacological tests, intervention was typically applied after 10 minutes of baseline recordings and 30 minutes prior to potassium solution exchange unless otherwise noted.

Compound muscle action potential (performed by Fenfen Wu)

Mice were anesthetized by isoflurane inhalation, an EMG needle electrode was inserted into the gastroc/soleus of the hind leg, and a stimulating electrode was place directly on the sciatic nerve. The compound muscle action potential (CMAP) was recorded in response to a single shock (0.1 msec) applied to the sciatic nerve.

Mice were pretreated for 4 days with fudge that contained sodium polystyrene sulfonate (22% by weight, Kayexalate; KVK-TECK Inc.) to deplete total body potassium. On the day of the

experiment, mice were anesthetized by intraperitoneal injection of a 10:1 (v/v) mixture of ketamine (10 mg/ml) and xylazine (1 mg/ml) at a dose of 0.1ml/10g, and maintained by a vaporizer with.5% isoflurane, and kept at 37 degrees using a heating blanket. To provocatively lower blood potassium further, a mixture of insulin (0.2 U/ml) plus glucose (0.175 g/ml) was administered by continuous infusion (0.5 ml/hr) of the jugular vein.

Computational Modeling

Simulations of muscle excitability were performed using a modified version of our two compartment model, T-tubular system and sarcolemma membrane, of a muscle fiber[16] (**figure ii**).

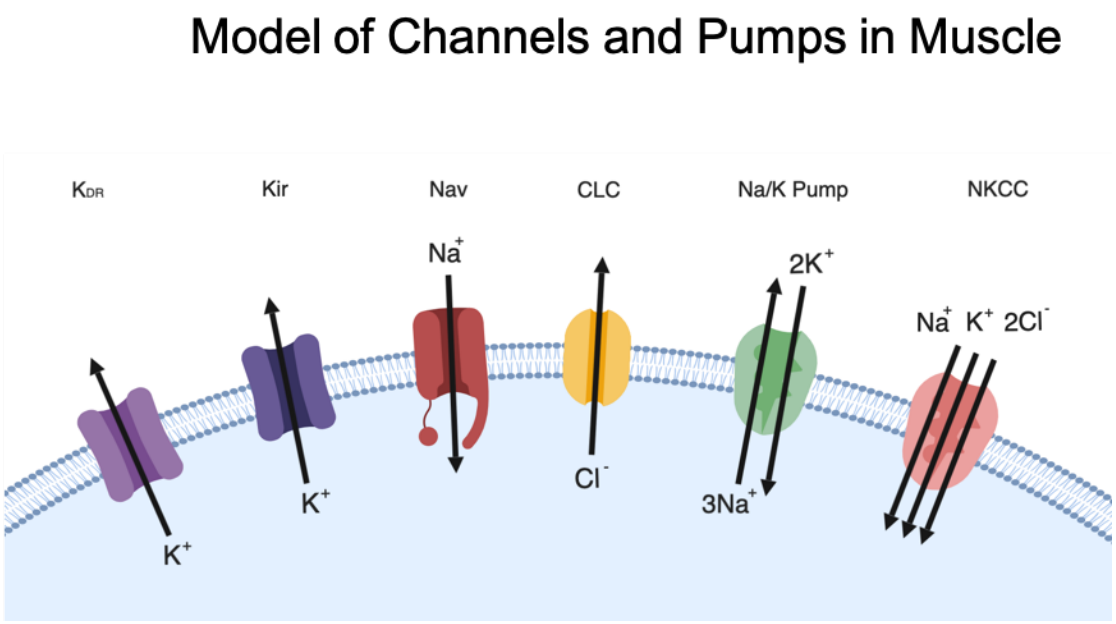

Figure ii. Diagram depicting the individual ion channels and pumps used to generate steady state current values used for computing membrane potential in the computational model. Arrows demonstrate the direction of ionic flux at a potential of -90mV.

The total current per unit area of the sarcolemma, I_m, was computed as the sum of multiple individual currents:

$$I_m = C_m \frac{dV}{dt} + \sum I_{ionic} + I_{pump} + I_{TT}$$

Where $C_m \frac{dV}{dt}$ is the capacitive current, I_{ionic} is the ionic current, I_{pump} is the contribution of the Na/K-ATPase, and I_{TT} is the net current of the T-tubule. The sum of ionic current and net t-tubular current is calculated as:

$$\sum I_{ionic} = I_{Na} + I_{Kir} + I_{Kdr} + I_{Cl} \quad \text{and} \quad I_{TT} = \frac{V - V_{TT}}{R_a} .$$

where R_a is the access resistance to the T-tubule.

The analysis was focused on determining possible values for the resting potential, V_{rest}, whereby an anomalously depolarized value (> -60 mV) represents the inexcitable state during an episode of periodic paralysis. The possibility of flux-dependent changes of ion concentrations in the intracellular compartment or the T-tubules adds another dimension to the calculation of V_{rest}. The extracellular ion concentrations remain fixed at constant values to simulate the "infinite" volume of the extracellular space in our ex vivo experiments in the tissue bath. For the fluctuations of intracellular ion concentrations that might occur under physiological conditions, the most important ion is Cl^- because of the large Cl^- conductance (80% of the total conductance) in resting fibers. Therefore, we included the major influx pathway for Cl^-, the electroneutral NKCC cotransporter, as well as the ClC-1 conductance (the major efflux pathway) in our model of a muscle fiber. For the NKCC cotransporter

$$J_{NKCC} = J_{max} \left\{ \log \frac{Na_o}{Na_i} + \log \frac{K_o}{K_i} + 2 \log \frac{Cl_o}{Cl_i} \right\}$$

and because of the cotransporter stoichiometry, $J_{NKCC}^{Cl} = 2J_{NKCC}$. The sign convention for this equation is flux > 0 implies influx. The mass-balance equations for Cl^- in the intracellular and T-tubular compartments are:

$$\frac{d[Cl]_i}{dt} = \frac{J_{NKCC}^{Cl} + I_{Cl}}{F(r/2)} + \frac{J_{TT\_NKCC}^{Cl} + I_{TT\_Cl}}{F\varsigma}$$

$$\frac{d[Cl]_{TT}}{dt} = -\frac{J_{TT_{NKCC}}^{Cl} + I_{TT_{Cl}}}{F\varsigma} - \frac{[Cl]_{TT} - [Cl]_{out}}{\tau_{Cl}}$$

where F is Faraday's constant, r is the fiber radius, ς is the volume to surface area ratio of the T-tubules, and τ_{Cl} is the time constant for equilibration of Cl^- in the T-tubule with the extracellular compartment.

V_{rest} is now determined by two constraints for the "true" steady-state when both ionic currents and ion concentrations are no longer changing with time:

(i) $\sum I_{ionic} + I_{pump} = 0$ the total current must be zero

(ii) $F \times J_{NKCC}^{Cl} + I_{Cl} = 0$ the net Cl flux must be zero

An iterative process was used to compute V_{rest} and $[Cl]_i$ for this complex set of coupled nonlinear equations.

(i) Guess $[Cl]_i$ and keep it fixed, then iteratively vary V until the sum of currents = 0.

(ii) Is the net Cl flux close enough to 0 (i.e. tolerance level)? YES → done, $V_{rest} = V$

(iii) If Cl flux > 0 then increase the guess for $[Cl]_i$, otherwise decrease the guess for $[Cl]_i$, then go back to step (i)

1.3 RESULTS

Generation of KCNJ2 cKO mice

Genetic model validation

A Kir2.1 defficiency, characteristic of Andersen Tawil Syndrome, was accomplished in a tissue-specific manner through the crossing of a floxed KCNJ2 mouse with a muscle specific cre. Flanking loxP sites bordered the second exon of the KCNJ2 open reading frame, which contains the entire protein coding sequence for the Kir2.1 subunit. For the remainder of this paper background C57B6 mice will be termed WT, mice homozygous floxed with no cre (fl/fl, -/-) will be termed control, heterozygous floxed and heterozygous cre (fl/+, cre,-) will be termed het-KCNJ2 cKO, and homozygous floxed and heterozygous cre (fl/fl, cre/-) will be termed homo-KCNJ2 cKO.

Mice were viable and developed normally into adulthood. There were no anecdotal accounts of spontaneous attacks of muscle weakness in the mice when observed or handled, and locomotor function was indistinguishable from that of WT mice.

KCNJ2 knockout efficiency was confirmed at a transcript level through qPCR analysis using primers that were complimentary for exon two of the KCNJ2 gene. Control WT samples which did not receive a reverse transcriptase during cDNA generation did not generate any detectable signal during qPCR amplification, confirming no contamination from genomic DNA. When compared to WT, KCNJ2 transcript levels decreased slightly in the control and the het-KCNJ2 cKO, however these changes were not statistically significant ($P = .99$, $P = .91$ respectively). Homo-KCNJ2 cKO transcript levels were reduced to $16.7 \pm 2.2\%$ that of WT muscle, $P < .0005$ (**figure 1A**). A second inward rectifying potassium channel subunit is expressed in skeletal muscle, Kir 2.2, coded for by KCNJ12. We tested for possible compensatory upregulation of KCNJ12 mRNA due to the knockout of KCNJ2 and found no detectable increase in expression from qPCR analysis (data not included).

To assess knockout efficiency at a protein level, western blot was used against Kir2.1 protein found in membrane fractions taken from of the soleus, a predominantly slow twitch muscle (**Figure 1B**) and the FDB, a predominantly fast twitch muscle (data not included). Equal loading in wells was confirmed both using a ponceau stain and by blotting against DHPR-α1s. In both cases, Western blot analysis displayed a reduced amount of protein in the heterozygous KCNJ2 cKO mouse with trace amounts in the homozygous KCNJ2 cKO mouse. We did not perform immunoblot analysis of Kir2.2 because commercially available antibodies lack sufficient specificity to distinguish Kir2.1 from Kir2.2.

Ionic current

Prior voltage-clamp studies of ATS mutant Kir2.1 subunits in oocytes, primary cultures of skeletal muscle myotubes, and iPSC-derived cardiomyocytes have all and demonstrated a dominant-negative effect with reduced Kir current to between 5% and 50% that of wild type[12,13]. While deletion of KCNJ2 is expected to reduce the Kir current density in muscle fibers through removal of Kir2.1, the expected extent of reduction is unknown because of the remaining presence of Kir 2.2 in the skeletal muscle. Two electrode voltage clamp studies were conducted in isolated muscle fibers dissociated from the flexeor digitorum brevis (FDB) muscle of WT and KCNJ2 cKO mice. Symmetrical K was used to set the Nernst potential of K to 0 mV and to generate large inward K^+ currents at negative membrane potentials and 9-anthracene carboxilic acid (9-AC) was used to suppress I_{Cl}. Ionic current was measured in response to voltage steps of 100 ms, varying from -160 to +80mV. The protocol was repeated in 1 mM Ba^{2+}, to block the I_{Kir} component, and digital subtraction was used to isolate the I_{Kir} current (**Figure 2A**). The current in the prescience of 1 mM Ba^{2+}, is primarily a nonspecific leakage current under our conditions of V_{hold} = 0 mV to

chronically inactivation sodium and calcium channels. This value was normalized to cell surface area that was calculated using measurements of the cell's length and diameter The I-V plot shows the expected strong inward rectification at approximately 0 mV (Fig. 2B). I_{Kir} current density was markedly decreased for FBD fibers from het-KCNJ2 cKO and homo-KCNJ2 cKO mice. The average inward current at -120mV for WT mice was -627.81 ± 41.68 μA/cm^2. Control mice (fl/fl, -/-) were indistinguishable from WT with average inward current at -120mV of -612.82 ± 49.2 μA/cm^2. The average inward current at -120mV was -374.49 ± 56.2 μA/cm^2 and -135.43 ± 15.47 μA/cm^2 for heterozygous and homozygous KCNJ2 cKO mice, respectively. This equates to a reduction in current to 59.65% and 21.57% in heterozygous and homozygous KCNJ2 cKO mice respectively when compared to WT (**figure 2C**).

Functional Studies of Skeletal Muscle in KCNJ2 cKO Mice

Transient attacks in periodic paralysis are often triggered by changes in the serum potassium that chronically depolarize the resting potential and thereby reduce or even abolish membrane excitability which compromises excitation contraction coupling. Because it is not clear whether hypokalemia or hyperkalemia is capable of triggering attacks of weakness in ATS, we conducted four independent and previously established tests of periodic paralysis in out lab to determine whether the phenotype in our KCNJ2 cKO mouse model of ATS is more consistent with hypoPP or hyperPP.

In vitro force measurement

Measurement of susceptibility to hypo and hyper periodic paralysis in our genetic model was assessed through measuring the peak isometric force of the soleus muscle in varying

extracellular potassium. Representative force transients elicited by tetanic stimulation in normal 4.75mM K^+ and the during provocative potassium challenge are shown in **figure 3A.** This example from a homo cKO soleus shows a steady isometric contraction during the entire 400 msec stimulus (100 Hz), and a clear decrease in steady-state force of the same preparation in the presence of a 10 mM K^+ challenge. Peak isometric force in control conditions (4.75 mM K^+) was smaller for homo-KCNJ2 cKO soleus compared to WT, while the heterozygous cKO was intermediate. (**figure 3B**). WT mice had an average baseline force of 20.36 ± .55g of force, het-KCNJ2 cKO mice had a reduced baseline force of 17.44 ± .91g ($P < .05$ when compared to WT), and homo-KCNJ2 cKO had a further baseline force of 14.8 ± .49g ($P < .0001$ when compared to WT).

Potassium sensitivity of contractility was determined by measuring the peak tetanic force every two minutes, during which a 30 min challenge of variable [K^+] was applied. For both WT and KCNJ2 cKO soleus, the baseline peak tetanic force in 4.7 mM K^+ was stable over tens of minutes, as shown by the pre-challenge interval (0-30 min) in Figure 3C&D. The effect of provocative K^+ testing is displayed as relative force, with each muscle serving as its own control from the pre-exposure force amplitude. A low-K^+ challenge (2 mM) produced only a slight 12% decrease in the relative force of soleus from WT mice. A larger, though not significant, drop of force was observed for het-KCNJ2 cKO soleus (22%, $P = .11$) with the biological significance of this difference is questionable. Unexpectedly, the relative force for homo-KCNJ2 cKO soleus did not have a large decrease. In fact, the relative force consistently showed an increase in every muscle tested and that on average was 7% (**figure 3C**). The response to a high-K^+ challenge (10 mM K^+) was concordant with a reduction in force for WT, het- and homo-KCNJ2 cKO soleus (Figure 3D). The loss of force was 16% for WT and while there appeared to be a slightly greater loss for het-KCNJ2 cKO (23%) the means were not statistically different ($p = 0.14$, $n = 6$).Homo-

KCNJ2 cKO mice had a large reduction of 62% ($P < .0001$, $n = 11$) when compared to WT. A full recovery to baseline force occurred upon washout of both the low and high K^+ challenges.

Resting Membrane potentials

The loss of force during an attack of periodic paralysis is due to a depolarization of the resting membrane potential, which inactivates voltage-gated sodium channels. We measured the resting membrane potential by microelectrode impalement of fibers in whole soleus muscle kept in constant flow of bicarbonate buffered physiological solution and maintained at 35°C. Based on our experience of assessing fiber excitability under current clamp, we used a cutoff of -60mV for excitability. Consistent with this value, the $V_{1/2}$ of sodium channel slow inactivation is also about -60 mV[17]. In 4.7 mM K WT mice had an average V_{rest} of -73.3 ± .91mV while homo KCNJ2 cKO mice had a marginally depolarized value (-71.0 ± 0.8 mV) that was 2.3mV more positive ($P < .01$, Welch's corrected unpaired T-test) (**figure 4A**). In response to a low potassium challenge of 2 mM K^+, WT fibers hyperpolarized more than 4mV to -77.67 ± 1.5mV, as expected due to a negative shift in the Nernst potential. In contrast, Vrest of homo KCNJ2 cKO muscle fibers remained relatively stable, hyperpolarizing by less than 1mV to -71.74 ± .86mV (**figure 4B**). Interestingly, while Homozygous KCNJ2 cKO muscle fibers did not hyperpolarize significantly in 2 mM K^+, only 1.8% of recorded fibers were depolarized to values more positive than -60mV compared to WT which had 12.7% of fibers depolarized to values more positive than -60mV. This lower percent of "depolarized' fibers for homo KCNJ2 cKO muscle may account unexpected increase of force in an a low-K^+ challenge compared to WT. In response to a high potassium challenge of 10 mM K^+, the average Vrest of WT fibers depolarized to -62.7 ± .71 mV, as expected due to a positive shift in the Nernst potential. A more depolarized mean value of -56.3 ± .87 mV was observed for

homo KCNJ2 cKO fibers (Figure 4C). In terms of predicted fraction of excitable fibers, 52.7% of the homo KCNJ2 cKO muscle fibers had a Vrest more positive than -60mV compared to 22.7% for WT.

pH challenge

A third test to detect the expected HypoPP phenotype is based on the loss of force that occurs after recovery from a 30-minute episode of acidosis (25% CO_2 in a bicarbonate buffer, pH 6.8) [18]. A large transient loss of force (nadir about 20% to 40% of baseline) is consistently observed two HypoPP models ($Na_V1.4$-R669H and $Ca_V1.1$-R528H) but not for WT or HyperPP ($Na_V1.4$-M1592V). We repeated this protocol for our KCNJ2 cKO mouse to assess whether in a different context the homo KCNJ2 cKO soleus would have the expected HypoPP phenotype, although neither outcome of the first two tests (force in a K challenge, or Vrest in a K challenge) was consistent with HypoPP. Peak tetanic isometric force of the soleus muscle was monitored every two minutes as the bath was exchanged from 4.7 bicarbonate buffered with 5% CO_2/95% O_2 to the same solution equilibrated with 25% CO_2/75% O_2. Historical data from our lab shown in grey demonstrates a consistent loss of more than 50% force within 6 to 8 minutes upon return to normal pH from acidosis in established hypoPP mouse models (**figure 5A**). Homozygous KCNJ2 cKO mice, however, did not show any loss of force upon recovery from acidosis, and instead remained within 10% of baseline force for the entirety of the experiment.

Muscle excitability, in vivo, during an insulin + glucose challenge

The fourth test to assess whether the homo KCNJ2 cKO mouse displayed a HypoPP phenotype was to monitor muscle excitability in vivo during a provocative low potassium

challenge accomplished by continuous infusion of insulin and glucose into potassium depleted mice. The insulin and glucose challenge further reduces serum potassium by shifting potassium into the muscle. Muscle excitability was assessed by measuring the compound muscle action potential (CMAP) of the soleus and gastrocnemius from anesthetized mice (isoflurane inhalation) in response to a single shock applied to the sciatic nerve once every minute. A stable baseline CMAP amplitude was established prior to sixty minutes of constant insulin + glucose infusion, which the Cannon Lab previously demonstrated leads to an average CMAP amplitude decrease of 70% or 80% for $Ca_V1.1$-R528H and $Na_V1.4$-R669H HypoPP mouse models, respectively. When the same protocol was tested on the homo KCNJ2 cKO mouse, the CMAP amplitude remained at a stable baseline that was not statistically different than WT.

Summary of functional studies for the homo KCNJ2 cKO model

Taken together, none of the outcomes from our four independent functional studies were consistent with a hypoPP phenotype in our KNCJ2 cKO model of ATS (**table 1**). Instead, isometric force measured in varying K support a Hyper PP phenotype rather than a hypoPP phenotype. The Vrest studies of KCNJ2 cKO muscle demonstrate a deviation from WT in low K, although the depolarization was not predicted to be sufficient to impair excitability and decrease the force. The recovery from acidosis assay and the insulin/glucose challenge are both tests for HypoPP that are able to distinguish HyperPP from WT. There was no evidence of a HypoPP phenotype for either of these tests in our KCNJ2 cKO mouse model of ATS.

Functional test	**Hypo PP**	**Hyper PP**	**KCNJ2 homo cKO**
[K+] challenge Isometric force	Loss of force in 2mM[K^+]	Loss of force in 10mM[K^+]	Hyper PP
[K+] challenge membrane potential	MP depolarization in 2mM[K^+]	MP depolarization in 10mM[K^+]	Hyper PP

Insulin Glucose challenge	Reduced CMAP and force	N/A	No hypo PP
pH challenge Isometric force	loss of force from acidosis	N/A	No hypo PP

***Table 1**: Summary of experimental results on KCNJ2 cKO mouse models using four independent established methods of testing for the potassium trigger of the periodic paralysis phenotype.*

A Ba^{2+} block model of ATS

Barium toxicity

Barium is a highly specific blocker of Kir channels, uniquely situating it as an optimal in vitro pharmacologic model to reduce Kir current (without affected other K conductances) and thereby provide a titratable model for the severity of the I_{Kir} loss in ATS. Moreover, a comparison of this acute model to our cKO mouse may reveal whether developmental compensatory changes have an impact on susceptibility to periodic paralysis for the genetic defect present at birth. Previous studies of in vivo Ba^{2+} administration to rats was interpreted as a model for hypokalemic periodic paralysis[19,20]. Moreover, severe weakness and low serum K^+ are common presenting symptoms for Ba^{2+} poisoning in humans, usually as a result of exposure to pesticides. While the findings for the Ba^{2+}-exposed rat contradict our findings in the KCNJ2 cKO mouse model, it should be recognized that the $BaCl_2$ dosage (16-25 mg/kg, i.v.) produced a high serum concentration of Ba^{2+} (25 to 500 μM) compared to concentrations of 50 μM or less in our model. This difference highlights the importance of titrating the [Ba^{2+}] in our ex vivo model to emulate the reduced I_{Kir} amplitude reported in ATS myotubes and cardiomyocytes for iPSCs.

Ba^{2+} sensitive I_{Kir}

Prior studies on Ba^{2+} block of Kir channels have focused on the blocking affinity for various heteromeric channel complexes (Kir2.x) expressed in heterologous systems, and its

voltage-dependence. Two Kir2.x isoforms are expressed in skeletal muscle, Kir2.1 and Kir2.2, both of which are Ba^{2+} sensitive, and the relative contribution of homomeric or heteromeric channel complexes to the measured Kir current in muscle is uncertain. Barium block of I_{kir} in skeletal muscle has not been previously reported.

The low solubility of Ba^{2+} is a potential limitation for studies of Kir block in physiological solutions. A bicarbonate / CO_2 buffer is the preferred bath solution for ex vivo functional studies of skeletal muscle because the sarcolemmal pH gradient is dependent upon diffusible CO_2. Barium carbonate, however, is poorly soluble in water (14 mg/liter ~70 μM). We therefore compared the block of I_{Kir} in voltage-clamp studies of FDB fibers for nominally-defined concentrations of Ba^{2+} in either HEPES (red, Fig. 6A) or HCO_3/CO_2 (black, Fig. 6A) buffered saline. These data enabled us to compare the potency of Ba^{2+} block of I_{Kir} in muscle fibers (HEPES) to published studies I_{Kir} block in other systems, and also to calibrate the Ba^{2+} block of I_{Kir} in our ex vivo contraction studies (HCO_3/CO_2). The Kir current was measured in dissociated FDB fibers, in the presence of variable barium from 1μM to 50μM, by subtraction of the background current remaining after a saturating concentration of 1 mM Ba^{2+}. Fractional block was calculated as:

$$Fraction\ blocked = \frac{I_{max} - I_{Kir}(Ba)}{I_{max}}$$

where I_{max} is the maximal Kir current and $I_{Kir}(Ba)$ is the Kir current in the presence of a (nominal) concentration of Ba^{2+}. The fractional block was fit to the Hill equation:

$$fraction\ blocked = \frac{1}{(\mathrm{IC}_{50}/[\mathrm{Ba}])^{n} + 1}$$

Where IC_{50} is the concentration that produces 50% block, and n is the hill coefficient. The hill coefficient of barium block at -80mV in HEPES and bicarbonate buffered solutions were both close to the expected value of 1; 1.02 ± .35 and .98 ± .15, respectively. I_{kir} at -80mV in a HEPES buffered solution was half blocked at 4.4 ± 2.0 μM, in close agreement to 4.5 ± 2.2 μM Ba^{2+} recorded by Schram et al (2003)[21]. when recording oocytes expressing Kir2.1 and 2.2 in equal ratios[21]. Because the available free barium is expected to be reduced in a bicarbonate bath, we anticipated a larger apparent IC_{50} of barium block. At -80mV in our bicarbonate buffered solution, the IC_{50} was 7.63 ± 1.3 μM. Nominal concentrations (based on molar mass) of 10 μM, 30 μM and 50 μM Ba^{2+} were used in bicarbonate buffered solutions for our acute barium block model of ATS, which is equivalent to 53.5 ± 3.9%, 22.4 ± 2.1%, and 6.4 ± 5.5% I_{kir} remaining, respectively.

The voltage sensitivity of barium block was readily apparent in the symmetrical K^+ solutions used for measuring I_{Kir}, as shown by the progressively larger fractional block at more negative potentials, in a constant Ba^{2+} solution (**figure 6B**). For each fiber, I_{Kir} was normalized to the amplitude measured at -120mV in barium free conditions, and then averaged.

Muscle Force in the Ba^{2+} block model of ATS

The peak isometric force in baseline conditions of 4.7 mM K^+ was relatively preserved over the entire operating range of 1 to 50 μM Ba^{2+}. Figure 7A shows the peak isometric force recorded in a single preparation, over a three-hour period, during which Ba^{2+} challenges were made from 1 to 50 μM. Even at the highest [Ba^{2+}], the loss of force was only about 10% and was fully reversible by washout. For the two operating concentrations of Ba^{2+} used in our ATS model, the average loss of baseline force was 2.98 ± 1.6% in 30 μM barium and 8.21 ± 1.8% in 50 μM Ba^{2+} (**figure 7B**).

Susceptibility to loss of force in either low K^+ (2 mM) or high K^+ (10 mM) was assessed for Ba^{2+} block models with 10, 30, or 50 μM Ba^{2+}, corresponding to residual I_{Kir} of 53%, 22%, and 6%. By comparison, a residual I_{Kir} of 22% was measured for the homo KCNJ2 cKO mouse (Figure 2). Both soleus muscles of a WT mouse were tested in parallel, with one exposed to barium and the other serving as a control. Force was normalized to the stable level over the 10 minutes before the K^+ challenge, whether that pre-exposure interval was in Ba^{2+} or a Ba^{2+}-free control. For the 2mM K^+ challenge, there was no discernable difference in the loss of force for control (0 μM), 10 μM, or 30 μM Ba^{2+} exposed soleus, with mean values of 12.2 ± 4.8%, 18%, and 15 ± 4.1% respectively. In 50 μM Ba^{2+}, however, there was a 35% loss of force from the 2 mM K^+ challenge ($P<.05$ one-way ANOVA) (**figure 7C**). For the high K^+ challenge, the loss of force was greater than control for Ba^{2+} exposed muscle at all concentrations tested (Figure 7D). On average, the control muscle had a 16.3 ± 4.8% loss of force, while the values for Ba^{2+} exposed soleus were 24.6 ± 4.6% (10μM), 31 ± 11.2% (30μM), and 59 ± 16.3% (50 μM). Using one-way ANOVA, 10 μM and 30 μM traces were not statistically different from WT ($P=.76$, $P=.15$ respectively), However 50 μM had a statistically significant reduction in force from WT ($P<.001$) and both 10 μM and 30 μM ($P<.05$)

Barium and homo KCNJ2 cKO combined

The acute Ba^{2+} block model of ATS, contrary to our homo KCNJ2 cKO model, exhibited an increased susceptibility to loss of force in low K, but only at the highest concentration of Ba^{2+} (50 μM) which corresponds to a residual I_{kir} of ~6%. This observation suggests the possibility of a threshold effect, whereby I_{Kir} must be reduced to a sufficiently low value in order for the muscle to have a HypoPP phenotype in response to the low K^+ challenge. If this hypothesis is correct, then

a lower dose of Ba^{2+} (i.e. < 50 μM) may be sufficient to induce a HypoPP phenotype in the homo KCNJ2 cKO background, where I_{Kir} is already reduced to 22% of control.

The relative peak isometric force in response to Ba^{2+} exposure, with a superimposed 2 mM K^+ challenge, for the homo KCNJ2 cKO soleus is shown in **Figure 8**. In panel (A), the force response of each muscle was normalized to the stable baseline in 4.7 mM K^+ and no Ba^{2+} (0-10 min.). At baseline K^+, the homo KCNJ2 cKO soleus is more sensitive to Ba^{2+} than WT muscle (compare to Figure 7A). The 2 mM K^+ challenge produced a substantial loss of force in the presence of 30 μM Ba^{2+}, whereas in the WT background this same amount of Ba^{2+} had no effect on the 2 K challenge (Figure 7C). This observation supports the notion that the Ba^{2+} block and homo KNCJ2 cKO had additive effects on reducing I_{Kir} that was now small enough to induce a HypoPP force response to low K challenge. The K-effect is more easily visualized by normalizing the peak force relative to the stable level attained in Ba^{2+} before the K challenge (30 to 40 min in Figure 8A). Re-normalizing the same data (from the grey box of figure 8A) demonstrates small increase of relative force in 2 K^+ for homo KCNJ2 cKO alone or with 10 μM Ba^{2+}. In the presence of 30 μM Ba^{2+}, however, the homo KCNJ2 cKO soleus had a 40% decrease ($P < .02$ $n = 3$) in force (**figure 8B**). Moreover, the data with a HypoPP phenotype when WT soleus exposed to 50 μM Ba^{2+} (from Figure 7C) is superimposable with a comparable loss of force in 2 mM K^+ (grey, Figure 8B).

Summary of functional studies

Taken together, the data show that the consequence of a K^+ challenge depends on the residual I_{Kir} amplitude. A loss of force in a 10 mM K^+ challenge, typical of HyperPP, begins to appear with 55% residual current (e.g. 10 μM Ba^{2+} WT soleus, Figure 7D; or in the het KCNJ2

cKO, Figure 2D), although not yet statistically different from control. As the residual I_{kir} is further reduced to about 20%, as occurred in the homo KCNJ2 cKO and WT in 30 μM Ba^{2+} models, the HyperPP phenotype is fully developed but the response to a 2 mM K^+ challenge is not different from WT (Figures 3 and 7). With a more severe loss of I_{Kir} (e.g. 6% for WT in 50 μM Ba^{2+} Figure 7 C and D; or homo KCNJ2 cKO in 30 mM Ba^{2+} Figure 8), the muscle is susceptible to loss of force in both low K^+ (2 mM) and high K^+ (10 mM). This concept of a I_{Kir} dependent phenotype in response to a K challenge is summarized in Figure 9.

Computational Modeling

We preformed computational modeling of muscle fiber excitability as an approach for elucidating the mechanism by which a reduction of I_{kir} causes a HyperPP phenotype or a combination of HyperPP and HypoPP, and also to provide insights on possible means of intervention. The total ionic current (I_{total}) was simulated as the sum of the contributions from the K-selective inward rectifier (I_{Kir}), the K-selective delayed rectifier (I_{Kdr}), the voltage-gated sodium channel (I_{Na}), the ClC-1 chloride channel (I_{Cl}) and the net outward current of the Na,K-ATPase pump (I_{pump}). For each ionic conductance, the open-channel I-V relation was approximated by the constant-field equation (GHK current equation). The steady-state I-V relations for these components are shown for a simulation in 4.0 mM external K^+ in Figure 10A.

The steady-state I-V for I_{Cl} as shown in Figure 10A includes an additional effect from a voltage-dependent shift of the Cl^- gradient. Flux-dependent shifts of intracellular ion concentrations were included in the model. The model used fixed concentrations of ions in the extracellular compartment to simulate our experimental conditions of a 25 ml tissue bath (equivalent to an infinite volume of the extracellular space with a fixed composition). Changes of

$[Cl^-]_i$ had a much greater effect than $[Na^+]_i$ or $[K^+]_i$ on the simulation responses for two reasons: (1) the resting Cl^- conductance is high in skeletal muscle fibers, (2) intracellular $[Cl^-]$ is relatively low (~ 4 mM) such that even modest Cl^- flux rates may cause a relatively large fold-change for $[Cl^-]_i$. To account for this pronounced effect of Cl^-, the simulation for steady-state conditions (including $[Cl^-]_i$ being at steady-state) required a net Cl^- flux of 0. This constraint means the sum of I_{Cl} (via ClC-1 channels, usually an efflux under physiological conditions) and the Cl^- flux from the NKCC co-transporter (a Cl^- influx under physiological conditions) must be zero. The overall effects of this variable $[Cl^-]_i$ are: (1) For the steady-state I_{Cl}-V relations shown in Figure 10, $[Cl^-]_i$ is not constant. $[Cl^-]_i$ is lower at hyperpolarized potentials and higher at depolarized potentials. (2) The apparent slope for I_{Cl}-V is much lower than is typically determined by voltage-clamp experiments that use brief test potentials (e.g. 200 msec) that are not long enough for the Cl^- shift to reach equilibrium. In other words, the classical I_{Cl}-V determination is steady-state for ClC-1 channels for a fixed initial value of $[Cl^-]_i$ determined by the holding potential, but the relation has not reached steady-state for the shift in the concentration gradient. (3) The apparent reversal potential for I_{Cl} is much more depolarized than the measured E_{Cl} when starting from a holding potential typical of V_{rest} (e.g. -90 mV). When the fiber is at a stable V_{rest} for a sufficiently long period of time (> 10 min), then E_{Cl} will be only a few mV depolarized relative to V_{rest} because the relatively modest influx rate of NKCC (about 20 pmol/cm^2-sec)[22] is able to keep $[Cl]_i$ only slightly higher than the passive equilibrium value (i.e. E_{Cl} only slightly depolarized from V_{rest}).

The resting potential in the model simulation is determined by the voltage at which the sum of ionic currents (via channels and the Na,K-ATPase pump) is zero. This condition also implicitly includes the constraint that the net Cl^- flux is zero. The simulation in 4.0 mM $[K^+]_o$ shows there is only one possible resting potential of about -92 mV, where $I_{total} = 0$ (Figure 8A). The I_{total}-V

relation does, however, have a region of negative slope between -80 mV and -60 mV. This behavior sets up the possibility for an I-V relation that intersects the I = 0 axis at multiple loci. Two ionic currents contribute to the negative slope: (1) I_{Kir} at V > EK, where the outward current amplitude is decreasing with more depolarization because of rectification, (2) the steady-state inward "window" current contributed by I_{Na}.

The effect of reducing I_{Kir}, at a fixed $[K^+]_o$ = 4.0 mM is shown in Figure 10B. The relative loss of outward current from I_{Kir} causes the I_{total} curve to shift downward over the voltage range from -85 mV to -60 mV. With a residual I_{Kir} = 20%, there are three points where I_{total} = 0: the original V_{rest} = -94 mV, an unstable equilibrium at -80 mV, and a second stable V_{rest} at -58 mV. This example illustrates how a reduction of I_{Kir} may create new anomalously depolarized V_{rest} values that are stable and occur at a voltage that would inactivate the majority of Na channels thereby reducing excitability and causing a loss of force. The plot in Figure 10C is a V_{rest} – $[K^+]_o$ phase diagram for which families of curves are shown, each with a differently scaled amplitude of I_{Kir}. When I_{Kir} is 100% of normal amplitude, V_{rest} shifts along the lowest set of blue circles (i.e. normally polarized) as K^+ varies over the entire physiological range of 2.0 to 5.5 mM. If only a residual I_{Kir} of 17% remains (purple circles), then a reasonably polarized V_{rest} (about -95 mV) is still maintained for K^+ between 2.0 and 4.0 mM. At an elevated $[K^+]_o$ of 5.5 mM, however, there will be an anomalous depolarization of V_{rest} to about -50 mV. This scenario simulates the HyperPP phenotype observed experimentally in homo KCNJ2 cKO mice or WT in 30 μM Ba^{2+}. When I_{Kir} is reduced even further to a residual of 14% (dark red circles, Figure 10C), then a reasonably polarized V_{rest} (-95 mV) exists for 2.3 < K < 3.9 mM. If $[K^+]_o$ is either lower (< 2.3 mM) or higher (> 4.0), however, then V_{rest} is anomalously depolarized. This example recapitulates the combined

HypoPP and HyperPP phenotype observed experimentally for the 50 μM Ba^{2+} block model or homo KNCJ2 cKO plus 30 μM Ba^{2+}.

The time course for a shift of V_{rest}, and its effect on excitability, in response to high K or low K challenge is shown in Figure 11. Simulated synaptic excitation occurs every 60 sec, by activating a conductance equally permeable to Na^+ and K^+ for 1 msec. On the compressed time scale of Figure 11, action potentials (inset 11B) appear as vertical lines. All simulations begin in 4.0 mM K^+. The top panel (A) simulates a residual I_{Kir} of 20% and even with this deficit the initial V_{rest} is stable at -90 mV. When K^+ is reduced to 2 mM (t = 0 sec, Fig. 11A, left), V_{rest} hyperpolarizes, as expected from the shift of E_K, and excitability is preserved. When K^+ is increased to 6 mM (t = 0 sec, Fig. 11B), only a modest depolarization of V_{rest} occurs and excitability is maintained. Over about 2000 sec, however, Cl^- shifts into the simulated fiber, V_{rest} depolarizes to about -60 mV and excitability is dramatically reduced. The consequences of a greater reduction of I_{Kir} (residual of 5%) is shown in Fig. 11B. Again, with the initial K^+ = 4.0 mM a stable V_{rest} of -90 mV exists and excitability is normal. When K^+ is reduced to 2 mM, the simulated fiber paradoxically depolarizes to -60 mV and excitability is severely compromised. This response emulates the properties of HypoPP. Starting again from an initial K^+ = 4.0 mM (Fig. 11B, right), when K^+ is increased to 6.0 mM the initial small depolarization of V_{rest} with preserved excitability (0 to 1500 sec), gives way to a larger depolarized shift and loss of excitability. This late shift is caused by equilibration of Cl^- (rise of $[Cl^-]_i$ with an associated depolarized shift of E_{Cl}) and is the equivalent of a HyperPP phenotype.

While there might be further improvements in the model parameters to slightly adjust the numerical values of K^+, V_{rest}, and scaled I_{Kir} that cause depolarization and loss of excitability, the model sufficiently captures the main features of our experimental observations. First, a normal

V_{rest} and fiber excitability are possible in normal K^+, even with a severe reduction of I_{Kir}. Second, as I_{Kir} is reduced (e.g. 20% residual), the initial phenotype is HyperPP with anomalous depolarization and loss of excitability in high K, but not low K. Third, as the reduction of I_{Kir} becomes more sever (e.g. 5% residual), then anomalous depolarization and loss of excitability occurs with either an increase of K^+ (6 mM) or a decrease of K^+ (2 mM), consistent with our experimentally observed phenotype of HyperPP and HypoPP.

Rational Approach to Pharmacologic Intervention

For all forms of periodic paralysis, the precipitating event is a failure to maintain V_{rest}, with depolarization and loss of excitability. For the first time, our experimental models of ATS demonstrate that the K-dependence for triggering a loss of force (i.e. high-K or low-K induced) depends upon the severity for the reduction of I_{Kir}. Because attacks may occur for both high K^+ or low K^+ when I_{Kir} is severely compromised, avoidance of trigger factors is less feasible and pharmacologic intervention has a higher priority. We strategically tested several approaches for pharmacologic intervention, based on the fundamental causes of anomalous depolarization. These approaches are summarized in the Table 2.

Intervention	Mechanism	Prevent Phenotype
Inhibit NKCC	↓ Cl^- influx, ↓ apparent g_{Cl}	HypoPP
Partially block $Na_V1.4$	↓ I_{Na} window current	HyperPP
b adrenergic stimulation	↑I_{pump}	HyperPP (HypoPP)
Carbonic anhydrase inhibition	? empirical use clinically	HyperPP or HypoPP
K_{ATP} channel activator	↑g_K	HyperPP or HypoPP

Table 2. Summary of pharmacological interventions

Each intervention was tested with the in vitro contraction assay. The paired soleus muscles from the same animal were studied two separate tissue chambers, one pretreated with the intervention and the other with no intervention as a control, after which both muscles were then tested in a high K or low K challenge.

Inhibition of NKCC with bumetanide (BMT)

Previous studies in our lab have demonstrated a beneficial effect of NKCC1 inhibition by bumetanide (BMT), which completely prevents a low-K induced loss of force in HypoPP muscle[23,24]. We therefore tested BMT (75 μM) in the 50 μM Ba^{2+} block model of ATS (in WT soleus) that has a HypoPP component of the phenotype (Figure 7C). Peak tetanic force was measured every two minutes, before and after washout of a 2 mM K challenge. The relative peak force in the Ba^{2+} block model was well maintained in 75 μM BMT (**Figure 11A** 20-40 min.), but there was no protection for the loss of force induced by the 2 mM K^+ challenge. In fact, the average loss of force tended to be greater in the presence of BMT, although this was not statistically significant (P = 0.8). As an additional test, we compared the loss of force for two thirty-minute low-K^+ exposures on the same muscle, either in the presence and absence of 75 μM BMT (**figure11B**). Again, the loss of force during the 2 mM K challenge was greater in the presence of BMT. The result for this alternative form of an internal control is remarkable because with repeated 30 min. challenges of low K there is usually a cumulative effect with a greater force deficit in the second exposure, but here the deficit was less. We conclude that inhibition of NKCC1 with BMT is not an effective means to reduce the susceptibility to HypoPP in the Ba^{2+} block model of ATS.

Partial block of $Na_V1.4$

A potential contribution of I_{Na} to the HyperPP phenotype is apparent from the steady-state IV relation in Figure 10A. An increase of $[K^+]_o$ will elicit a modest depolarization of V_{rest} because of the positive shift in E_K. This small depolarization may activate a substantial inward I_{Na} from the window current (i.e. overlap of incomplete inactivation and onset of activation). Normally this window current is balance by a contribution to the outward current by I_{Kir}. The reduced I_{Kir} in ATS creates an imbalance, and we reasoned that reducing I_{Na} could restore the balance to promote a normal V_{rest} (as confirmed in the computational model). We tested two agents to partially block I_{Na}. Ranolazine is an FDA approved anti-anginal drug with a complex mechanism of action but has an established effect on preferentially blocking the late I_{Na} in cardiomyocytes, of which Na^+ window current is a known contributor[25]. Moreover, ranolazine has been used for investigational studies of reducing myotonia[26]. In the homo KCNJ2 cKO model, ranolazine at 10, 30 or 50 μM elicited a large drop in force that was further exacerbated by the 10 mM K^+ challenge (**Figure 12A**). Both effects were partially reversible, upon return to 4.7 mM K and washout of ranolazine.

As a proof of concept, low dose TTX was also tested because of its higher specificity than ranolazine for blocking Nav channels. In the homo KCNJ2 cKO soleus, pretreatment with 10 nM TTX did not substantially reduce the baseline (4.7 mM K^+) peak tetanic force (**Figure 12B**). The 10 mM K^+ challenge elicited a substantial loss of force in the low-dose TTX treated muscle, surpassing that of the untreated muscle. Upon return to 4.7 mM K^+, TTX treated muscle did not fully recover to baseline, but did recover slightly upon washout of the toxin.

Based on these unfavorable responses for two different drugs at concentrations that partially block $Na_V1.4$ channels, we conclude this mechanism is not effective for reducing the severity of a high-K induced loss of force in the homo KCNJ2 cKO model of ATS.

β adrenergic stimulation with salbutamol

Model simulations show that increasing I_{pump} is an effective means to reduce the susceptibility to anomalous depolarization in high K, and thereby be beneficial in preventing HyperPP. A possible benefit also exists for preventing HypoPP, but the computational model shows this is a much smaller effect because the risk of the anomalous depolarization in HypoPP occurs from a more hyperpolarized range of normal V_{rest} (because K is low) where I_{pump} is smaller because of its $[K^+]_o$ and voltage dependencies. We therefore tested the efficacy of salbutamol (1 or 10 μM) to prevent loss of force in high K for the homo KCNJ2 cKO model of ATS. In control conditions, before the high K^+ challenge, application of 10 μM (**Figure 13A**) or 1 μM (**Figure 13B**) salbutamol produced a substantial increase of relative force. This effect is consistent with the notion that homo KCNJ2 cKO soleus may be in a "partial attack" of periodic paralysis even before the K challenge (**Figure 3B**). When a 10 mM K^+ challenge was applied in the continued presence of salbutamol, a large decrease of peak tetanic force still occurred. The limited available data suggest that the rate of force decrease was slowed by salbutamol (1 or 10 μM), and perhaps the magnitude for the loss of force was modestly attenuated in 10 μM drug.

The benefit of β adrenergic stimulation with salbutamol was modest, at best, in the homo KCNJ2 cKO model of ATS. Because the use of β adrenergic agents has potential risks for the arrhythmias associated with ATS, we did not pursue more detailed studies of this intervention.

Inhibition of carbonic anhydrase with acetazolamide

The benefit of carbonic anhydrase inhibitors for prophylactic management of HyperPP and HypoPP was discovered empirically[27], and subsequently a controlled cross-over trial showed efficacy for dichlorphenamide over placebo[28]. The frequency of a favorable response in HypoPP

patients is about 50%[29]. The mechanism of action for reducing the risk of periodic paralysis remains to be fully established, but a leading proposal is a protective effect from the systemic metabolic acidosis caused by increased renal excretion of bicarbonate. Consistent with this hypothesis, we previously showed acetazolamide is not very effective at preventing HypoPP in an ex vivo assay (where the drug will not cause metabolic acidosis), whereas in vivo administration was clearly efficacious[23]. This caveat should be considered when interpreting the results of our ex vivo acetazolamide studies.

The in vitro contraction assay was used to test for an effect of 100 μM acetazolamide on the high-K induced loss of force for the homo KCNJ2 cKO model of ATS (**Figure 14**). In the limited available data, acetazolamide did not have a detrimental effect on relative force in control conditions (4.7 mM K). The loss of force in the 10 mM K challenge, however, was similar or perhaps even a bit worse (83% loss vs 83% loss) in the acetazolamide-treated muscle. We conclude that under these in vitro testing conditions, acetazolamide does not provide protection against a high-K induced loss of force for the homo KCNJ2 cKO model of ATS.

Activation of K_{ATP} channels with pinacidil

In general, hyperpolarization of V_{rest} in skeletal muscle would be an effective therapy for reducing the severity and frequency for any form of periodic paralysis. Activation of a K-selective conductance in muscle is a potential universal mechanism to achieve this goal. Model simulations show that even a very modest increase of the resting g_K can have a substantial benefit in compensating for the reduced I_{Kir} in ATS. Prior studies in human HypoPP fibers have shown the K_{ATP} channel openers (cromakalim or pinacidil) are effective for repolarizing fibers and promoting recovery from loss of force. While pinacidil is used clinically to reduce vascular resistance and

blood pressure, it has not been applied to the routine management of HypoPP because at dosages required to improve muscle function patients experience hypotension and suppressed insulin secretion. Nevertheless, we explored the use of pinacidil to prevent the K-induced loss of force in our models of ATS.

The in vitro contraction assay was used to test for a beneficial effect of pinacidil. The homo KCNJ2 cKO model was used for the high-K induced loss of force assay, and the 50 μM Ba^{2+} block model (in the WT background) was used for the low-K assay. Similar to the salbutamol effect, the application of pinacidil (100 μM) produced an increase in relative baseline force for homo KCNJ2 cKO soleus (**Figure 15A**). The increase was larger for muscle preparations starting from a lower initial peak force, and the force in pinacidil was comparable to WT soleus. These effects are consistent with the view that homo KCNJ2 cKO soleus may have a reversible partial loss of force, even at baseline 4.7 mM K^+, that improves with 100 μM pinacidil. For the 10 mM K challenge, 100 μM pinacidil substantially attenuated the loss of force from 64% (no drug) to 18% (**Figure 15B**). In a single trial of 1 μM pinacidil, however, there was no protection for loss of force. In the 50 μM Ba^{2+} block model of ATS, 100 μM pinacidil completely prevented the loss of force induced by a 2 mM K^+ challenge (**Figure 15C**). Just as with the high K assay, however, 1 μM pinacidil did not protect against a loss of force induced by the K^+ challenge.

In vitro contraction assays for two different models of ATS, homo KCNJ2 cKO and 50 μM Ba^{2+} block, both showed beneficial effects of 100 μM pinacidil for attenuating or preventing the loss of force in high-K or low-K challenge, respectively. At 1 μM, however, there was no evidence for a beneficial effect of pinacidil.

1.4 DISCUSSION

Generation of an animal model for ATS provides a unique opportunity to characterize the pathomechanism for the muscle phenotype associated with the disease. Contrary to both hyperkalemic periodic paralysis and hypokalemic periodic paralysis, where the relationship of extracellular potassium to provoking an attack of weakness is well established, the role of serum potassium is poorly understood in ATS[2]. Historically, experiments have demonstrated hyper-, hypo-, and normo-kalemia during spontaneous attacks of weakness in patients[1,14,15] leading to the current classification of dyskalemic periodic paralysis in ATS. Accurate characterization of the K^+ dependence is imperative for optimal disease management, and yet provocative testing in humans is not feasible due to the risk of ventricular arrhythmia.

Current management for ATS is not well established, due to the uncertainty of a K^+ trigger, and treatment plans are often based on the assumption that that low-K is deleterious[30]. This treatment approach is also influenced by the preference of cardiologists to keep serum K high and thereby reduce the incidence of PVCs and ventricular tachyarrhythmias in ATS. Moreover, for skeletal muscle a decreased outward current through reduction of I_{kir} was predicted to increase the susceptibility to paradoxical depolarization and loss of excitability in low-K. The analogous situation has been demonstrated for HypoPP mice, wherein the current imbalance is caused by an anomalous gating pore leak[31]. To address this question, we used a mouse model of ATS that enabled us to explore fiber excitability and contraction, whereas a limited insight would be gained from studying cell culture based systems. We show that a reduction of I_{kir} in muscle fibers, either through a KCNJ2 cKO or Ba^{2+} block, produces a dyskalemic periodic paralysis phenotype that has features of both HypoPP and HypePP, depending on the severity of Kir loss.

Moderate loss of I_{kir} produced a HyperPP phenotype

While there is a clear consensus agreement that ATS mutations have a dominant-negative effect on I_{Kir} amplitude, a wide range of severity has been reported, and this variability depends on the particular mutation and the experimental preparation. Co-expression of WT and ATS-mutant Kir2.1 in oocytes results in as little as 10% of the normal current amplitude, with most mutations falling between 20 and 50% that of WT[12]. Studies in cultured ATS myotubes have shown similar reductions in I_{kir}, averaging around 50% remaining[13]. While our het-KCNJ2 cKO did not reduce current to this level, our homo KCNJ2 cKO had 30% I_{kir} remaining, poising it within the optimal range to recapitulate the ATS phenotype. Our in vitro force studies showed that baseline force in the homo-KCNJ2 cKO was reduced by 27% compared to WT. While statistically significant, the variance was high with considerable overlap with WT. This "baseline" may actually represent a spontaneous partial attack of weakness, before a provocative challenge is applied. In support of this concept, several manipulations unexpectedly caused an increase of force compared to "baseline". For example, in the homo-KCNJ2 cKO soleus muscle, but not WT, the peak force increased in response to β adrenergic stimulation, low K, K_{ATP} openers, or acidosis. These increases brought the peak force of homo KCNJ2 cKO soleus to a level comparable to WT. Taken together this suggests a partial attack in normo-K, rather than a fixed myopathy.

The response of homo KCNJ2 cKO muscle to a provocative K^+ challenge was unexpected, given the previously mentioned first principles of current balance. A low-K challenge produced a small, but consistent, increase of force whereas a high-K challenge elicited a substantial loss of force. Curiously, we did not observe a low-K induced increase in force for the Ba^{2+} block model with a comparable residual I_{Kir} (30 μM Ba^{2+}). This discrepancy might be caused from two possible mechanisms: (1) the Ba^{2+} was applied after the muscle had recovered for ~ 30 min from the stress

of the muscle dissection, whereas for the KCNJ2 cKO muscle, which had a pre-existing I_{Kir} deficit, the dissection may have triggered a partial spontaneous attack. In other words, the KCNJ2 cKO soleus was able to display an increase of force from recovery, while the Ba^{2+} block model did not have a spontaneous attack and so there was no loss to recover from. (2) The time course for developing a loss of force in normal K (4.7 mM) might be very slow. In this case, the KCNJ2 cKO preparation had about 30 min post dissection in which to develop an attack whereas in the Ba^{2+} model the blocker was applied for only 10 or 20 min and then the K challenge was performed.

Because the response to the K challenges were directly opposite to the expected HypoPP phenotype, we preformed several additional tests previously developed in our lab to provoke a loss of force in HypoPP, besides the in vitro K^+ challenge. These tests included peak force after recovery from acidosis, in vivo CMAP response to insulin and glucose infusion, and the shift of V_{rest} in response to changes in extracellular K. As summarized previously in Table 1, none of these three additional tests produced a result consistent with HypoPP. Interpretation of the data, however, is not always a definitive yes or no. For example, the resting membrane potential in homo KCNJ2 cKO fibers did show a paradoxical depolarization in response to a low K, a phenomenon consistent with HypoPP. However, this depolarization was not severe enough to sufficiently inactivate Na channels and thereby suppress excitability to cause weakness. Taken collectively, these studies of muscle function by in vitro contraction in response to K challenges or recovery from acidosis, fiber excitability as reflected by CMAP amplitude during an in vivo glucose plus insulin challenge, and microelectrode recordings of V_{rest} are most consistent with a HyperPP phenotype in the homo KCNJ2 cKO mice.

Severe loss of I_{kir} produces a Dyskalemic Periodic Paralysis with features of HypoPP and HyperPP.

In other contexts, the effect of Ba^{2+} on mammalian skeletal muscle shows many features of HypoPP. For example, acute Ba^{2+} administration to the rat, in vivo, [19] causes hypokalemia and a loss of muscle force. However, this study used large doses of barium chloride (16-25 mg//kg i.v.) with measured serum concentrations of Ba^{2+} (25 to 500 μM), and so the potential off target effects are in question. Barium poisoning in humans occasionally occurs in the setting of pesticide exposure. Clinical case reports of barium poisoning state that 55.3% of patients present with paralysis while only 17.3% had hypocalemia[32]. This dissociation suggests the loss of force may be a primary event, in the absence of hypokalemia. In vitro studies of Ba^{2+} treated rat muscle[20] demonstrated an initial increase of force over 5 to 10 min that then transitioned to a profound loss of force. These effects were more pronounced in low K (nominally 0-1 mM). It should be noted, however, that exceptionally high [Ba^{2+}] was used in this study (nominally, up to 10 mM), which raises questions about achievable solubility, specificity for blocking only I_{Kir}, and relevance to our low-dose (10-50 μM) Ba^{2+} block model. Because these studies raise more questions than answers, we revisited the Ba^{2+} block model using a carefully titrated approach to produce a loss of I_{Kir} comparable to that observed in ATS. This pharmacologic model was an important extension for our studies of ATS because we were unable to reduce I_{Kir} to less than 30% of control by using the homo KCNJ2 cKO model.

The impact on peak isometric force of a reduced I_{Kir} secondary to Ba^{2+} block was examined in normal (4.7 mM), low-K and high-K. Unlike the prior studies in rat muscle, in normal [K^+] the peak isometric force of the soleus muscle remained within 10% of control values over the entire experimental range of 10 to 50 μM [Ba^{2+}]. At a nominal free [Ba^{2+}] of 50 μM, we observed a near

complete block (94%) of I_{Kir}. This observation suggests the profound loss of force observed in normal K^+ for (high) Ba^{2+} exposed rat muscle may be caused by effects on targets other than Kir channels. Conversely, our Ba^{2+} block model of ATS shared many features with the homo KCNJ2 cKO model, suggesting that in the range of [Ba^{2+}] used in our studies, the effects of this divalent were primarily the result of blocking I_{Kir}. Thirty μM Ba^{2+} reduced I_{Kir} to a comparable level detected in the homo KCNJ2 cKO mouse, i.e. a residual of ~20%. Both of these scenarios caused a HyperPP phenotype with loss of force during a 10 mM K^+ challenge, but preserved force in 2 mM K^+.

Some ATS patients unequivocally have attacks of weakness with a K-sensitivity more consistent with HypoPP[2], and functional studies of some ATS mutations have demonstrated > 80% loss of I_{Kir}. While these two phenomena are not tightly coupled, they suggest that a greater range of I_{Kir} loss should be investigated to more fully explore the pathogenesis of ATS. A more complete block of I_{kir} (residual of 6%) in 50 μM Ba^{2+} produced a dyskalemic state wherein either high K or low K elicited a substantial loss of isometric force. We tested the notion that the dyskalemic phenotype is determined by the extent of I_{Kir} loss, rather than being a unique feature of the Ba^{2+} block model. In support of this hypothesis, a lower [Ba^{2+}] of 30 μM, which produces purely HyperPP in WT, now caused the mixed Hyper/Hypo dyskalemic PP when applied to homo KCNJ2 cKO soleus. Taken together, the Ba^{2+} block and KCNJ2 cKO models show that a loss of up to ~50% of I_{Kir} has no significant impact on contractility, but as the loss of I_{Kir} approaches 80% the muscle becomes susceptible to HyperPP, and with a ~95% loss then a dyskalemic form of PP occurs with features of HyperPP and HypoPP.

Pathomechanism for I_{Kir}-dependent K-sensitivity for loss of force demonstrated through computational modeling.

The computational model of V_{rest} for a simulated fiber provides insight on how the K-dependent susceptibility to anomalous depolarization varies with the magnitude of the I_{Kir} reduction and also provides a platform to identify potential interventions to stabilize V_{rest}. The transient attack of muscle weakness, which is an essential feature for all forms of periodic paralysis, is caused by an anomalous depolarization of V_{rest} which inactivates $Na_V1.4$ channels and reduces fiber excitability[33]. It remains unclear however, how changes in extracellular K^+ are mechanistically linked to this depolarization in muscle fibers with reduced I_{kir} such as in ATS. The possibility of two stable resting potentials, one normally polarized and the other depolarized, is an intrinsic feature of the nonlinear conductances in skeletal muscle, including the simulation of WT. This bistable V_{rest} occurs when there are multiple values of V for which the total ionic current is zero. Under steady-state conditions, the major inward ionic currents are I_{Na} (small window current) and I_{Cl}; whereas the major outward ionic currents are I_{Kir}, I_{Kdr}, and I_{pump}. Flux dependent changes of $[Cl^-]_i$ must be included, if the model is to exhibit bistability. This requirement is a consequence of the large resting Cl^- conductance (about 80% of the total resting conductance) that in the absence of a shift for $[Cl^-]_i$ would constrain V_{rest} to remain within a few mV of a constant E_{Cl}, regardless of how large a $[K^+]_o$ was imposed. Another way to view this same effect is to recognize the steep I_{Cl}-V relation (for constant $[Cl^-]_i$) that prevents the nonlinear inflection of the total I-V from causing multiple values of V where $I_{total} = 0$. In our model, $[Cl^-]_o$ is held constant, and $[Cl^-]_i$ is determined from the balance of Cl^- eflux via ClC-1 and influx via the NCKK co-transporter. In summary, the value of V_{rest} from out model is determined by a pair of constraints: $I_{total} = 0$ and the net Cl^- flux = 0.

For our computational model, V_{rest} was sensitive to both $[K^+]_o$ and the scaled value of I_{Kir}. When I_{Kir} was simulated for normal conditions (i.e 100%), V_{rest} maintained a normal polarized value as $[K^+]_o$ was varied from 1 mM to 8 mM. This result implies the simulation of a WT muscle fiber is not susceptible to periodic paralysis for any $[K^+]_o$ value in this operating range. When I_{Kir} was scaled to 17% of normal (Figure 10C, purple symbols), anomalous depolarization of V_{rest} occurred for $[K^+]_o > 5$ mM. Mechanistically, this depolarization was caused by an insufficient outward I_{Kir} current compared to the normal I_{Na} window current. The anomalous depolarization is high-K dependent because a modest depolarization from the rightward shift of E_K is necessary to activate I_{Na}, all of which is normal but now overwhelms the reduced I_{Kir}. These insights suggest a partial block of I_{Na}, to reduce the steady-state window current, may be beneficial to prevent anomalous depolarization in high K^+. To complete the model description, a reduced I_{Kir} at 17% of normal does also create susceptibility to depolarization in low-K, but this occurs only at extremely low values < 1.5 mM. Over the intermediate interval $2 < [K^+]_o < 5$, the model has a bistable V_{rest} with both normally polarized and depolarized values. Therefore, the overall phenotype is Normo-PP or HyperPP when I_{Kir} is 17%. When I_{Kir} is further reduced to 14%, the anomalous depolarization in high K^+ persists and now paradoxical depolarization occurs in 2 K^+ as well (Fig. 10C). A small "island" of permissible $[K^+]_o$ exists where V_{rest} remains polarized, and outside this range there is both HyperPP and HypoPP. The low-K depolarization occurs because the normal inward I_{Cl} overwhelms the outward currents from attenuated I_{Kir} and I_{pump} decreases in low $[K^+]_o$. This mechanism suggests two possible interventions increase I_{pump} or decrease I_{Cl}. Rather than directly block ClC-1 (e.g. 9-anthracene carboxylic acid) a more effective way to reduce I_{Cl} is to promote low $[Cl^-]_i$ by inhibition of NKCC with bumetanide.

Pharmacological Intervention

Interventions designed to suppress high-k induced loss of force

Understanding the individual currents responsible for establishing V in response to a depolarizing shift in E_K allows us to identify potential candidates for pharmacological manipulation in an effort to reestablish a stable hyperpolarized resting membrane potential. As described above, the I_{Na} window current likely contributes to the depolarization during HyperPP. Therefore we tested ranolazine, an anti-anginal drug that is reported to preferentially block the window current, in the high-K challenge for our homo KCN2 cKO model. Unfortunately, even at the lowest dosage studied (10 μM, Fig. 12), ranolazine caused a pronounced loss of force in normal K^+ that was further exacerbated by high K^+. Others have used ranolazine (5 – 100 μM) to suppress myotonic discharges in the ClC-1 null mouse (Ref: Novak Ann Neurol, 2015). It is not clear why those mice tolerated much high concentrations of ranolazine, but perhaps excitability was preserved in the setting of low Cl^- conductance. As an alternative to ranolazine, we tested low-dose TTX (10 nM, IC_{50} ~ 30 nM) to partially block Nav1.4 channels. For homo KCNJ2 cKO soleus in normal K^+ (4.7 mM), TTX did not impair the baseline isometric force, but a 10 K^+ challenge elicited a near complete loss of force that was worse than the 80% decrease in the paired muscle without drug. While it may be possible that additional titration of NaV1.4 blockers could reveal a dosage that protects against HyperPP, the negative results so far led us to pursue other approaches.

Another possible method to prevent high-K induced loss of force in ATS is to increase the outward current through the Na^+/K^+ ATPase, as computational modeling shows this dramatically suppresses the anomalous depolarization in high-K. For our in vitro assay, we used the β_2 adrenergic agonist salbutamol as a proof of principle, while this may be detrimental for the

arrhythmia in ATS patients. At baseline (4.7 mM K^+), the application 1 μM or 10 μM salbutamol elicited a 20% to 60% increase in isometric force for homo KCNJ2 cKO soleus. We interpret increase as recovery from a partial loss of force in this ATS model at baseline conditions. The potential benefit to protect against high-K^+ induced loss of force is less clear. In 1 μM salbutamol the nadir for relative force in 10 K^+ was comparable to the no-drug control. For 10 μM, the high-K induced loss of force was reduced by about half. Overall, these data suggest that a therapeutic level of salbutamol (1 μM) may provide some benefit for recovery of mild weakness in normokalaemia or perhaps even in mild hyperkalemia, especially when considering that increased pump activity in vivo will lower serum K^+ (unlike the situation in the tissue bath). Our data suggest that with a more severe elevation of K^+, however, adrenergic stimulation of the Na,K-ATPase may not produce a sufficient outward current to prevent anomalous depolarization and loss of force.

Interventions designed to suppress low-k induced loss of force

Previous studies in our lab have demonstrated that inhibition of the NKCC co-transporter with 1 μM bumetanide completely prevents the loss of force during a 2 mM K^+ challenge in both of our knock-in HypoPP mouse models.[24,31]. Susceptibility to paradoxical depolarization in low K for these models is caused by an inward gating pore current. The combination of this inward leakage current and inward I_{Cl} overwhelms the outward current of I_{Kir} under low K conditions, which reduces I_{Kir}. We reasoned that an analogous current imbalance occurs in low K for ATS, except the primary defect is a reduced outward I_{Kir}. We tested the efficacy of 75 μM bumetanide (a saturating dose) to protect against a low-K induced loss of force for the 50 μM Ba^{2+} block model of ATS. Surprisingly, a 2 mM K^+ challenge produced a greater loss of force in bumetanide treated muscle than controls. Perhaps the inhibition of Cl^- influx with bumetanide does not sufficiently

reduce I_{Cl} to prevent depolarization in the setting of a severely impaired I_{Kir}? Afterall, bumetanide does not block I_{Cl}, but instead it biases the Cl^- gradient at equilibrium such that the apparent Cl^- conductance is reduced and E_{Cl} is more hyperpolarized. These considerations raise the possibility that a ClC-1 blocker such as 9-anthracene may be worth exploring in future studies, as a means to prevent anomalous depolarization in low K^+ for ATS muscle with an impaired I_{Kir}.

Assessment of Empirical Interventions in Clinical Use

Carbonic anhydrase inhibitors (acetazolamide and dichlorphenamide) are used prophylactically to reduce the frequency and severity for episodes of weakness in HypoPP and HyperPP[27]. The efficacy to prevent weakness for HyperPP and for HypoPP is intriguing, both in terms of understanding the mechanism and in consideration of ATS patients who may have either HyperPP or HypoPP. The response rate in classical HypoPP is only about 50%[29] and the mechanism of action is unknown, although the accompanying metabolic acidosis is a leading hypothesis. Anecdotal case reports of ATS patients suggest carbonic anhydrase inhibitors may be beneficial to reduce attacks of weakness[30], although there is one report of weakness being worsened with the drug[34]. For the homo KCNJ2 cKO model, we did not observe a protective effect of 100 μM acetazolamide to prevent a loss of force in the high-K challenge. One caveat is that the efficacy of acetazolamide may be dependent upon inducing metabolic acidosis, which does not occur in the tissue bath preparation. Indeed, our lab previously reported that while acetazolamide was clearly inferior to bumetanide in preventing a loss of force in low K for the HypoPP mouse (CaV1.1-R528H), when tested in vivo both drugs were equally effective[23].

Interventions directed at increasing the K conductance of resting muscle

An increase in the K conductance (g_K) of resting muscle (i.e. at -80 to -95 mV) is, in principle, a generalized strategy for treating all forms of periodic paralysis because this manipulation would tend to polarize V_{rest} toward E_K. Moreover, an increase of gK would precisely address the membrane defect in ATS. While not currently used as a prophylactic agent for periodic paralysis, K_{ATP} channel openers (pinacidil, cromakalim, and other investigational drugs) have been shown to improved muscle force both in patients and in ex vivo preparations. Limited studies in small groups of patients showed about half had an improvement in baseline strength or were protected from a carbohydrate-load induced attack in HypoPP[35]. In ex vivo studies of biopsies from HyperPP and HypoPP patients, pinacidil was able to restore force in muscle that was subjected to K challenges[36,37]. While the K channel openers were clearly effective in ameliorating the depolarization-induced weakness in PP, the drug concentrations used for these ex vivo studies were much higher than can be achieved therapeutically (e.g. 100 μM pinacidil experimentally, whereas a therapeutic level is at most 2 μM[38]). Such high dosages are limited by K_{ATP}-dependent side effects in vivo, such as relaxation of smooth muscle that lowers blood pressure and inhibition of insulin secretion by pancreatic β cells.

As a proof of concept, we tested the ability of pinacidil to prevent a high-K induced loss of force in our KCNJ2 cKO model or to prevent a low-K induced loss of force in the Ba^{2+} block model. At 100 μM, pinacidil completely prevented the loss of force in 2 mM K^+ and substantially attenuated the loss of force in 10 mM K^+. Similar to the effect of salbutamol, pinacidil also improved the baseline force in 4.7 mM K^+ for the homo KCNJ2 cKO soleus, which is again consistent with "rescue" from a spontaneous partial attack at baseline. This highly efficacious outcome for 100 μM pinacidil is consistent with prior studies on HypoPP or HyperPP. Unfortunately, at a more realistic concentration of 1 μM for therapeutics usage, there was no

benefit from pinacidil. It may be possible that at some intermediate value of 2-5 μM, pinacidil may provide meaningful protection from weakness in ATS. Alternatively, these studies demonstrate that if a muscle-specific K channel opener could be developed, then this would be an ideal compound for management of periodic paralysis, especially in ATS.

1.5 FIGURES

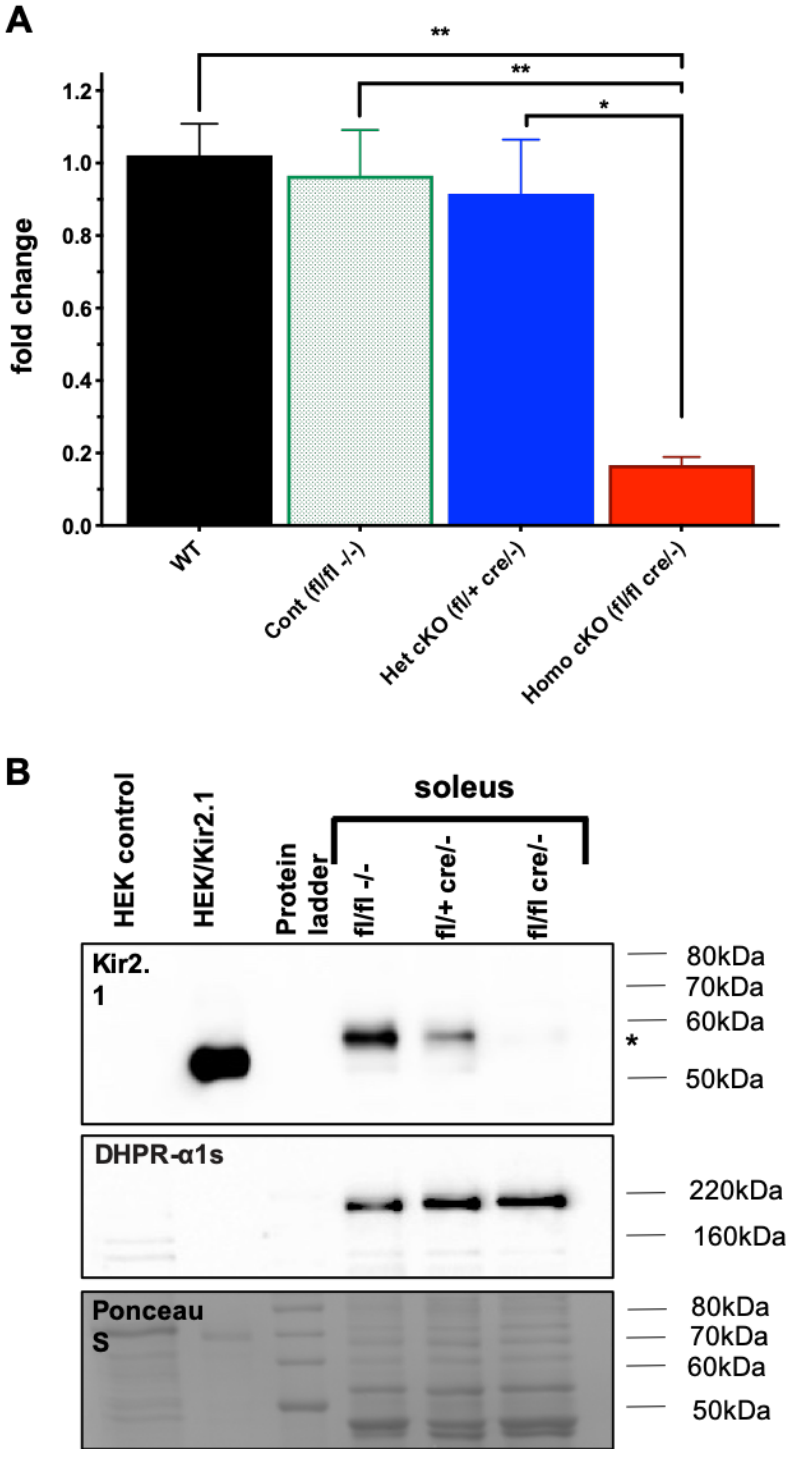

Figure1-1. KCNJ2 RNA transcript and Kir2.1 protein are reduced in genetic knockout model of ATS. (**A**) KCNJ2 transcript levels assessed by qPCR from excised soleus muscle demonstrate a statistically significant five fold reduction reduction in the homo-KCNJ2 cKO mouse model. C57B6 background, control,

and het-KCNJ2 cKO did not show a statistically significant difference in KCNJ2 transcript levels. Significance levels were determined with one-way ANOVA, **P < .001, *P <.05. (**B**) Immunoblots of the membrane fraction from the soleus muscle probed with anti-Kir2.1. show no detectable protein in homo-KCNJ2 cKO, and reduced amounts in het-KCNJ2 cKO compared to control, HEK cells were transiently transfected with Kir2.1 to provide a positive control. DHPR-α1s immunoblot and Ponceau S stain were used to verify equal loading among wells

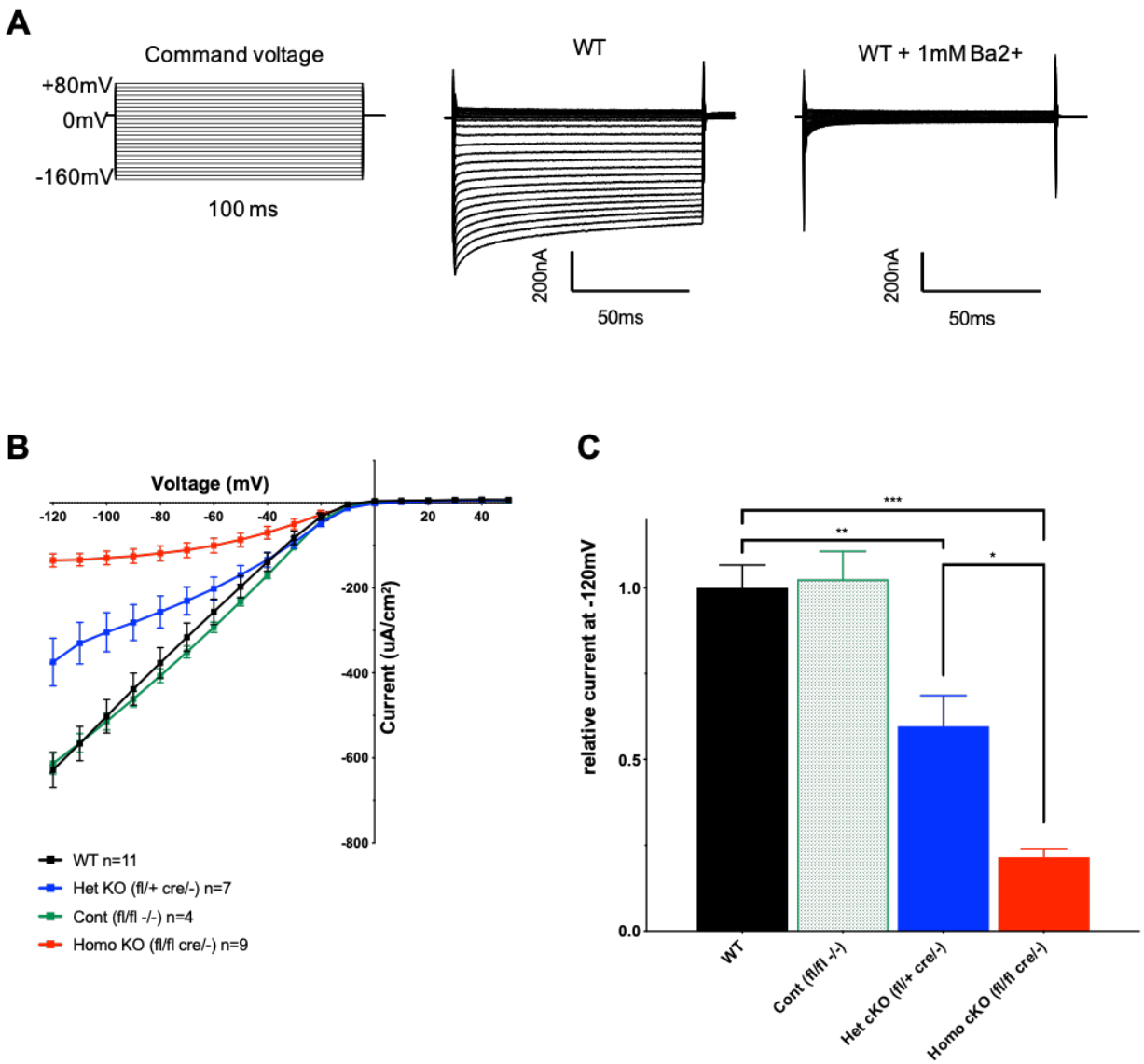

Figure1-2. Kir currents recorded from isolated skeletal muscle fibers from the FDB and IO in symmetrical K^+. (**A**) Raw currents measured in response to 100ms voltage pulses increasing in 10mV steps from -160mV to +80mV using symmetrical (100mM) K^+ external solution. Raw currents show clear inward rectification with complete block in 1mM Ba^{2+}, Subtraction of these two currents removed background leak current generating the barium sensitive Ikir current. (**B**) Current Voltage relationship normalized to cell size between all genetic mouse models. (**C**) IKir current amplitude at -120mV normalized to average current density of WT demonstrate current density is reduced by 70% and 40% in homozygous and heterozygous KCNJ2 cKO mouse models respectively. There is no difference between WT (C57B6 background) and Control. ***P <.0001, **P < .001, *P <.05, one-way ANOVA.

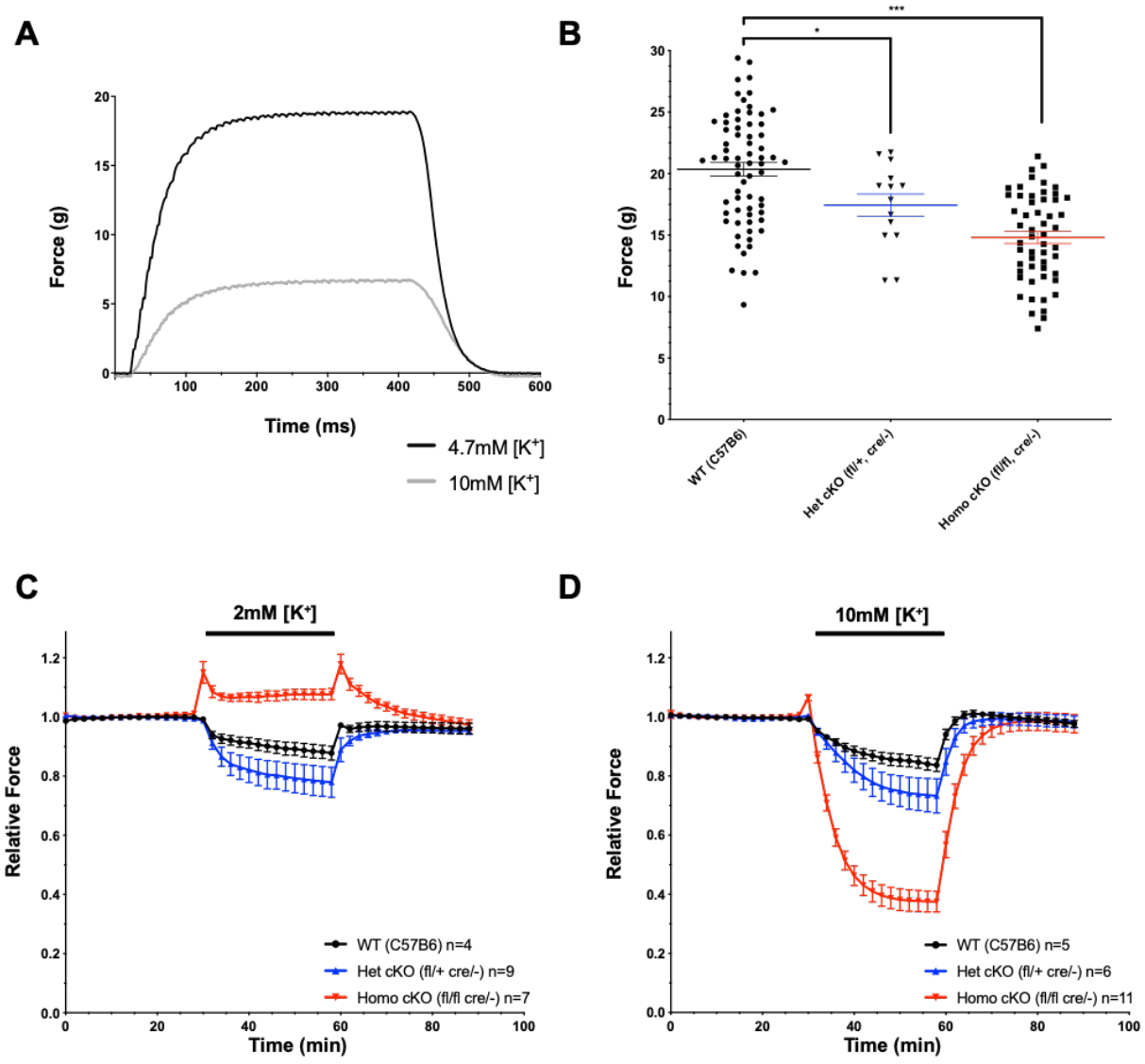

Figure1-3. Ex vivo Isometric force response elicited by current stimulation in variable K conditions. (**A**) Raw force trace generated by 100 Hz stimulation for 400ms on the soleus muscle of KCNJ2 cKO mice suspended in a bath of 4.7 mM K^+ as compared to when provoked with a10mM potassium challenge. Peak force was recorded from intermittent stimulation every two minutes to prevent muscle fatigue. (**B**) Peak force recorded in mice aged three to five months in 4.7 mM external [K+] demonstrate marked reduction of Isometric force for KCNJ2 cKO mice at baseline. (**C**) Average responses generated from a 30 minute exposure to low (2 mM) external K^+. Peak force was normalized to the average force in 4.7mM K^+ solution, before the K challenge. Solution exchange to a the low potassium solution elicited an increase of force of the homo cKO soleus, as shown by the mean and also occurred in every individual

fiber. (red triangles n=7). (**D**) Solution exchange to a 30 minute exposure of high (10 mM) K^+ solution demonstrates a large reduction of force by 63% in homo-KCNJ2 cKO compared to a 16% reduction in C56B7 WT mice.

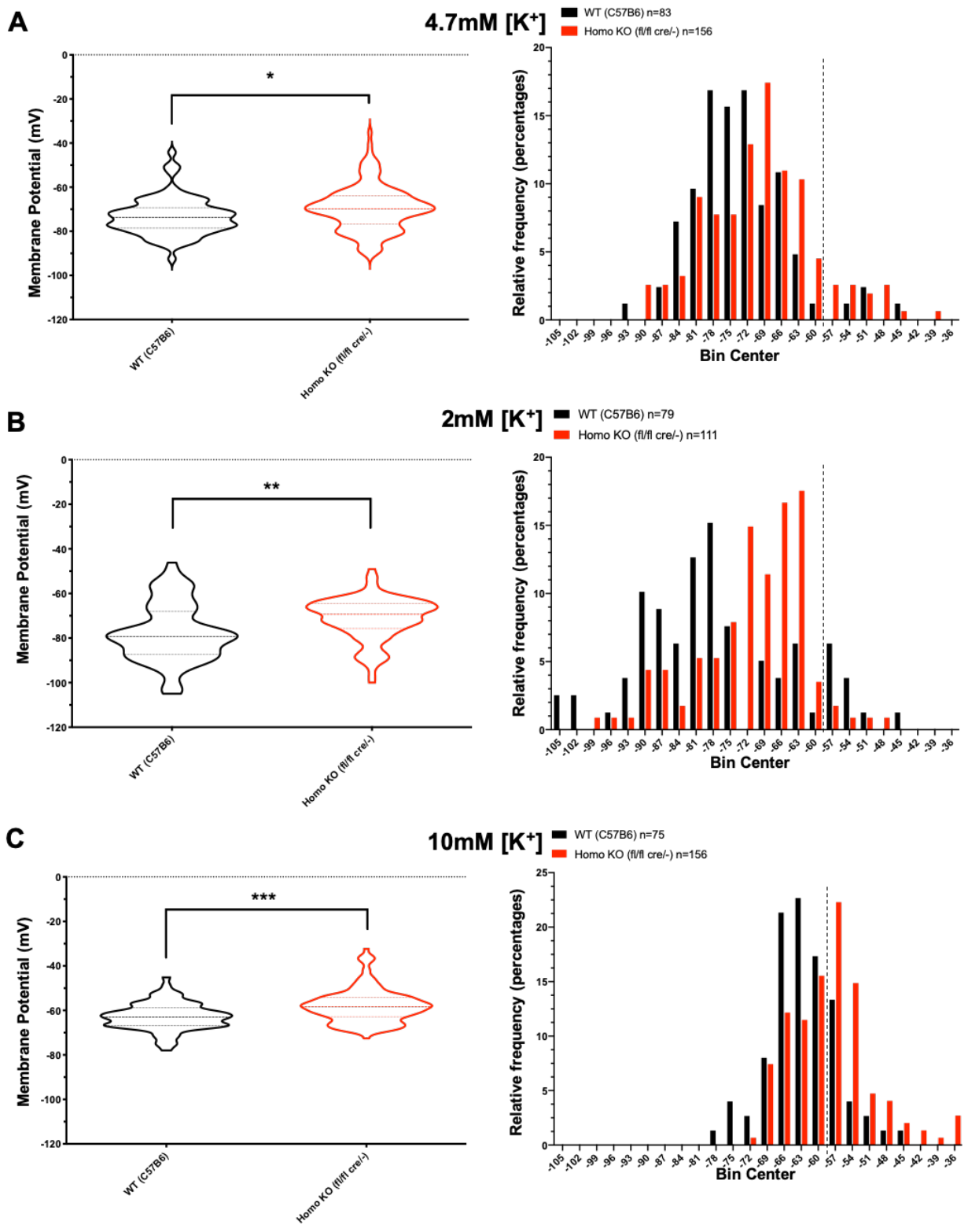

Figure1- 4. Membrane potential recorded from a strip of soleus muscle maintained ex vivo, in varying extracellular potassium.

Median and quartile range recorded from multiple fibers impaled from whole soleus muscle in physiological 4.7mM external K+ (**A**), in low (2mM) external K^+ (**B**), and in high (10mM) external K^+ (**C**). Significance levels were determined by comparing the mean membrane potentials with Welch's T-test , ***P <.0001, **P < .001, *P <.05. Histogram with a bin size of 3 mV demonstrates the variation of resting membrane potential. Dotted line at -60mV represents a hypothetical point of in-excitability as it is roughly the $V_{1/2}$ of sodium channel slow inactivation.

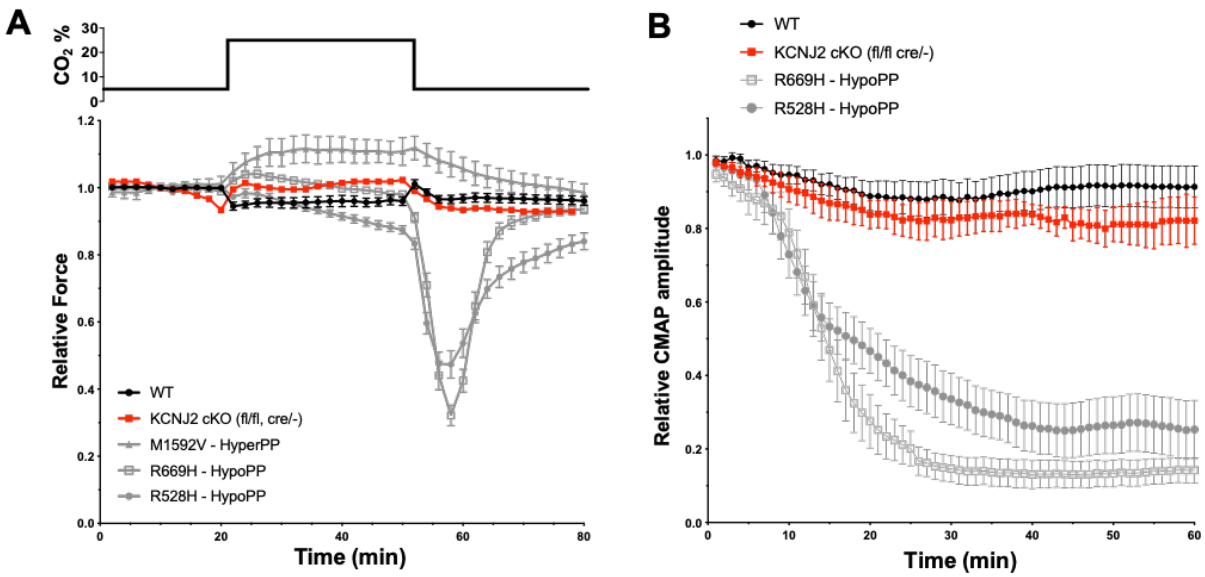

Figure1-5. Comparison of KCNJ2 cKO muscle to historical data of established tests for hypoPP phenotype.

(**A**) Isometric force production is unchanged in response to recovery from acidosis driven by a decrease from 25% to 5% CO_2. Historical data from our lab (Mi et al. JGP 2019) demonstrates a post-acidosis loss of force for HypoPP, but not WT or HyperPP muscle.The KCNJ2 cKO mouse demonstrated no loss of force post acidosis. (**B**) Amplitude of the in vivo compound muscle action potentials elicited from a .1ms shock to the sciatic nerve every minute was stable for KCNJ2 cKO mice during a continuous infusion of insulin and glucose. Historic data from our lab (Wu et al. JCI 2011, Wu et al. JCI 2012) demonstrates a pronounced decrease in CMAP amplitude in established KI mouse models of hypoPP.

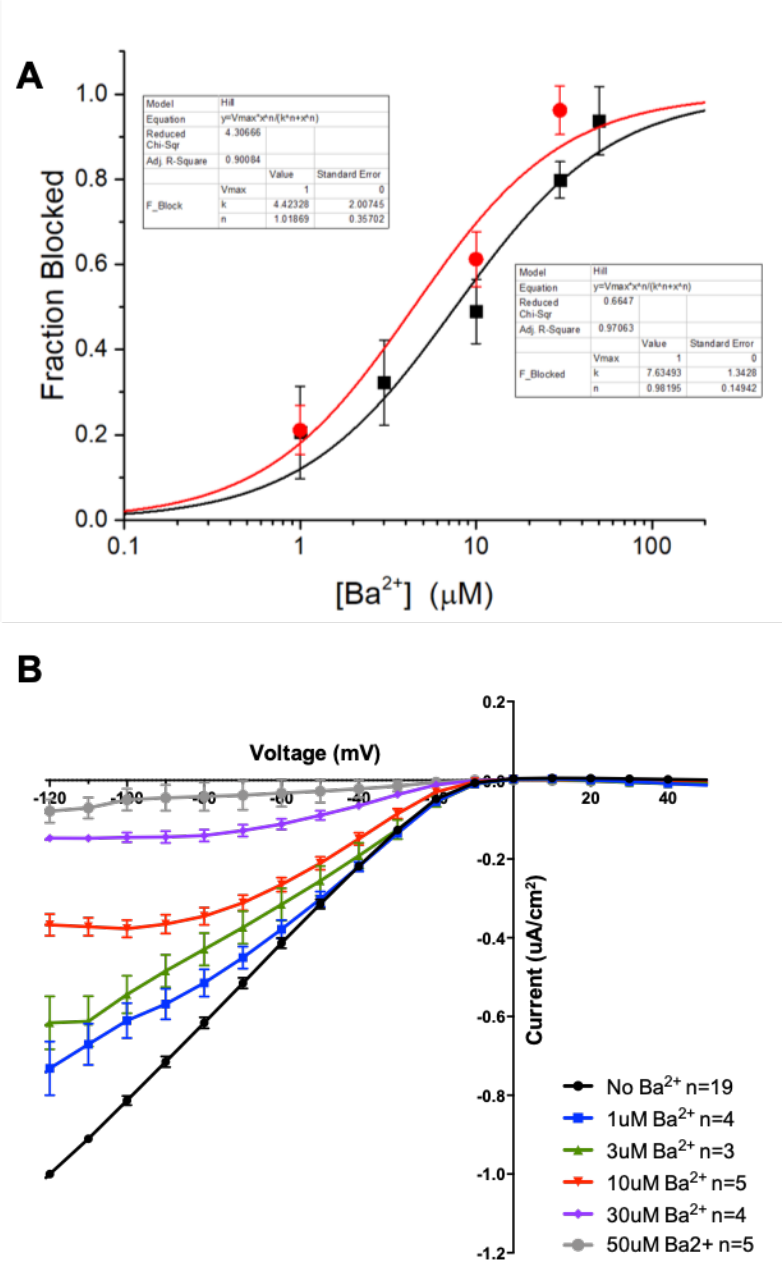

Figure1-6. Barium block of Ikir in dissociated muscle fibers.

(**A**) Fractional current remaining from varying levels of barium block at -80mV in either HEPES or bicaronate buffered solutions, demonstrating the interfering effect of bicarbonate on the available free barium. Hill constant was = 1.01 in HEPES buffered solution and .98 in the bicarbonate buffered solution. 50% of inward rectifying current was blocked with 4.4µM Ba^{2+} in HEPES and with 7.6µM Ba^{2+} in bicarbonate buffered solution. All contraction experiments were performed in a bicarbonate buffered solution. (**B**) Current voltage relationship of barium block in a bicarbonate buffered symmetrical K solution demonstrates increased block at more hyperpolarized potentials.

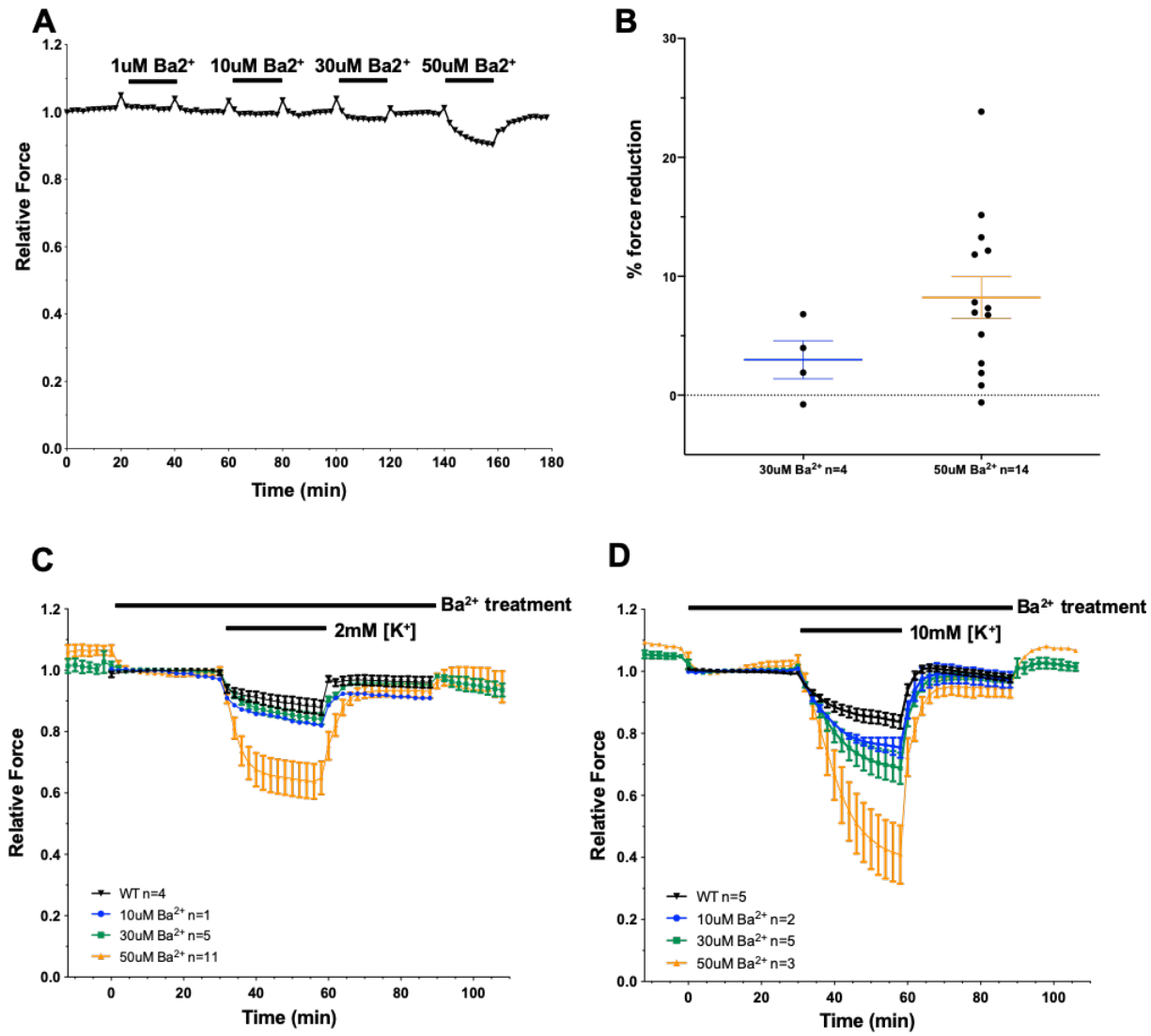

Figure1-7. Isometric force responses in varying levels of barium block.

(**A**) Time course and severity of force reduction upon administration of varying levels of barium in 20 minute intervals. Steady state is reached within 20 minutes, with effective barium washout noted by the complete return to baseline. (**B**) percentage reduction of force generated through administration of barium in normal (4.7 mM) K^+. On average baseline force was reduced in 30 mM barium and a larger reduction occurred in 50 mM Ba^{2+}. Some individual muscles, however, can remain completely unaffected. (**C**) Peak isometric force was measured every two minutes and normalized to the average force generated in 4.7 mM K^+ solution containing barium. Solution exchange to a 2 mM K^+ solution generated no additional loss of force in 10 μM Ba^{2+} and in 30 μM Ba^{2+} when compared to WT control without barium. However,

reduction if Ikir to ~6% of WT using 50 μM Ba^{2+} resulted in a 35% reduction in force when subjected to a 2 mM K^+ challenge. (**C**) Similar force experiments using a high potassium challenge of 10 mM K^+ instead, demonstrate a reduction of force to 75%, 69% and 40% of baseline in 10 μM, 30 μM and 50 μM Ba^{2+} respectively.

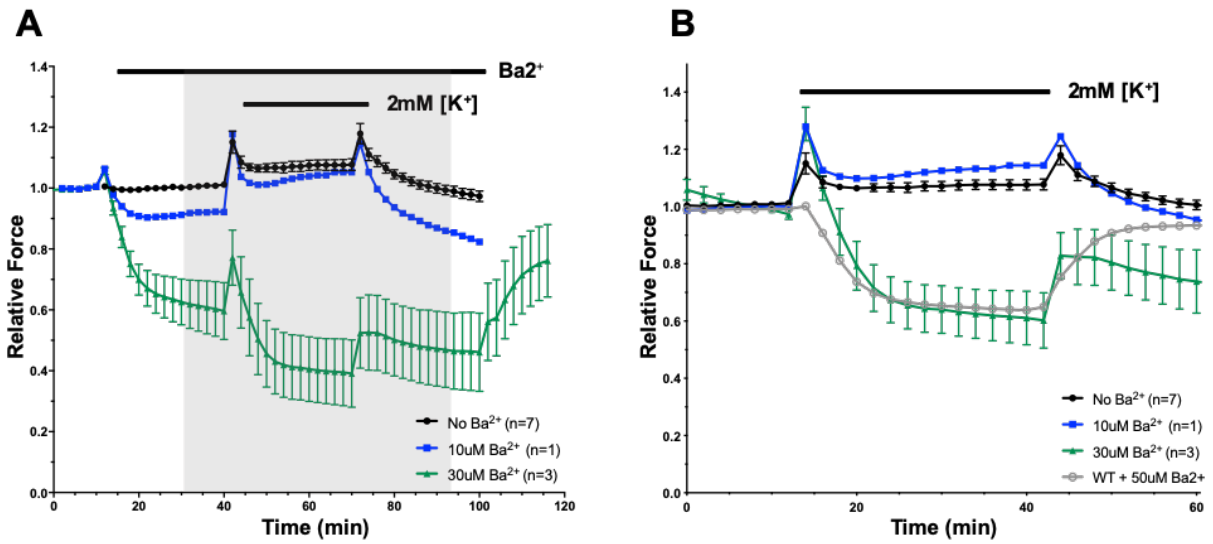

Figure1-8. homo KCNJ2 cKO mouse force response when exposed to a low K challenge in the presence of barium.

(**A**) In vitro contraction test of KCNJ2 cKO mice normalized to average peak force prior to any intervention demonstrate a a force reduction of 8% and 40% when subjected to 10 μM and 30 μM Ba^{2+}, respectively. While exposed to 30mM Ba^{2+}, a 30 minute 2mM K^+ challenge elicited a loss of force for KCNJ2 homo cKO mice, contrary to the increase in force displayed in the absence of Ba^{2+}. (**B**) Normalizing the data in the grey box of figure 8 to the average force generated just prior to the low-K^+ challenge more clearly demonstrates the HypoPP phenotype. Overlaying with averages of WT with 50μM barium, demonstrates remarkable consistency in force amplitude lost.

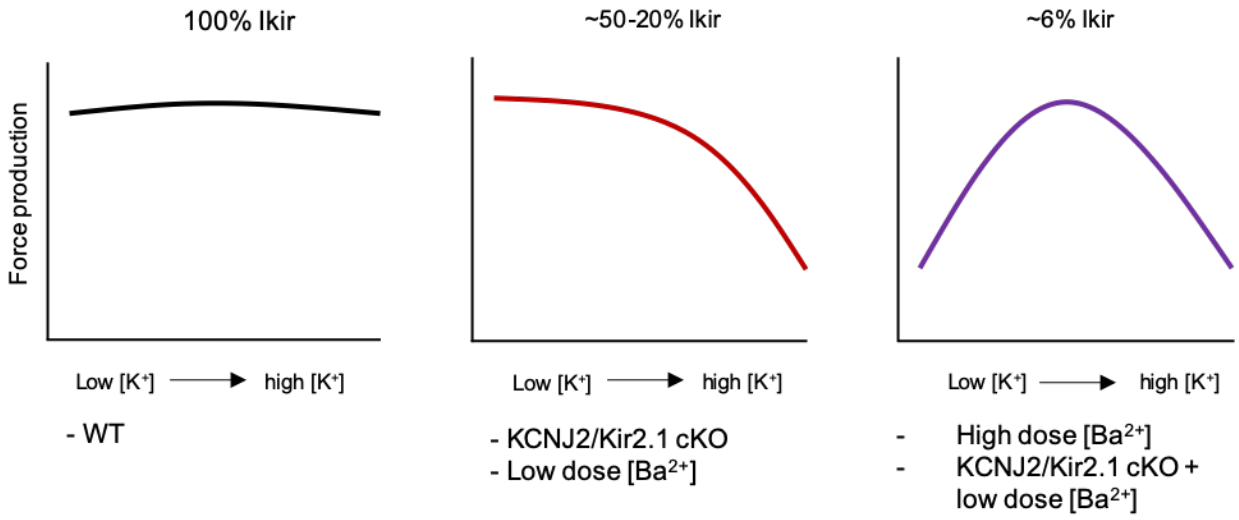

Figure1-9. Summary schematic of in vitro Isometric force reduction based on severity of Ikir deficit. Peak isometric force of for WT soleus muscle in vitro is relatively insensitive the changes of extracellular $[K^+]$ over a range of 2 mM to 10 mM. Upon slight reduction of Ikir through the use of either KCNJ2 knockout or pharmacological block with Ba^{2+}, there is a reduction of force when muscle is subjected to a high external potassium but not when subjected to a low. When Ikir is further reduced through the use of high dose barium block (50 mM) in a WT soleus or a low dose (30 mM) in a KCNJ2 cKO muscle, peak isometric force is substantially diminished in both high and low external potassium.

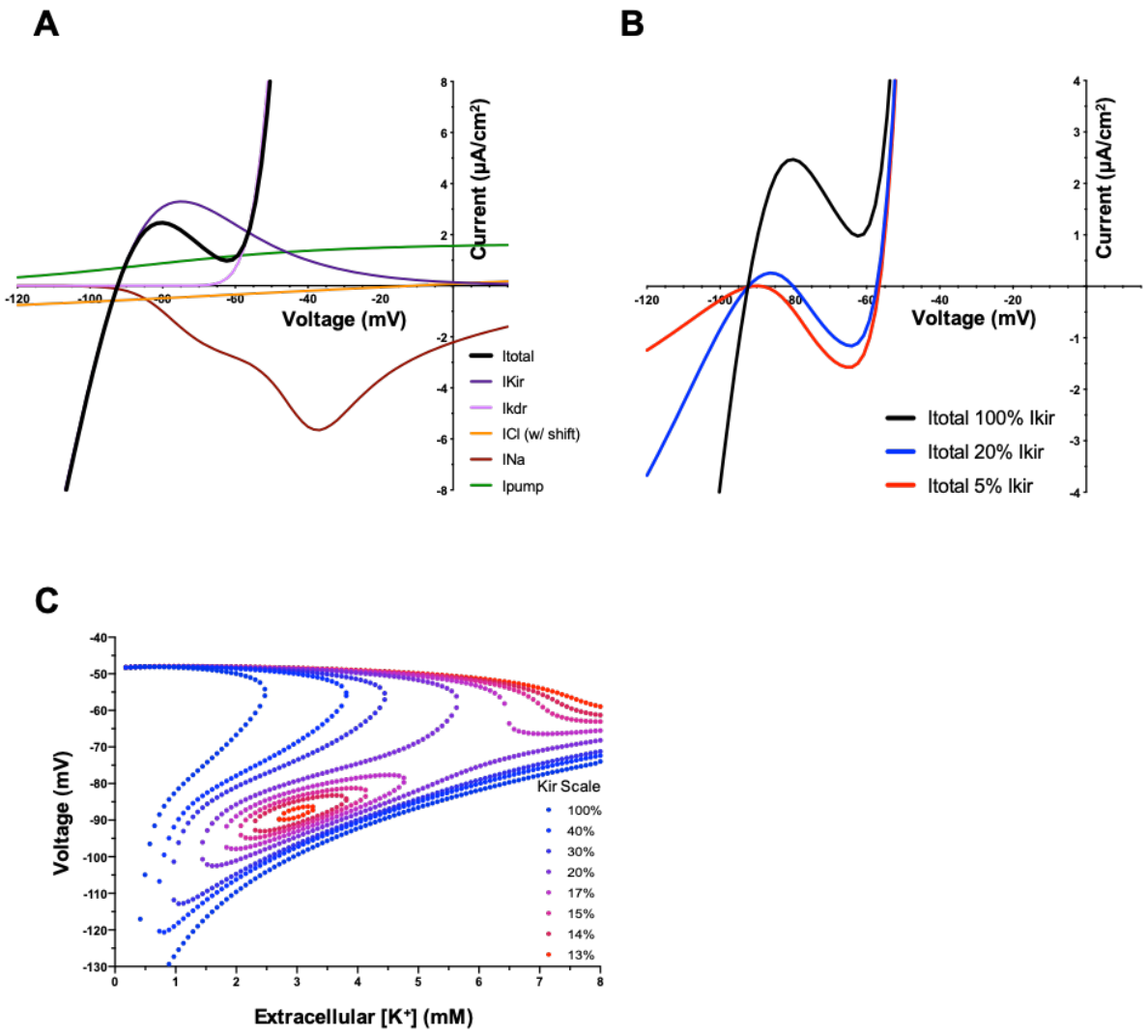

Figure1-10. Computational modeling of the effect of reduced I_{kir} on membrane potential.

(**A**) Steady state current-voltage relation for the individual ionic currents in the simulated muscle fiber. The intracellular [C^-] is variable, in response to the net Cl^- current and influx via the NKCC cotransporter. I_{total} is calculated as the sum of all individual inward and outward currents at any given voltage. The resting potential, Vrest, is determined by the membrane voltage at which I_{total} = 0. (**B**) Reduction of Ikir decreases the outward current at membrane potentials > E_K , thereby causing the I_{total} curve to shift downward and intersect the I = 0 axis at multiple values of V These multiple points where Itotal = 0 cause a bistable Vrest, with one being severely depolarized. Further reduction of I_{kir} to 5% of WT further shifts I_{total} to where a stable resting membrane potential is only established at depolarized voltages. (**C**) Effect of altering

extracellular potassium on Vrest with varying reduction of I_{kir}. As the reduction of IKir becomes more severe, first there is a loss of the normally polarized Vrest in high K and then with further reduction of Ikir Vrest becomes depolarized in low K as well.

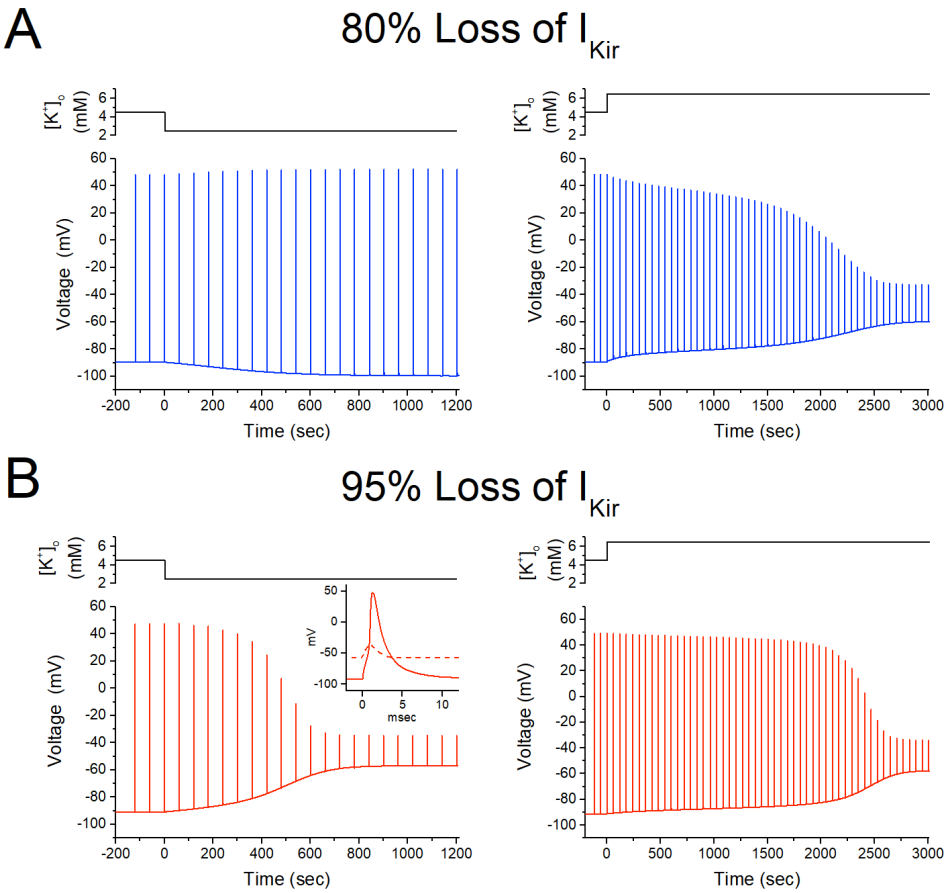

Figure1-11. Model simulations of excitability demonstrate the K sensitivity of periodic paralysis phenotype is dependent upon the magnitude of I_{kir} reduction.

Action potentials, seen as vertical lines on this time scale, are elicited through modeling of 1 msec nAChR activation every 60s. (A) High K^+ (6.7 mM), but not low K^+ (2.7 mM), triggers depolarization and refractory block of action potentials when Ikir is reduced by 80% (B) With 95% reduction of Ikir either high K or low K triggers depolarization and reduced excitability.

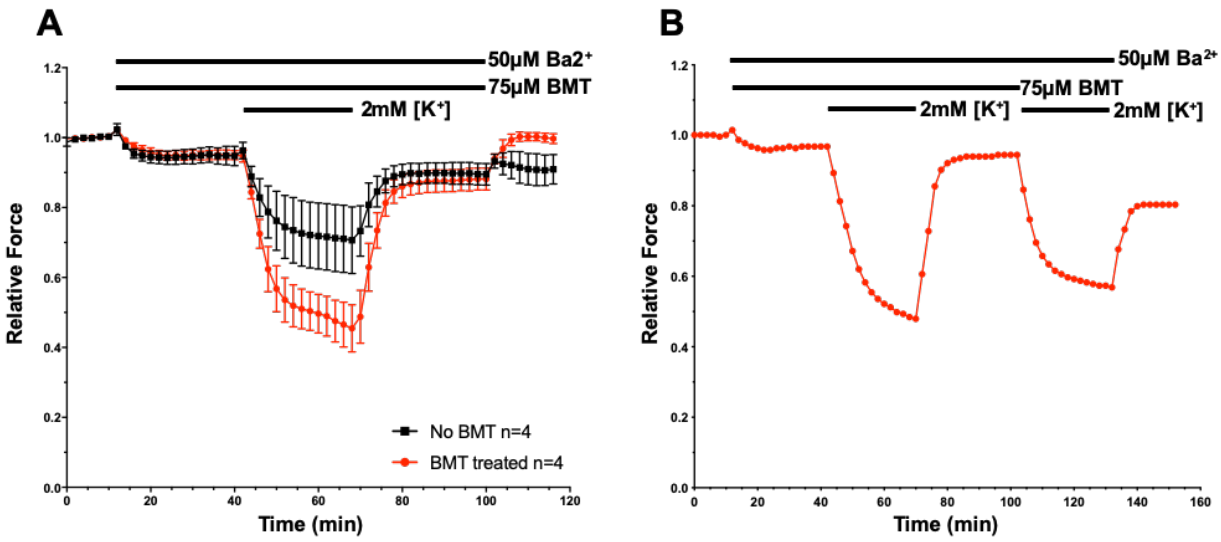

Figure1-12. In vitro force assay demonstrates lack of effect from bumetanide (BMT) to provide protective intervention for low K induced weakness in Ba^{2+} block model of ATS.

(**A**) Isometric force of WT soleus muscle pairs measured in parallel every two minutes in drug (75μM BMT) and drug free conditions. Peak isometric force is normalized to the average of the first five contractions in 4.7 K, prior to the addition of either 50 μM Ba^{2+} only (black trace), or of 50 μM Ba^{2+} and 75 μM BMT (red trace). Average loss of force across four muscles was 55% in the presence of BMT compared to 30% loss of force with no treatment. (**B**) In vitro force assay demonstrating the exacerbation in the loss of force by BMT using a repeated low K^+ challenge in the same muscle. Typically, larger force reductions occur with subsequent K^+ challenges.

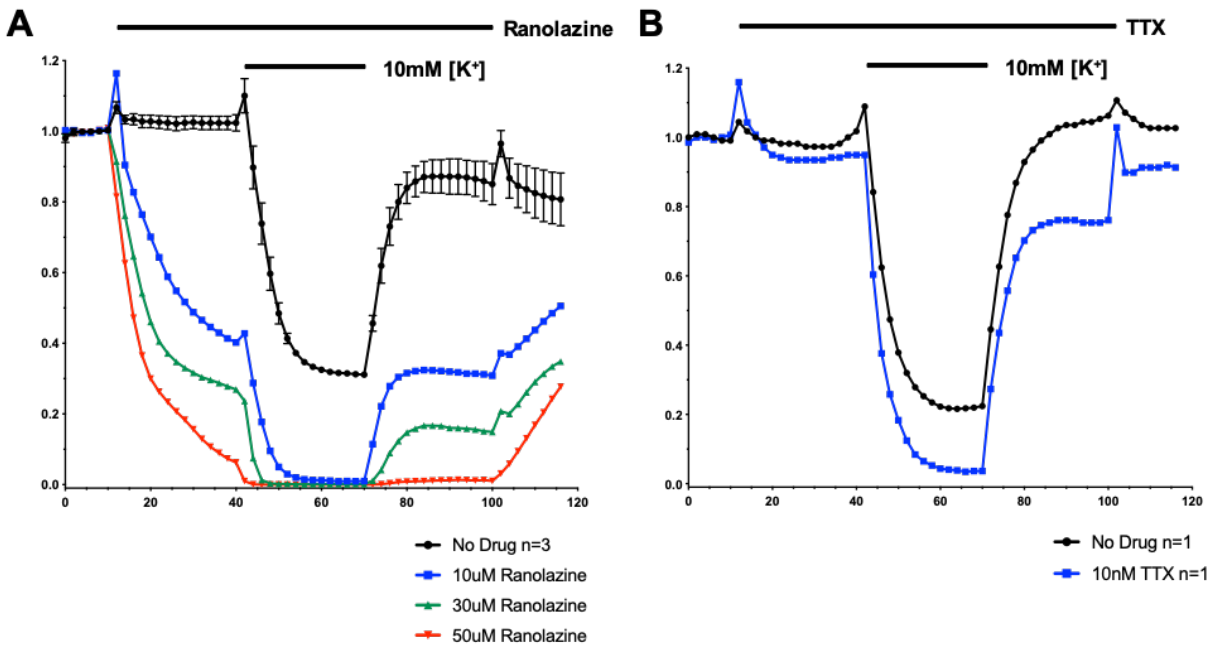

Figure1-13. In vitro force assay demonstrates lack of protection by sodium channel blockers, ranolazine or TTX, to attenuate the loss of force in response to a high K challenge in the KCNJ2 cKO mouse model of ATS.

(**A**) Relative peak isometric force measured in soleus muscle as in figure 10. Addition of 10μM to 50μM ranolazine to while in a 4.7 mM [K^+] bath caused a marked loss of force prior to any potassium challenge. Contraction was not detectable upon the addition of a 10 mM [K^+], although some recovery occurred upon returning to physiological K and wash out of the drug (**B**) Partial block of $Na_V1.4$ by addition of 10 nM TTX produced only a minor loss of force prior to potassium challenge. However, a 10 mM [K^+] challenge induced a loss of force greater than in the absence of the drug.

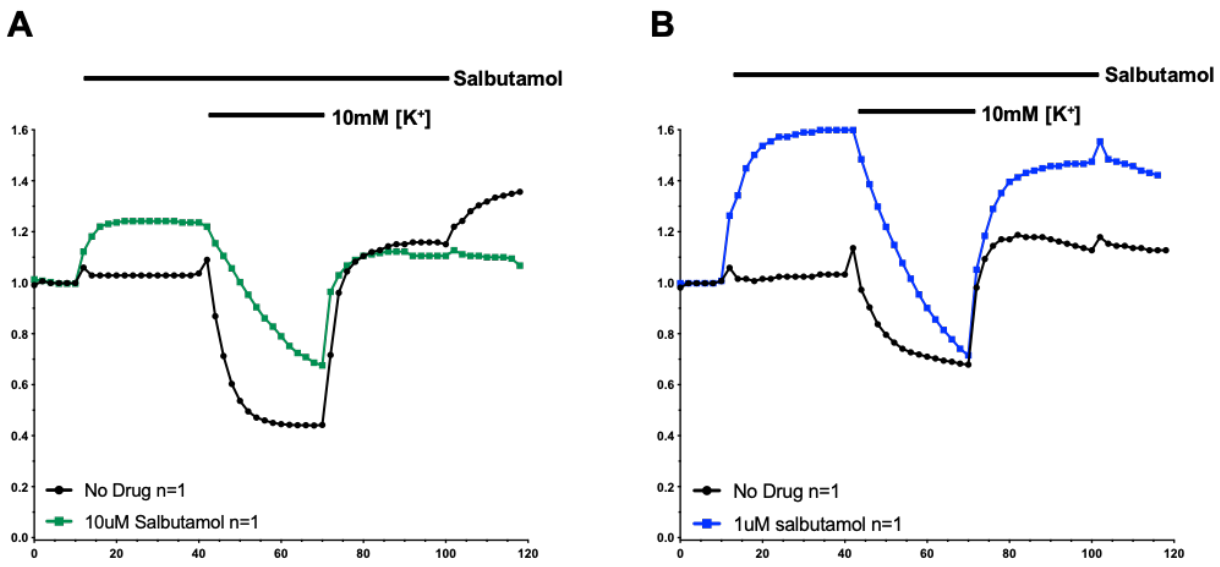

wFigure1-14. In vitro force assay demonstrates minimal benefit if any from salbutamol, a sodium potassium ATPase activator, to provide protective intervention for high K induced weakness in KCNJ2 cKO mouse model of ATS.

Relative peak isometric force increased at baseline for homo cKO soleus by the addition of salbutamol (1mM or 10mM). (A) Pretreatment with 10mM salbutamol provided modest protection against high K induced loss of force (33% loss vs 45% in the absence of drug). (**B**) The addition of 1μM salbutamol did not substantially reduce the severity of the loss of force when given a 10mM K^+ challenge.

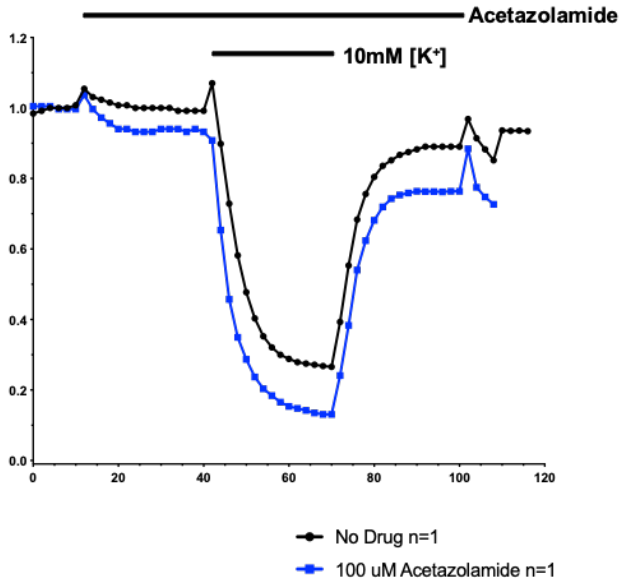

Figure1-15. In vitro force assay demonstrates no benefit from Acetazolamide, a carbonic anhydrase inhibitor, to provide protective intervention for high K induced weakness in KCNJ2 cKO mouse model of ATS.

Soleus muscle pairs were assayed and normalized as mentioned in figure 10. Addition of 100μM acetazolamide generated a slight decrease in force that was exacerbated by high-K^+ challenge.

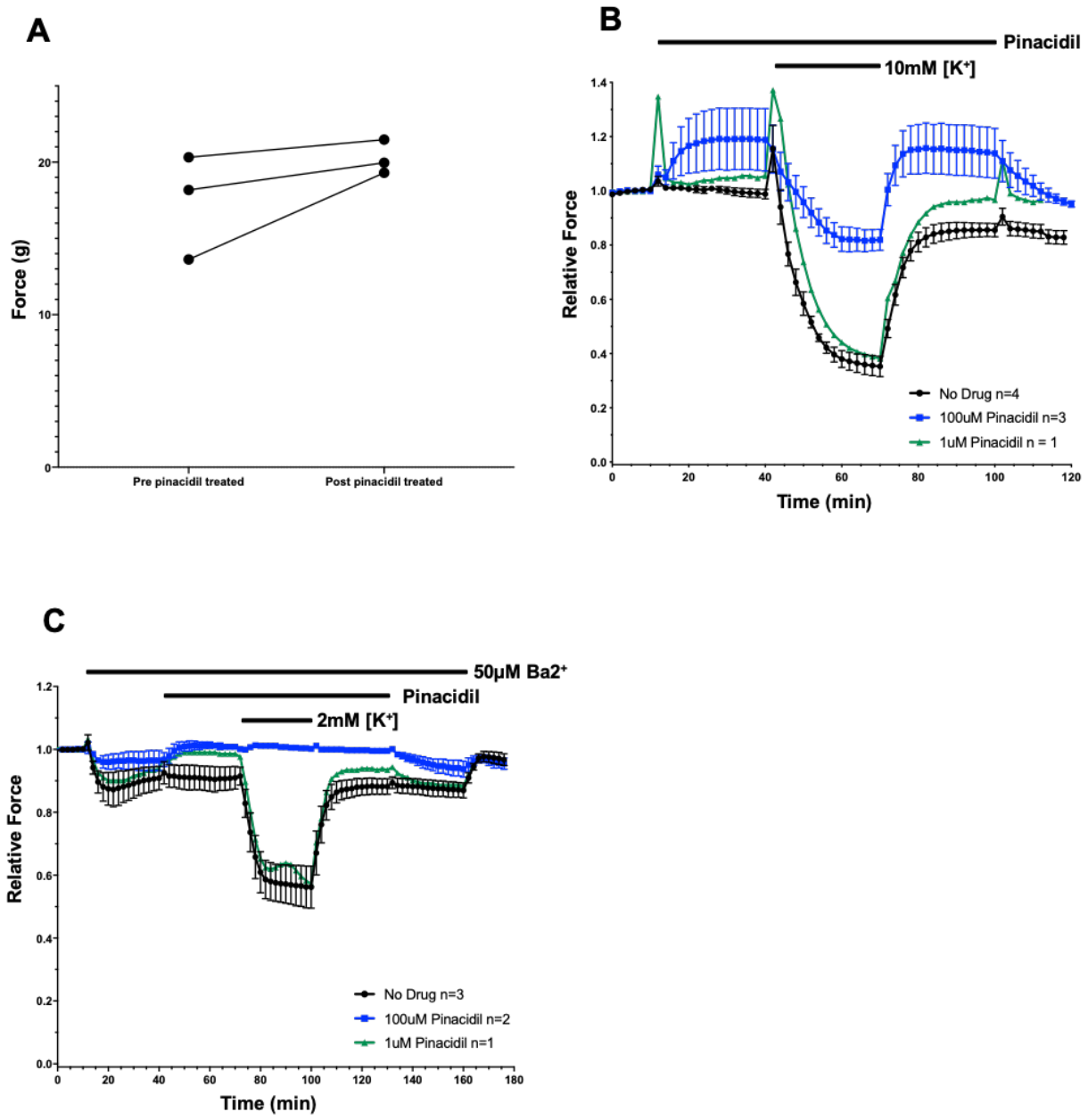

Figure1-16. In vitro isometric force assay demonstrates a beneficial effect of pinacidil, a K_{ATP} channel opener, to protect against both high-K and low-K induced loss of force in mouse models of ATS. Relative force was measured in paired soleus muscles, from the same mouse. (**A**) In the KCNJ2 homo cKO model,100 μM pinacidil elicited a substantial increase in baseline force. The change was greater for muscles that started with lower peak force at baseline and the post-pinacidil amplitude of peak force was comparable to that of WT. (**B**) In the KCNJ2 homo cKO soleus,100 mM pinacidil attenuated the loss of

force elicited by a high K challenge (10 mM). Low-dose pinacidil (1 mM), however, did not provide protection. (**C**) In the 50 mM Ba^{2+} model of ATS, which does not have a substantial loss of baseline force (Fig. 7), addition of 100μM pinacidil did not increase in force. However, this dose of pinacidil completely prevents any loss of force upon challenge with 2mM K^{+}. No protection was observed for pretreatment with1μM pinacidil.

2.6 REFRENCES

1. Rabi T, J. PL, G. PS, et al. Andersen's syndrome: Potassium-sensitive periodic paralysis, ventricular ectopy, and dysmorphic features. *Ann Neurol*. 1994;35(3):326-330. doi:10.1002/ana.410350313

2. Sansone V, Griggs RC, Meola G, Z LJP, Barohn R. Andersen's Svndrome : A Distinct Periodic Paralysis. *Ann Neurol*. 1997:305-312.

3. Nguyen H-L, Pieper GH, Wilders R. Andersen–Tawil syndrome: Clinical and molecular aspects. *Int J Cardiol*. 2013;170(1):1-16. doi:10.1016/J.IJCARD.2013.10.010

4. Horga A, Rayan DLR, Matthews E, et al. Prevalence study of genetically defined skeletal muscle channelopathies in England. *Neurology*. 2013. doi:10.1212/WNL.0b013e31828cf8d0

5. Kubo Y, Baldwin TJ, Nung Jan Y, Jan LY. Primary structure and functional expression of a mouse inward rectifier potassium channel. *Nature*. 1993. doi:10.1038/362127a0

6. Sacco S, Giuliano S, Sacconi S, et al. The inward rectifier potassium channel Kir2.1 is required for osteoblastogenesis. *Hum Mol Genet*. 2015. doi:10.1093/hmg/ddu462

7. Donaldson MR, Yoon G, Fu YH, Ptacek LJ. Andersen-Tawil syndrome: A model of clinical variability, pleiotropy, and genetic heterogeneity. In: *Annals of Medicine*. ; 2004. doi:10.1080/17431380410032490

8. Stanfield PR, Nakajima S, Nakajima Y. Constitutively active and G-protein coupled inward rectifier K+ channels: Kir2.0 and Kir3.0. *Rev Physiol Biochem Pharmacol*. 2002. doi:10.1007/bfb0116431

9. Plaster NM, Tawil R, Tristani-Firouzi M, et al. Mutations in Kir2.1 cause the developmental and episodic electrical phenotypes of Andersen's syndrome. *Cell*. 2001;105(4):511-519. doi:10.1016/S0092-8674(01)00342-7

10. Tristani-Firouzi M, Etheridge SP. Kir 2.1 channelopathies: The Andersen-Tawil syndrome. *Pflugers Arch Eur J Physiol*. 2010;460(2):289-294. doi:10.1007/s00424-010-0820-6

11. Donaldson MR, Jensen JL, Firouzi MT, et al. PIP 2 binding residues of Kir2 . 1 are common targets of mutations causing Andersen syndrome. *Neurology*. 2003;60:1811-1816. doi:10.1212/01.WNL.0000072261.14060.47

12. Tristani-Firouzi M, Jensen JL, Donaldson MR, et al. Functional and clinical characterization of KCNJ2 mutations associated with LQT7 (Andersen syndrome). *J Clin Invest*. 2002;110(3):381-388. doi:10.1172/JCI200215183

13. Sacconi S, Simkin D, Arrighi N, et al. Mechanisms underlying Andersen's syndrome pathology in skeletal muscle are revealed in human myotubes. *Am J Physiol Physiol*. 2009;297(4):C876-C885. doi:10.1152/ajpcell.00519.2008

14. Andersen ED, Krasilnikoff PA OH. Intermittent muscular weakness, extrasystoles, and multiple developmental anomalies. A new syndrome? *Acta Pædiatrica*. 1971;60(5):559-564. doi:10.1111/j.1651-2227.1971.tb06990.x

15. Davies NP, Imbrici P, Fialho D, et al. Andersen-Tawil syndrome: New potassium channel mutations and possible phenotypic variation. *Neurology*. 2005. doi:10.1212/01.wnl.0000178888.03767.74

16. Cannon SC, Brown RH, Corey DP. Theoretical reconstruction of myotonia and paralysis caused by incomplete inactivation of sodium channels. *Biophys J*. 1993. doi:10.1016/S0006-3495(93)81045-2

17. Hayward LJ, Brown RH, Cannon SC. Slow inactivation differs among mutant Na channels associated with myotonia and periodic paralysis. *Biophys J*. 1997. doi:10.1016/S0006-3495(97)78768-X

18. Mi W, Wu F, Quinonez M, DiFranco M, Cannon SC. Recovery from acidosis is a robust trigger for loss of force in murine hypokalemic periodic paralysis. *J Gen Physiol*. 2019. doi:10.1085/jgp.201812231

19. Schott GD, McArdle B. Barium-induced skeletal muscle paralysis in the rat, and its relationship to human familial periodic paralysis. *J Neurol Neurosurg Psychiatry*. 1974;37(1):32-39. http://www.ncbi.nlm.nih.gov/pubmed/4813426. Accessed October 22, 2018.

20. Gallant EM. Barium-treated mammalian skeletal muscle: similarities to hypokalaemic periodic paralysis. *J Physiol*. 1983. doi:10.1113/jphysiol.1983.sp014552

21. Schram G, Pourrier M, Wang Z, White M, Nattel S. Barium block of Kir2 and human cardiac inward rectifier currents: evidence for subunit-heteromeric contribution to native currents. *Cardiovasc Res*. 2003;59:328-338. doi:10.1016/S0008-6363(03)00366-3

22. Mølgaard H, Stürup-Johansen M, Flatman JA. A dichtomy of the membrane potential response of rat soleus muscle fibres to low extracellular potassium concentrations. *Pflügers Arch Eur J Physiol*. 1980. doi:10.1007/BF00581880

23. Wu F, Mi W, Cannon SC. Beneficial effects of bumetanide in a CaV1.1-R528H mouse model of hypokalaemic periodic paralysis. *Brain*. 2013. doi:10.1093/brain/awt280

24. Wu F, Mi W, Cannon SC. Bumetanide prevents transient decreases in muscle force in murine hypokalemic periodic paralysis. *Neurology*. 2013. doi:10.1212/WNL.0b013e3182886a0e

25. Horvath B, Bers DM. The late sodium current in heart failure: pathophysiology and clinical relevance. *ESC Hear Fail*. 2014. doi:10.1002/ehf2.12003

26. Hawash AA, Voss AA, Rich MM. Inhibiting persistent inward sodium currents prevents myotonia. *Ann Neurol*. 2017. doi:10.1002/ana.25017

27. Griggs RC, Engel WK, Resnick JS. Acetazolamide treatment of hypokalemic periodic paralysis. Prevention of attacks and improvement of persistent weakness. *Ann Intern Med*. 1970. doi:10.7326/0003-4819-73-1-39

28. Tawil R, McDermott MP, Brown R, et al. Randomized trials of dichlorphenamide in the periodic paralyses. *Ann Neurol*. 2000. doi:10.1002/1531-8249(200001)47:1<46::AID-ANA9>3.0.CO;2-H

29. Matthews E, Portaro S, Ke Q, et al. Acetazolamide efficacy in hypokalemic periodic paralysis and the predictive role of genotype. *Neurology*. 2011. doi:10.1212/WNL.0b013e31823a0cb6

30. Sansone V, Tawil R. Management and Treatment of Andersen-Tawil Syndrome (ATS). *Neurotherapeutics*. 2007. doi:10.1016/j.nurt.2007.01.005

31. Wu F, Mi W, Burns DK, et al. A sodium channel knockin mutant (NaV1.4-R669H) mouse model of hypokalemic periodic paralysis. *J Clin Invest*. 2011. doi:10.1172/JCI57398

32. Bhoelan BS, Stevering CH, van der Boog ATJ, van der Heyden MAG. Barium toxicity and the role of the potassium inward rectifier current. *Clin Toxicol*. 2014;52(6):584-593. doi:10.3109/15563650.2014.923903

33. Cannon SC. Channelopathies of skeletal muscle excitability. *Compr Physiol*. 2015;5(2):761-790. doi:10.1002/cphy.c140062

34. Nagamine S, Sakoda S, Koide R, et al. A case of Andersen-Tawil syndrome presenting periodic paralysis exacerbated by acetazolamide. *J Neurol Sci*. 2014. doi:10.1016/j.jns.2014.09.040

35. Ligtenberg JJM, Van Haeften TW, Van Der Kolk LE, et al. Normal insulin release during sustained hyperglycaemia in hypokalaemic periodic paralysis: Role of the potassium channel opener pinacidil in impaired muscle strength. *Clin Sci*. 1996. doi:10.1042/cs0910583

36. Iaizzo PA, Quasthoff S, Lehmann-Horn F. Differential diagnosis of periodic paralysis aided by in vitro myography. *Neuromuscul Disord*. 1995. doi:10.1016/0960-8966(94)00036-9

37. Quasthoff S, Spuler A, Spittelmeister W, Lehmann-Horn F, Grafe P. K+ channel openers

suppress myotonic activity of human in vitro. *Eur J Pharmacol*. 1990. doi:10.1016/0014-2999(90)94068-9

38. Goldberg MR, Rockhold FW, Thompson WL, DeSante KA. Clinical pharmacokinetics of pinacidil, a potassium channel opener, in hypertension. *J Clin Pharmacol*. 1989. doi:10.1002/j.1552-4604.1989.tb03234.x

CHAPTER 2

2.1 INTRODUCTION

Several allelic disorders of skeletal muscle are caused by mutations of *SCN4A* that encodes the pore-forming subunit of the voltage-gated sodium channel ($Na_V1.4$)[1]. Missense mutations with gain-of-function changes (GOF; too much inward Na^+ current) are found in hyperkalemic periodic paralysis, paramyotonia congenita, and several variants of sodium channel myotonia[2]. Leaky channels resulting from mutations of arginine residues in the voltage sensor domain cause hypokalemic periodic paralysis type 2[3, 4]. These traits are all dominantly inherited.

Loss-of-function (LOF) mutations of *SCN4A* are encountered far less frequently and are associated with recessively inherited phenotypes. A congenital myasthenic syndrome with ptosis, bulbar weakness, respiratory difficulties and prolonged episodes of weakness more typical for periodic paralysis has been associated with missense mutations of *SCN4A* that cause a LOF by markedly enhancing channel inactivation[5-7]. More recently, congenital myopathy with neonatal hypotonia has been reported in patients with null mutations in SCN4A[8]. A homozygous null is embryonic lethal, while compound heterozygous mutations (null allele plus an LOF allele) result in congenital myopathy with survival to adulthood. Remarkably, family members with a single *SCN4A* null allele are healthy.

In this report, we describe the molecular and clinical consequences of two additional LOF mutations, both of which are at residue p.1460. The index cases presented with congenital myopathy plus fluctuating weakness and were found to have biallelic mutations of SCN4A as either p.R1460Q plus p.R1059X or homozygous p.R1460W. Expression studies of the p.R1460 mutant channels also revealed GOF changes that account for the myotonia in some carriers of p.R1460Q. Moreover, the phenotype for some carriers of the p.R1460Q mutation in the primary

Finnish family was complexed by the independent co-segregation of a known *CLCN1* mutation p.R894X associated with recessive myotonia congenita.

2.2 MATERIALS AND METHODS

Clinical examination

The proband (III:3) and six of her relatives were examined in a Finnish family (F1, Figure 1A). In addition, one of her aunts (II:6) and her maternal grandfather (I:1) had similar symptoms (larynx spasms) but were not available for further studies. The patients underwent neurological examination, electromyogram (EMG) and DNA extraction. Further, a single unrelated Finnish patient (P2) with myotonia was similarly examined. Muscle histology was available for two patients and muscle MRI for one patient. The proband from family 2 and her parents were examined neurologically, and whole blood was collected for DNA analysis.

Clinical electrophysiology

Standard neurography and EMG investigation was performed in nine patients with p.R1460Q mutation. Compound muscle action potentials (CMAP) exercise test was carried out in three patients. A Fournier protocol was used with short (10-12 s) and long (5 min) exercise test[9, 10]. CMAPs were evoked by supramaximal nerve stimulation. The proband of Family 1 also underwent repetitive nerve stimulation at 30 Hz and single-fiber jitter examinations. The proband of Family 2 was studied by needle EMG and repetitive nerve stimulation at 3 Hz and 50Hz. Because cooperation was limited in a 6 year-old, she did not complete a CMAP exercise test.

Molecular genetics

For the members of Family 1 the sequencing of relevant exons of *SCN4A* and *CLCN1* genes was performed using traditional Sanger sequencing. For some of the patients the *CLCN1* gene was studied by targeted mutation detection using TaqMan Sequence Detection System (ABI). DNA sample of the proband was also studied by whole exome sequencing. DNA of the patient P2 was sequenced using MYOcap targeted gene panel[11].

Functional assessment of mutant sodium channels

Sodium channels were transiently expressed in fibroblasts (HEK cells) as previously described[12], except transfection was performed with lipofectamine. Cells expressed the human wild type $Na_V1.4$ pore-forming α subunit (WT), or mutant constructs encoding R1460Q or R1460W, plus the β_1 accessory subunit. Sodium currents were recorded using the whole cell voltage-clamp configuration. The electrode contained in mM: 100 CsF, 35 NaCl, 5 EGTA, 10 HEPES, pH to 7.3 with CsOH while the bath solution contained in mM: 140 NaCl, 4 KCl, 2 $CaCl_2$, 1 $MgCl_2$, 2.5 glucose, 10 HEPES, pH to 7.3 with NaOH. After whole-cell access was achieved, cells were allowed to equilibrate for five to ten minutes before recording. For the data set to determine the voltage-dependence of gating, cells with maximal peak Na^+ currents < 1 nA were excluded to minimize the contribution from endogenous Na^+ currents (typically < 0.1 nA), and those with peak current > 5 nA were excluded to minimize series resistance errors. To reduce the selection bias for the current density measurements (Figure 2), cells with peak Na^+ currents from 0.5 nA to 10 nA were included. For the experiments to test for gating pore currents (Figure 6), channels were expressed in toad oocytes, and currents were recorded using two-electrode voltage-clamp as previously described[8]. Oocytes were harvested from adult female *X. laevis* in accordance

with the UK Animal (Scientific Procedures) Act 1986. The bath solution contained in mM: 60 Na^+-methansulfonate, 60 guanidine sulfate, 1.8 $CaSO_4$, 10 HEPES plus 1 μm tetrodotoxin to block sodium currents conducted by the central core.

The functional properties of WT and mutant sodium channels were compared quantitatively by obtaining parameter estimates to functions describing the voltage-dependent changes of the ionic currents. Channel activation of was quantified by fitting the peak amplitude (I_{peak}) to a linear conductance (G_{max}) with a reversal potential (E_{rev}) that was scaled with a Boltzmann function: $I_{peak} = G_{max}(V - E_{rev})/(1 + e^{-(V - V_{1/2})/K})$. The voltage-dependence for activation of the channel is characterized by $V_{1/2}$, the voltage at which half the channels are activated, and K a steepness factor. The relative conductance (see Figure 2C) was calculated as I_{peak} divided by $G_{max}(V - E_{rev})$. The time constant for entry to inactivation was estimated from a single exponential fit of the current decay (fast inactivation) or of the change in peak current after progressively longer conditioning pulses (closed-state inactivation). Steady-state fast inactivation was quantified by fitting the relative peak current at -10 mV after a 300 msec conditioning pulse (V_{cond}) to a Boltzmann function $I_{peak}(V_{cond})/I_{peak\_max} = 1/(1 + e^{(V_{cond} - V_{1/2})/K})$. For slow inactivation, a conditioning depolarization was used to induce inactivation, then a recovery pulse at -120 mV for 20 msec was applied to remove fast inactivation, and finally the available current (i.e. not slow-inactivated) was measured for a test pulse to -10 mV. For the steady-state voltage dependence, a plateau term (S_0) was included because slow inactivation does not reduce channel availability to 0 at strongly depolarized potentials (Fig. 5C). Estimated values for parameters are presented as mean ± SEM. Error bars in all graphs show ± SEM.

2.3 RESULTS

Clinical Presentation and Assessment

Family 1

The proband (III-3), a 30-year-old female, had congenital hypotonia that was severe at birth but resolved to milder non-progressive muscle weakness and fatigue during the first years of life. She had severe weakness in the facial muscles, mild dysphonia, and fixed ptosis bilaterally. Otherwise, muscle strength was 4/5 MRC (the Medical Research Council Scale) in all limbs. She had marked fatigability especially when climbing stairs, otherwise there was no large variability in her muscle strength. Clinical myotonia was not detected.

Muscle biopsy showed myopathic changes with fiber size variation, increased internal nuclei, structural abnormalities and neckless fibers. Some non-rimmed vacuolated fibers were seen. Several EMG studies were performed and one showed definite myotonic discharges. Single fiber test was myasthenic jitter and exercise test showed 40% decrease of CMAP amplitude after long exercise. The proband had two mutations in *SCN4A* gene: one missense p.R1460Q inherited from the mother and a nonsense p.R1059X inherited from the father. In addition, she had inherited a heterozygous *CLCN1* mutation p.R894X from her mother (Figure 1).

The proband's mother, three siblings of the mother and two cousins were identified with the p.R1460Q mutation. In addition, one unrelated patient (P2) carried the same mutation. They all had myotonic muscle symptoms and signs starting during young adulthood that either showed myotonic discharges or increased insertional activity on EMG and clinical myotonia, or related to muscle stiffness, exercise induced myalgia and cramps (Table 1). Most of the p.R1460Q carrying patients in Family 1 had larynx spasms that were evident in cold weather or at night. The *CLCN1* p.R894X mutation was also identified in the mother and one of her siblings. They had myotonic

discharges on EMG but that was also seen in other siblings without *CLCN1* mutation. The father who carried the nonsense *SCN4A* mutation found in the proband possibly had mild fixed ptosis but was otherwise healthy.

Family 2.

The proband was born with hypotonia. She exhibited poor feeding and respiratory insufficiency, requiring gastrostomy as well as intubation and mechanical ventilation. She was hospitalized for the first month of life. Motor milestones were attained including standing and walking, albeit delayed, but she also exhibited fluctuating weakness and recurrent breathing difficulty. Around 6 years of age she developed worsening motor function, intermittent respiratory distress, and was referred to the UCLA Neuromuscular Clinic for further evaluation. Her exam at that time demonstrated significant weakness of axial and appendicular muscles. She was not able to stand or support her head while in a seated positon. Reflexes were present, although mildly diminished. Repetitive stimulation of the median and accessory nerves at 3 Hz did not demonstrate a decrement in CMAP amplitude, and 50 Hz repetitive nerve stimulation of the median nerve did not elicit significant increment. No myotonic discharges were detected by needle EMG. The patient's mother reported improvement of strength and breathing with inhaled albuterol, but the benefit was not sustained on oral therapy. A trial of pyridostigmine did not improve strength, but the family reported improved mobility when acetazolamide and albuterol were tried separately. The parents have no motor symptoms. An older sister reportedly had bulbar weakness, was never able to sit without support, and died at age 1 year from respiratory complications. The proband is homozygous for c.4378C>T p.R1460W in *SCN4A*, and both parents are asymptomatic carriers although there is no history of consanguinity in the family.

Molecular results

The *SCN4A* variants in these families cause missense substitutions at the same amino acid, arginine 1460, which is in the highly conserved S4 transmembrane segment in domain IV of the sodium channel (Figure 1B). The allele frequency for p.R1460W in the ExAC database is 1 per 119522, and the p.R1460Q allele has not been reported. The S4 segments in the voltage sensors contain positively charged basic amino acids (arginine or lysine) at every third residue[13], and R1460 is the fifth of eight such residues in S4 of domain IV. Although mutation at R1460 in $Na_V1.4$ has not previously been reported in neuromuscular disorders, all three *SCN4A* mutations associated with a congenital myasthenic syndrome, and for which myopathy with fluctuating weakness is a prominent feature, are missense mutations of the voltage sensor in domain IV, and two are at other arginines in the S4 segment (p.R1454W and p.R1457H)[5-7]. All three previously reported mutations are also unusual because they cause LOF changes for the sodium channel and recessive inheritance of the syndrome, whereas GOF changes are found in *SCN4A* mutations associated with myotonia, paramyotonia, or hyperkalemic periodic paralysis[1]. We therefore tested the functional consequences of p.R1460Q and p.R1460W by recording sodium currents for channels heterologously expressed in fibroblasts or toad oocytes.

Functional Characterization of R1460 Mutant Sodium Channels

R1460 mutant sodium channels were expressed in the plasma membrane, but current density was reduced.

Sodium currents were detected in HEK cells transfected with wild type (WT) as well as R1460W and R1460Q mutant channels (Figure 2). Peak current amplitudes were smaller,

however, for cells expressing mutant channels. The peak current density (pA/pF to normalize for variations in cell size, Figure 2B) for cells expressing mutant channels was about 30% to 50% that of WT. At a test potential of – 5 mV, where the sodium current is largest, the amplitude was statistically smaller for each mutant compared to WT ($p < 0.01$, ANOVA) but the difference between the two mutants was not distinguishable (R1460W -73.8 ± 11 pA/pF (n = 9), R1460Q -140 ± 26 pA/pF (n = 7), WT 278 ± 46 pA/pF (n = 12)).

Channel activation was not altered by R1460Q or R1460W

The voltage dependence of sodium channel activation is shown in Figure 1C, where the relative conductance is plotted as a function of the test potential (see Methods). The data are completely overlapping between WT and R1460 mutant channels. Quantitatively, there was no detectable difference in the voltage midpoint of activation with $V_{1/2}$ of WT, R1460Q and R1460W being -18.7 ± 1.1 mV (n = 16), -17.6 ± 1.7 mV (n = 12), and -19.0 ± 1.4 mV (n =16), respectively. Additionally, the steepness of the voltage dependence was similar for all three: WT, R1460Q and R1460W being 7.7 ± 0.22 mV, 9.1 ± .34 mV, and 9.2 ± 0.23 mV, respectively.

Fast inactivation had mixed, loss- and gain-of-function, defects for R1460 mutant channels

Sodium channels undergo two forms of inactivation; fast inactivation on a time scale of milliseconds which contributes to termination of the action potential and limits repetitive firing, and slow inactivation over a time course of tens of seconds to minutes. To test the steady-state voltage dependence of fast invitation (also referred to as availability), we measured the peak current elicited at -10 mV, after a 300 msec conditioning pulse to potentials over a range from -130 mV to -40 mV (Figure 3A). Depolarization promotes inactivation (reduces availability), and

the voltage-dependence was markedly left-shifted for R1460 mutant channels ($V_{1/2}$ value for R1460Q -78.1 ± 0.67 mV, n= 10; R1460W -86.1 ± 1.5 mV, n = 12; and WT -70.5 ± 0.91 mV, n = 15). Additionally, the steepness of the voltage dependence of steady-state invitation was reduced for R1460 mutant channels (*k* value for WT 5.5 ± 0.88 mV, R1460Q 8.6 ± 0.2 mV, R1460W 7.7 ± 0.2 mV). Combined, these changes in the voltage dependence of steady-state fast inactivation produce a substantial LOF, as can be seen by the reduced availability (Figure 3A) of mutant channels (R1460Q = 0.7, R1460W = 0.5 compared to WT = 0.9) at the resting potential of -85 mV for skeletal muscle.

The voltage-dependent kinetics of fast inactivation were assessed for both entry to and recovery from inactivation. The entry rate was slower for R1460 mutant channels, which can be observed directly as a prolonged decay in a superposition of sodium currents elicited by a step depolarization to 10 mV (Figure 3B). This slower entry rate was observed over a range of test potentials (-20 mV to +60 mV), as shown by the larger amplitude time constant of the current decay (Figure 3D). Recovery from fast inactivation was recorded using a two-pulse protocol. Channels were fast inactivated using a 30 ms conditioning pulse to -10 mV, then after a variable duration recovery at a hyperpolarized potential (-80 mV to -130 mV), a test pulse to -10mV was delivered to determine the relative amplitude of the peak sodium current (Figure 3C, inset). The time course of recovery at -80 mV is shown in Figure 3C, and demonstrates the faster recovery (left shift) for R1460 mutant channels. A faster recovery rate (smaller time constant) of R1460 mutant channels was observed over a potential range from -50 mV to -130 mV (Figure 3D). Finally, the kinetics of closed-state fast inactivation (Figure 3D, -40 to -70 mV), was measured using a two-pulse protocol with a 30 ms conditioning pulse to induce inactivation, followed by a test pulse at -10 mV to measure the relative current. The altered entry and recovery kinetics for

fast inactivation of R1460 mutants both contribute to a GOF change, in other words more inward sodium current. In the physiological context of an action potential, mutant channels are predicted to inactivate more slowly at the peak of depolarization and then recover more quickly when the membrane potential returns to its resting value (-85 mV).

The impact of the altered kinetics of fast inactivation can be observed directly by measuring the peak amplitudes of sodium currents elicited by a train of brief depolarizing pulses. Normally, sodium channels do not have time to fully recover in the interval between action potentials with high-frequency discharges. We simulated this scenario by measuring sodium channel availability as the relative peak current elicited by a 2 ms depolarization to 10 mV, with an intervening recovery interval at -80 mV, over a range of pulse frequencies (Figure 4). Use-dependent inactivation was pronounced for WT channels (e.g. 30% decrease at 60 Hz and 50% decrease at 100 Hz), but was substantially less for R1460 mutant channels. These data demonstrate a GOF for R1460 mutant channels that would manifest, for example, as myotonic bursts.

Slow inactivation was unaffected for both R1460Q and R1460W mutant channels

Prolonged depolarizations lasting seconds or sustained bursts of discharges both cause sodium channels to become slow inactivated, and derangements of slow inactivation are known to cause susceptibility to periodic paralysis[14] or congenital myasthenia[6]. We characterized slow inactivation by using prolonged step depolarizations (up to 60 s) to induce slow inactivation, followed by a 20 ms recovery period at -120 mV to remove fast inactivation, and then applied a test pulse to -10 mV to detect the presence of slow inactivation as a reduced peak current. The time course of entry to slow inactivation at -10 mV was indistinguishable between WT and R1460 mutant channels (Figure 5A). Similarly, the rate of recovery was comparable for WT and R1460

mutant channels at -100 mV (Figure 5B). The small rightward shift represents about a 1.5-fold slower rate of recovery for R1460 mutants, although the fitted time constants were not statistically distinguishable from those of WT channels. The voltage-dependence of steady-state slow inactivation, as determined by 30 s conditioning pulses, was identical for WT and R1460 mutant channels (Figure 5C).

R1460 mutant channels do not conduct a gating pore leakage current

Missense mutations at arginine residues in the S4 segments of the voltage sensor domains of sodium or calcium channels account for almost all cases of hypokalemic periodic paraysis[3], and have a common functional defect, the gating pore leakage current, caused by a mutation-induced anomalous ion conduction pathway[4]. Since R1460 is an arginine in the S4 segment of domain IV in $Na_V1.4$ (Figure 1B), we tested whether R1460Q or R1460W mutant channels have a detectable gating pore leakage current. Channels were studied in frog oocytes to achieve high expression levels sufficient to observe gating pore currents when the main pore was blocked by tetrodotoxin. Currents recorded from oocytes expressing R1460Q or R1460W channels were no different from WT (Figure 6), as compared to the positive control with the HypoPP mutation R1132Q for which a large gating pore current was detected (inward current a negative potentials).

2.4 DISCUSSION

This report identifies a new residue in $Na_V1.4$ (p.R1460) where missense mutations were identified in patients with congenital myopathy plus fluctuating weakness. The clinical manifestations overlap considerably with prior reports of a recessive congenital myasthenia

syndrome plus periodic paralysis that is associated with LOF mutations in SCN4A[5-7]. These cases and the two recessive phenotypes herein are likely part of a continuum, if not a single entity. The consistent features are hypotonia at birth, respiratory distress, and feeding difficulties often requiring tube feeds. Motor function at infancy and early childhood is notable for delayed milestone attainments, fixed ptosis, myopathic weakness especially of the face and neck, episodes of hypoventilation, myalgia and fatigability.

Electrophysiological signs of myasthenia are variable. The first published report (p.S246L/p.V1442E) was notable for pronounced CMAP decrement during repetitive nerve stimulation (at 2Hz after a 10 Hz load and at all frequencies of 10 Hz or higher)[5]. For the two subsequent single-case reports of *SCN4A*-associated CMS, one had increased jitter[7] (as observed for patient F1 III:3 herein) but neither had a CMAP decrement with repetitive stimulation. Conversely, in the series of 6 families with congenital myopathy associated with *SCN4A* recessive mutations, one of four available surviving patients had a 60% CMAP decrement with 10Hz stimulation[8].

A consistent pattern is emerging for the genotype-phenotype associations with LOF mutations in *SCN4A*. A single mutant allele, whether a partial loss or complete null, is asymptomatic although a mouse model revealed a latent susceptibility to myasthenia[15]. A biallelic deficit with homozygous LOF mutations leads to moderate congenital myopathy with fluctuating weakness and variable electrodiagnostic signs of myasthenia. Compound heterozygous mutations with a null plus a LOF defect cause moderate to severe congenital myopathy, including an increased risk of infant mortality. Finally, biallelic null mutations, whether from nonsense mutations or missense mutations with no detectable sodium current, are lethal in utero or at birth[8]. In hindsight, this paradigm suggests the original report of *SCN4A*-associated CMS was indeed

caused by a recessive compound heterozygote (p.S246L / p.V1442E)[5]. The LOF was much greater for V1442E, which raised the possibility that S246L was a benign polymorphism. Recognizing now that a single LOF allele is asymptomatic and that S246L does not appear in the ExAC database, strongly supports the notion that S246L is a functionally relevant LOF mutation.

The clinical phenotypes associated with mutations at p.R1460 described herein were more varied, which we attribute to the mixed LOF and GOF changes observed for both R1460Q and R1460W mutant channels. In the primary Finnish family, inheritance of congenital myopathy was recessive (p.R1460Q / p.R1059X) but myotonia was a partially dominant trait. Latent myotonia was detected by needle EMG in p.R1460Q carriers, and the coincident occurrence of an independently segregating mutation of the chloride channel gene *CLCN1* (p.R894X associated with recessive myotonia congenita) led to symptomatic myotonic stiffness. Combined GOF mutations in *SCN4A* and LOF mutations in *CLCN1* are known to synergistically aggravate the severity of myotonia[16, 17]. The LOF defects for R1460W channels were more severe than those of R1460Q (smaller amplitude, Figure 2; greater left shift of inactivation, Figure 3), which explains why the parents shown to be p.R1460W carriers did not have myotonia. Unusual clinical phenotypes have also been reported for missense mutations of the second arginine in the voltage sensor of domain IV (p.R1451L and p.R1451C)[18, 19]. In the heterozygous state, p.R1451L is associated with myotonia aggravated by cold and rare episodes of periodic paralysis typical for paramyotonia congenita, which is consistent with GOF defects manifest as slower entry and faster recovery from inactivation. An individual homozygous for p.R1451L had more frequent and severe episodes of weakness, one of which with serum K^+ 2.8 mM suggestive of HypoKPP[19]. Expression studies of R1451L did not reveal a gating pore leakage current – the canonical defect in HypoKPP – but instead showed LOF changes (reduced peak current and enhanced inactivation)

that may cause this unusual form of periodic paralysis in homozygous patients[19]. Unlike the cases herein, however, the LOF aspects of the mixed channel defects for p.R1451L did not result in congenital myopathy or a CMS syndrome in the homozygous proband.

Our report is the third case of a homozygous recessive mutation in *SCN4A* found in CMS / congenital myopathy, and all three missense mutations are at arginine residues in the S4 segment of the domain IV voltage sensor (p.R1454W[6], p.R1457H[7], and p.R1460W). Expression studies for all three mutations show a similar pattern of LOF changes with aberrant enhancement of inactivation, consistent with the established structure-function behavior of voltage-gated sodium channels; the domain IV sensor is coupled to inactivation[20] whereas domains I-III control activation. All 11 mutations of $Na_V1.4$ that cause HypoPP type 2 are also missense substitutions of arginines in S4 segments within voltage sensors[1, 3]. These mutations all create anomalous "gating pore" leakage currents that are mechanistically implicated in episodic attacks of depolarization and weakness in HypoPP[4]. The HypoPP mutations of S4 are in domains I – III, whereas a homologous mutation in domain IV (p.R1448C) causes paramyotonia congenita and does not create a gating pore leak[21]. Scanning mutagenesis studies have shown that a missense substitution of any single arginine in S4/DIV is insufficient to create a gating pore leak[22], and we have confirmed herein that the p.R1460 mutations found in recessive congenital myopathy do not produce a leak (Figure 6).

Further investigations are required to understand the mechanism for the fluctuating weakness in CMS / congenital myopathy caused by mutations in *SCN4A*. Fluctuating weakness reminiscent of periodic paralysis is not likely to be caused by fiber depolarization, as with attacks of HyperPP or HypoPP, because this clinical symptom occurs with CMS mutations that lack GOF changes (e.g. p.R1454W[6]). The fluctuation in strength is more likely to be a consequence of

impaired generation and conduction of action potentials caused by a marginal sodium current density that may be exacerbated by use-dependent trapping of sodium channels in an inactive state.

2.5 FIGURES

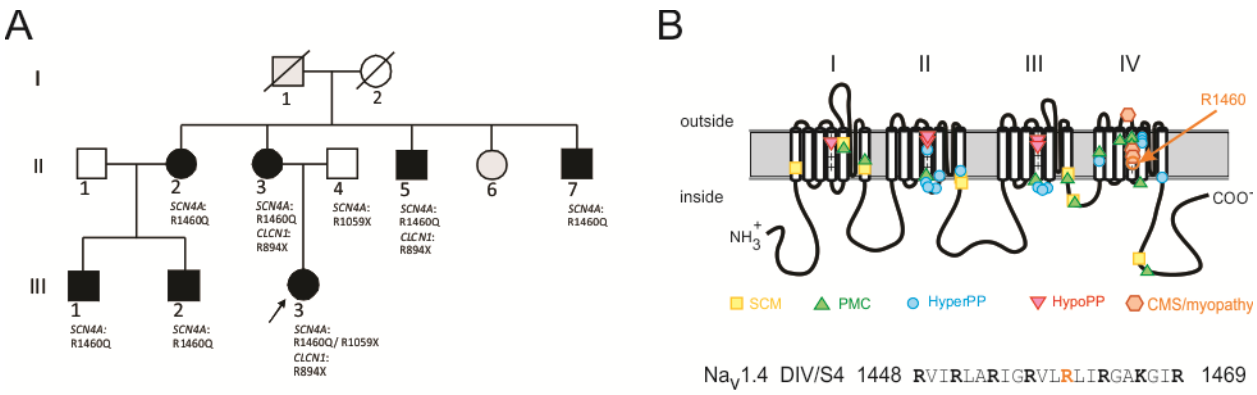

Figure 2-1 Sodium channel mutations. (**A**) Segregation of clinical phenotype and genotype amongst seven carriers of p.R1460Q in family 1 from Finland. (**B**) Location of p.R1460 in the pore-forming subunit ($Na_V1.4$) along with established sites for sodium channelopathies of skeletal muscle (SCM - sodium channel myotonia, PAM - paramyotonia congenita, HyperPP – hyperkalemic periodic paralysis, HypoPP – hypokalemic periodic paralysis, CMS – congenital myasthenic syndrome).

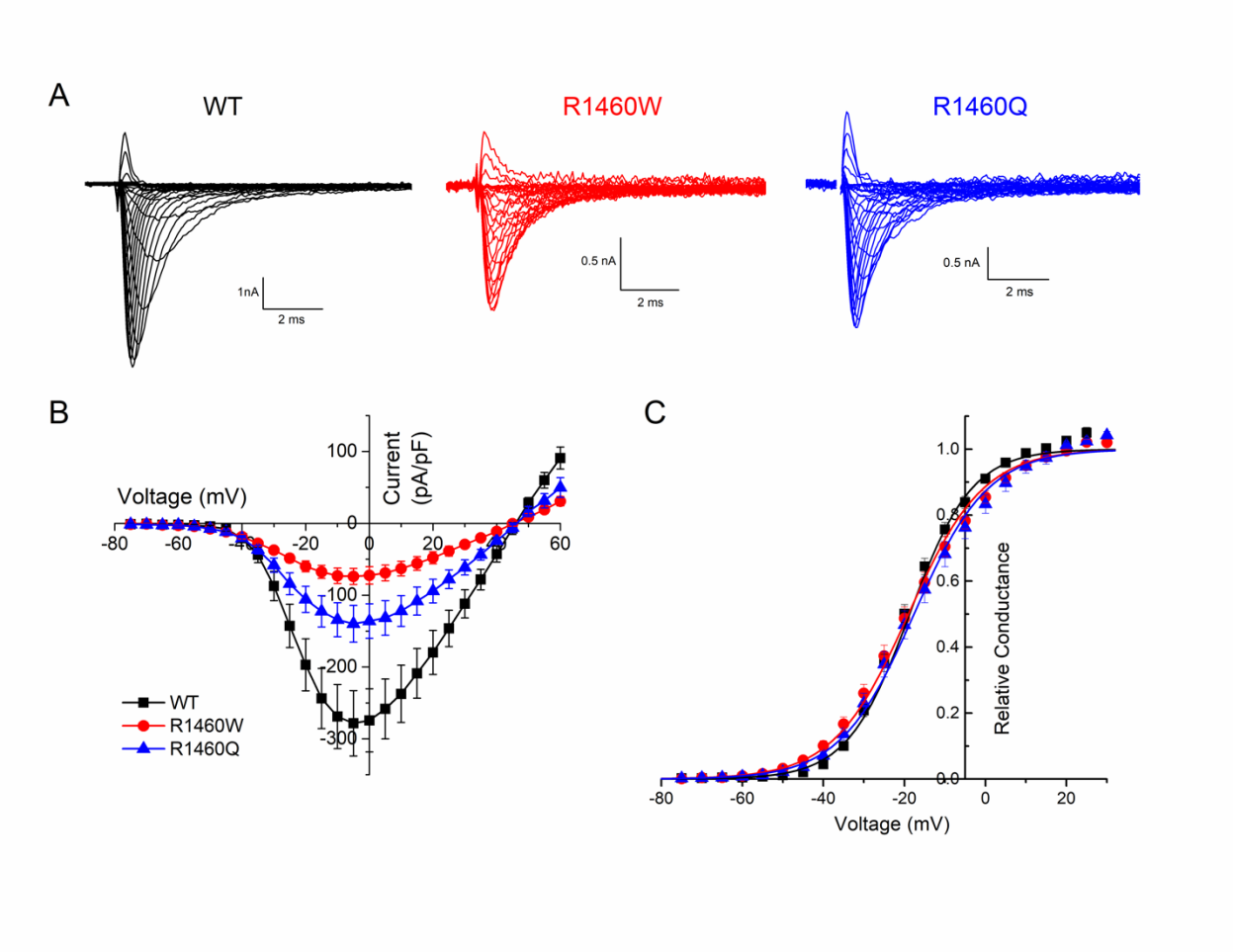

Figure 2-2. Sodium current density was reduced for cells transfected with R1460 mutant constructs, but the voltage-dependence of activation was not altered. (**A**) Traces show sodium currents elicited by depolarization from -120mV to test potentials between -75 and +60mV. Note the higher gain for the scale bars in the mutant channel traces. (**B**) Peak current density is shown as a function of test potential and displays a marked reduction in current amplitude for both mutants. (**C**) The voltage dependence of channel activation, as shown by relative conductance, was indistinguishable between the WT and mutant channels. Black squares, blue triangles, and red circles correspond to WT (n = 16), R1460Q (n = 12), and R1460W (n = 16) respectively.

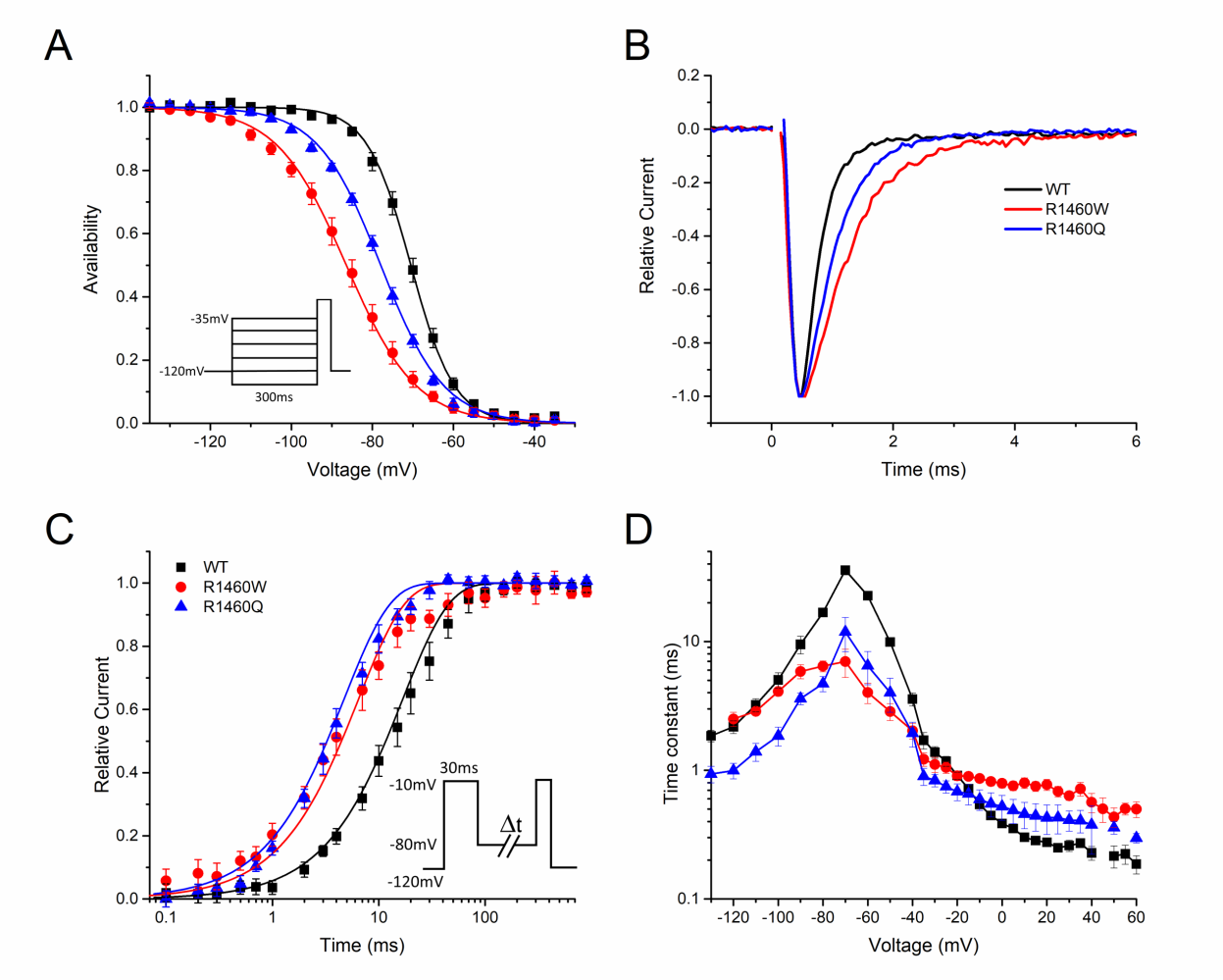

Figure 2-3. Fast inactivation of R1460 mutant channels had both gain of function and loss of function defects. (**A**) The steady-state voltage dependence of fast inactivation was shifted leftward (hyperpolarized) for both R1460 mutant channels relative to WT. Inset shows the voltage protocol used to measure inactivation produced by a 300 ms conditioning pulse at various potentials. (**B**) The rate of inactivation was slower for R1460 mutant channels at depolarized potentials, as shown by the superposition of amplitude normalized currents elicited at 10mV. (**C**) Recovery from fast inactivation was faster for both R1460Q and R1460W, compared to WT channels (Tau recovery of 4.7 ± 0.6 ms, $p < 0.0001$ (n=5); 6.4 ± 0.6 ms, $p < 0.0001$ (n = 7); 16.8 ± 0.4 ms (n = 4) respectively). Data show the time course for the recovery of peak current amplitude at a holding potential of -80 mV, after channels were inactivated with a conditioning pulse of 30 msec at -10 mV (inset). (**D**) Plot summarizing the voltage-dependent kinetics for entry to or recovery from fast inactivation. Three separate protocols were used to measure inactivation kinetics, over the entire

voltage range (see text, Results). Overall, the changes in steady-state fast inactivation (A) are loss of function; whereas the slower entry and more rapid recovery from fast inactivation are GOF changes.

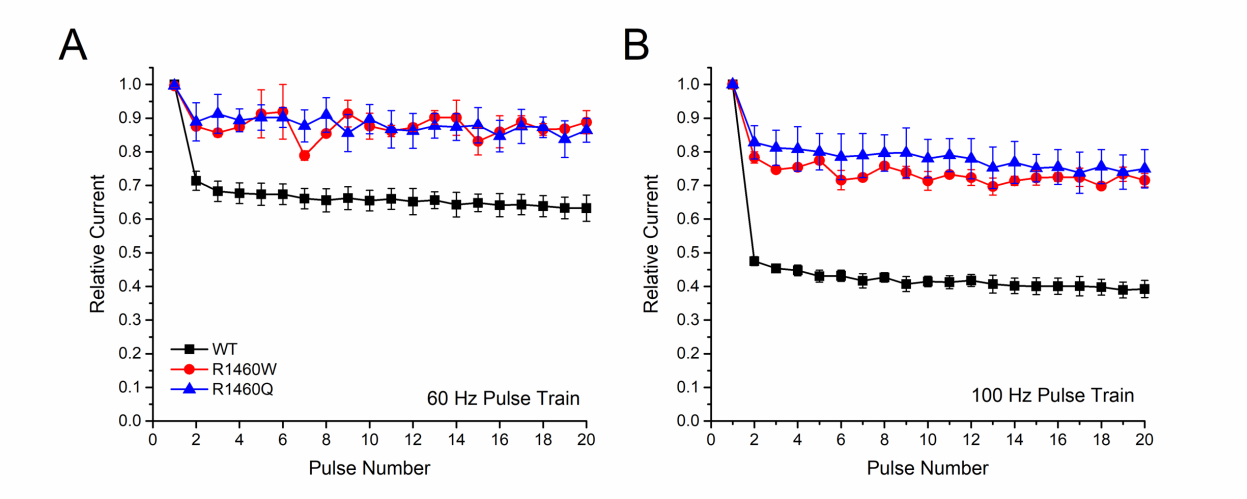

Figure 2-4. The use-dependent reduction in sodium current peak amplitude was less pronounced in R1460 mutants than in WT channels. Data show relative peak sodium current elicited by 2 msec depolarizing pulses to 10 mV applied at 60 Hz (**A**) or 100 Hz(**B**), from a holding potential of -80 mV.

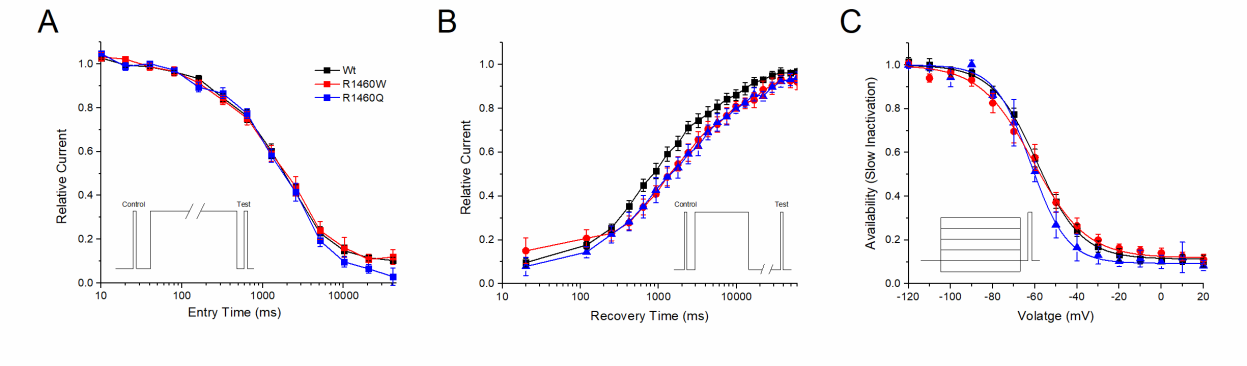

Figure 2-5. Slow inactivation was not altered by either R1460W or R1460Q. (**A**) Onset of slow inactivation showed identical kinetics between WT and mutant channels. Inset shows the voltage protocol to characterize the onset of slow inactivation by stepping to -10 mV for a variable duration (Entry Time), and then measuring the decline in relative loss current that fails to recover within 20 ms at -120 mV. (**B**) The rate of recovery from slow inactivation was comparable between WT and R1460 mutant channels. Channels were slow inactivated by a 30 s step to -10 mV (inset), and the data show recovery as the relative increase in current after repolarizing to -80 mV for a variable duration (Recovery Time). (**C**) The voltage-dependence of steady-state slow inactivation was indistinguishable between WT and R1460 mutant channels. 30 s conditioning pulses to various conditioning potentials (inset) were used to determine the voltage dependence of inactivation. Smooth curves show best fits to the data with $V_{1/2}$ of -59.1 ± 1.9 mV for WT, -60.9 ± 2.8 mV for R1460Q, and -63.4 ± 2.6 mV for R1460W. The number of cells for the mean values shown in the data was 5 to 8 for WT and both R1460 mutant channels.

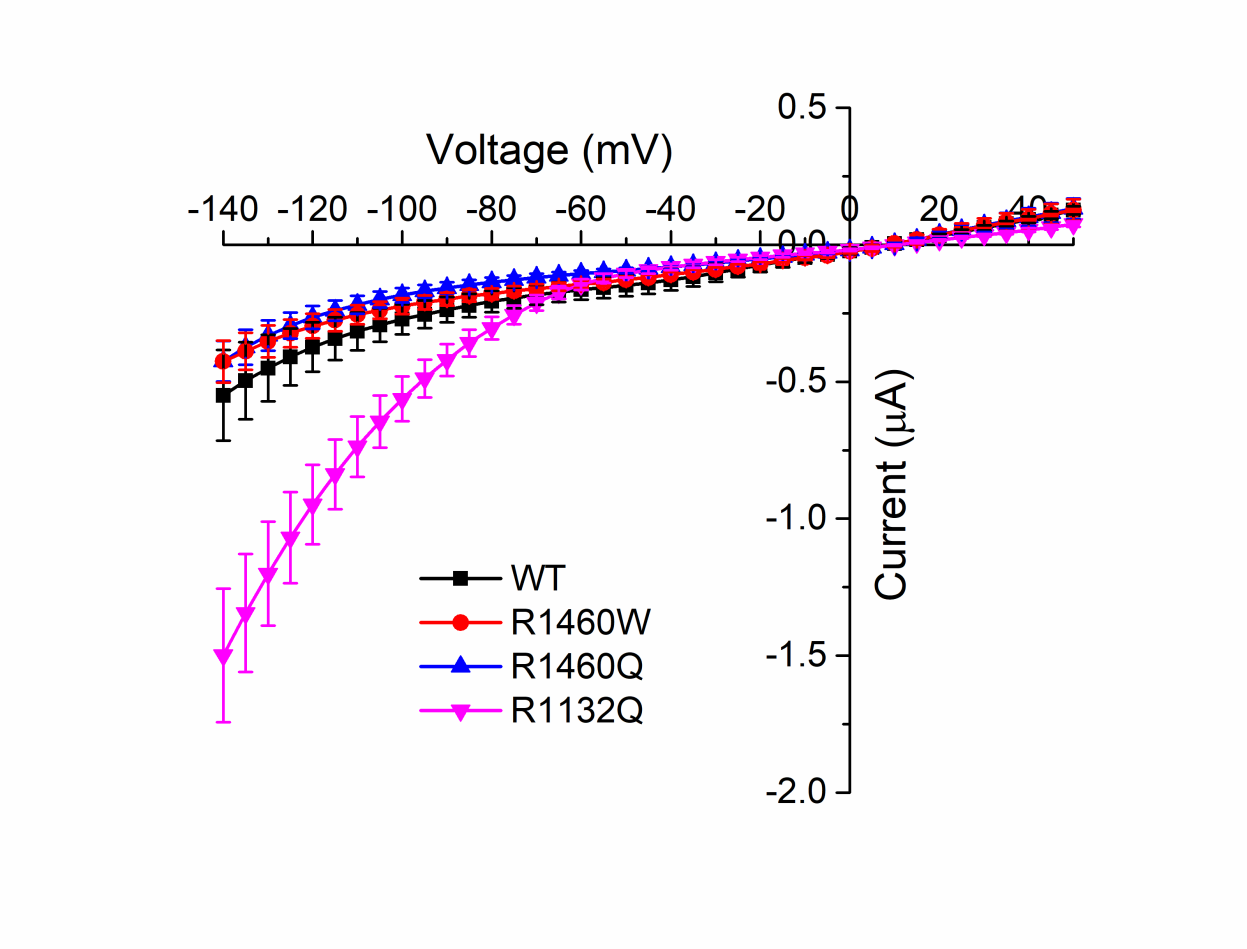

Figure 2-6. The R1460 mutations did not cause a gating pore leakage current. The steady-state current (without subtraction of the non-specific leak) recorded from oocytes expressing high levels of WT or R1460 mutant channels is plotted as a function of the membrane potential. Tetrodotoxin was added to block sodium currents through the main pore. The I-V relation was identical for WT and R1460 mutant channels, while the positive control for the p.R1132Q mutation in hypokalemic periodic paralysis showed a gating pore leakage current (large negative current for membrane potentials more negative than -80 mV). Data are from 6-8 oocytes per construct.

2.6 REFRENCES

1. Cannon SC. Sodium Channelopathies of Skeletal Muscle. Handb Exp Pharmacol 2018;246:309-330.

2. Lehmann-Horn F, Rüdel R, Jurkat-Rott K. Nondystrophic myotonias and periodic paralyses. In: Engel AG, Franzini-Armstrong C, eds. Myology, 3rd ed. New York: McGraw-Hill, 2004: 1257-1300.

3. Matthews E, Labrum R, Sweeney MG, et al. Voltage sensor charge loss accounts for most cases of hypokalemic periodic paralysis. Neurology 2009;72:1544-1547.

4. Cannon SC. Voltage-sensor mutations in channelopathies of skeletal muscle. J Physiol 2010;588:1887-1895.

5. Tsujino A, Maertens C, Ohno K, et al. Myasthenic syndrome caused by mutation of the SCN4A sodium channel. Proc Natl Acad Sci U S A 2003;100:7377-7382.

6. Habbout K, Poulin H, Rivier F, et al. A recessive Nav1.4 mutation underlies congenital myasthenic syndrome with periodic paralysis. Neurology 2016;86:161-169.

7. Arnold WD, Feldman DH, Ramirez S, et al. Defective fast inactivation recovery of Nav 1.4 in congenital myasthenic syndrome. Ann Neurol 2015;77:840-850.

8. Zaharieva IT, Thor MG, Oates EC, et al. Loss-of-function mutations in SCN4A cause severe foetal hypokinesia or 'classical' congenital myopathy. Brain 2016;139:674-691.

9. Fournier E, Arzel M, Sternberg D, et al. Electromyography guides toward subgroups of mutations in muscle channelopathies. Ann Neurol 2004;56:650-661.

10. Fournier E, Viala K, Gervais H, et al. Cold extends electromyography distinction between ion channel mutations causing myotonia. Ann Neurol 2006;60:356-365.

11. Evila A, Palmio J, Vihola A, et al. Targeted Next-Generation Sequencing Reveals Novel TTN Mutations Causing Recessive Distal Titinopathy. Mol Neurobiol 2017;54:7212-7223.

12. Hayward LJ, Brown RH, Jr., Cannon SC. Inactivation defects caused by myotonia-associated mutations in the sodium channel III-IV linker. J Gen Physiol 1996;107:559-576.

13. Gamal El-Din TM, Lenaeus MJ, Catterall WA. Structural and Functional Analysis of Sodium Channels Viewed from an Evolutionary Perspective. Handb Exp Pharmacol 2018;246:53-72.

14. Hayward LJ, Brown RH, Jr., Cannon SC. Slow inactivation differs among mutant Na channels associated with myotonia and periodic paralysis. Biophys J 1997;72:1204-1219.

15. Wu F, Mi W, Fu Y, Struyk A, Cannon SC. Mice with an NaV1.4 sodium channel null allele have latent myasthenia, without susceptibility to periodic paralysis. Brain 2016;139:1688-1699.

16. Skov M, Riisager A, Fraser JA, Nielsen OB, Pedersen TH. Extracellular magnesium and calcium reduce myotonia in ClC-1 inhibited rat muscle. Neuromuscul Disord 2013;23:489-502.

17. Kato H, Kokunai Y, Dalle C, et al. A case of non-dystrophic myotonia with concomitant mutations in the SCN4A and CLCN1 genes. J Neurol Sci 2016;369:254-258.

18. Poulin H, Gosselin-Badaroudine P, Vicart S, et al. Substitutions of the S4DIV R2 residue (R1451) in NaV1.4 lead to complex forms of paramyotonia congenita and periodic paralyses. Sci Rep 2018;8:2041.

19. Luo S, Sampedro Castaneda M, Matthews E, et al. Hypokalaemic periodic paralysis and myotonia in a patient with homozygous mutation p.R1451L in NaV1.4. Sci Rep 2018;8:9714.

20. Capes DL, Goldschen-Ohm MP, Arcisio-Miranda M, Bezanilla F, Chanda B. Domain IV voltage-sensor movement is both sufficient and rate limiting for fast inactivation in sodium channels. J Gen Physiol 2013;142:101-112.

21. Francis DG, Rybalchenko V, Struyk A, Cannon SC. Leaky sodium channels from voltage sensor mutations in periodic paralysis, but not paramyotonia. Neurology 2011;76:1635-1641.

22. Gosselin-Badaroudine P, Delemotte L, Moreau A, Klein ML, Chahine M. Gating pore currents and the resting state of Nav1.4 voltage sensor domains. Proc Natl Acad Sci U S A 2012;109:19250-19255.

CHAPTER 3

3.1 INTRODUCTION

Sodium channels are required for action potential generation and propagation. The sodium channel alpha-subunit gene (*SCN4A*) encodes the isoform $Na_V1.4$ which is the most abundant isoform in skeletal muscle.

Mutations affecting one *SCN4A* allele are often associated with a gain-of-function resulting in muscle stiffness (myotonia) that may worsen with repeated contraction (paramyotonia) as well as episodes of hyperkalemic periodic paralysis (Cannon, 2015). Phenotypic variability has been reported among family members regarding the age of onset and clinical severity of myotonia (Yoshinaga et al., 2015). Another class of heterozygous *SCN4A* mutations allow an anomalous leakage of ions through the voltage sensor of the channel, distinct from the sodium-conducting pore, and cause hypokalemic periodic paralysis (Cannon, 2018).

With increased accessibility to genetic testing, the phenotypic spectrum of *SCN4A* mutations has been expanding. We now recognize *SCN4A* mutations to cause isolated exercise- or cold-induced myalgia (Palmio et al., 2017). De novo heterozygous *SCN4A* mutations, often at p.Gly1306Glu, have been linked to a severe neonatal phenotype with episodic laryngospasm (Lion-Francois et al., 2010; Caietta et al., 2013; Singh et al., 2014; Portaro et al., 2016), stridor (Matthews et al., 2011) or in other cases with apneic episodes (Gay et al, 2008). .

More recently, biallelic mutations in *SCN4A* have been reported in congenital myasthenic syndromes (Tsujino et al., 2003; Arnold et al., 2015; Habbout et al., 2016), at times with myopathy (Elia et al., 2019), and in severe congenital myopathy with fetal hypokinesia (Zaharieva et al., 2016). All these syndromes have recessive inheritance, with a single loss-of-function allele being asymptomatic, including even a functional null from a premature stop. Moderate loss-of-function

mutations from enhanced inactivation are associated with congenital myasthenia (Tsujino et al., 2003), whereas biallelic mutations that include a single null cause congenital myopathy with fetal hypokinesia and biallelic null mutations are embryonic or neonatal lethal (Zaharieva et al., 2016). We report a patient who presented with arthrogryposis multiplex congenita, congenital myopathy, and episodes of bronchospasm who has the c.2386C>G, p.L796V variant in *SCN4A*. Expression studies of L796V channels revealed two forms of gain-of-function, enhanced activation and impaired slow inactivation, and which in model simulations led to prolonged bursts of myotonic discharges. We propose L796V is a pathogenic mutation and that the clinical features shared with previously described cases defines a new *SCN4A* syndrome of myotonic myopathy with secondary deformities of joints and bone.

3.2 MATERIALS AND METHODS

Sodium channel currents

Sodium currents were measured from fibroblasts (HEK cells) transiently transfected with plasmids encoding the wild type (WT) or mutant L796V human $Na_V1.4$ □ subunit and the □1 accessory subunit as previously described (Hayward et al., 1996). Currents were recorded in whole-cell mode with a patch electrode that contained in mM: 100 CsF, 35 NaCl, 5 EGTA, 10 HEPES, pH to 7.3 with CsOH. The extracellular bath contained in mM: 140 NaCl, 4 KCl, 2 $CaCl_2$, 1 $MgCl_2$, 2.5 glucose, 10 HEPES, pH to 7.3 with NaOH. Cells with maximal peak Na^+ currents less than 1 nA were excluded to minimize the contribution from endogenous Na^+ currents (typically < 0.1 nA), and cells with peak Na^+ currents greater than 5 nA were excluded to avoid series resistance errors.

The voltage-dependent activation of sodium currents was quantified by fitting the peak amplitude (I_{peak}) to a linear conductance (G_{max}) with a reversal potential (E_{rev}) that was scaled with a Boltzmann function: $I_{peak} = G_{max}(V - E_{rev})/(1 + e^{-(V - V_{1/2})/K})$. The voltage-dependence for activation of the channel is reflected by $V_{1/2}$, the voltage at which half the channels are activated, and K a steepness factor. The voltage dependence of the relative conductance (see Fig. 1D) was calculated as I_{peak} divided by $G_{max}(V - E_{rev})$. The time constant, τ, for entry to inactivation was estimated from a single exponential fit of the current decay (fast inactivation) or of the change in peak current after progressively longer conditioning pulses (slow inactivation). The voltage dependence of steady-state fast inactivation was quantified by fitting the relative peak current after a 300 msec conditioning pulse at a voltage of V_{cond} by a Boltzmann function $I_{peak}(V_{cond})/I_{peak\_max} = 1/(1 + e^{(V - V_{1/2})/K})$. For the steady-state voltage dependence of slow inactivation, a plateau term (S_0) was included because slow inactivation does not reduce channel availability to 0 at strongly depolarized potentials (Fig. 3D). Estimated values for parameters are presented as mean ± SEM.

Simulated muscle action potentials

The functional consequences of altered sodium currents observed for the L796V mutant channels on muscle excitability were explored using computer simulation. The two-compartment model of a muscle fiber (modified from Cannon et al., 1993) consisted of the plasma membrane (sarcolemma) and the transverse tubular membrane, each of which contained voltage-dependent conductances to simulate sodium channels, chloride channels, inward-rectifying potassium channels, and delayed-rectifier potassium channels. Mutant L796V channels were simulated by modifying the parameter values so that the currents predicted by a Hodgkin-Huxley model

matched the currents we measured in the HEK cell expression system (See Supplementary material for details).

3.3 RESULTS

Clinical Presentation and Genetic Analysis

A 7 year old boy of Morrocan descent was the first child to healthy, non-consanguineous parents. Routine antenatal ultrasounds at 13, 21 and 30 weeks gestation revealed normal fetal anatomy and amniotic fluid levels. Good fetal movements were reported throughout gestation. Repeat ultrasound at 41 weeks showed decreased amniotic fluid levels prompting a planned Caesarian section. Apgar scores were 1 at 1 min, 5 at 5 minutes and 7 at 10 minutes. Although no chest compressions were required, he was intubated at birth and empiric surfactant was administered. His birth weight was 2,995 g (3-10%ile) and head circumference 36.0 cm (50%ile). He was noted to have facial weakness and arthrogryposis multiplex congenita with extensive bilateral contractures at the elbows, wrists, fingers, hips, knees and ankles. He did demonstrate antigravity movements of his arms and legs. Nerve conduction studies at 2 weeks of age revealed normal median and medial plantar nerve sensory responses. Median and tibial motor responses revealed abnormally low compound motor action potential (CMAP) amplitude. Needle EMG of his biceps, vastus lateralis, gastrocnemius and abductor hallicus revealed increased insertional activity (Supplemental Video 1).

Beginning at 2 weeks old, he began having episodes of bronchospasm associated with cessation of chest movement and desaturation. Episodes lasted for 30 seconds to 2 minutes and

showed minimal response to supplemental oxygen and positive pressure ventilation. Video EEG was unremarkable with no epileptiform activity noted at the time of clinical events.

MRI brain, echocardiogram, serum creatine kinase and quadriceps muscle biopsy were unremarkable. Repeat EMG of the deltoid, first dorsal interosseous and tibialis anterior at 6 weeks of age again revealed increased insertional activity; however, there were long runs of myotonic discharges with typical waxing and waning variation in frequency and amplitude (Supplemental Video 2) that were not seen on the earlier study.

Although the bronchospasm did not show any appreciable response to phenobarbital, it abruptly stopped with empiric carbamazepine 20 mg/kg/day. He remains on carbamazepine. At 5 years of age he has reported some cold-induced episodes of eyelid and facial muscle paramyotonia but no episodes of periodic paralysis.

The patient's medical history was also relevant for severe gastroesophageal reflux due to a sliding hiatus hernia. He required a fundoplication and gastro-jejunostomy (GJ) tube placement (removed at 4 years old). He had strabismus which required surgical correction at 16 months of age. He had bilateral cryptorchidism requiring orchidopexy. He required multiple orthopedic surgeries including bilateral ankle casting and eventual contracture release (at 15 months); treatment of the developmental dysplasia of the left hip with open reduction (at 3 years).

His language development has progressed normally. He is fluent in three languages and requires no modification to his academic curriculum. Gross motor development was significantly delayed; he rolled independently at 6 months and sat independently at 18 months. At 2-1/2 years he was able to walk using a walker. At 3-1/2 years he was able to rise and walk independently.

Array CGH and molecular testing for myotonic dystrophy type 1 were normal. HSPG2 gene sequencing revealed that the patient was heterozygous for a G>A transition in a highly

conserved residue (nucleotide 4877, exon 39) (seen in 0.8% of the population) that had not been reported as either a mutation or a polymorphism. MLPA testing revealed no deletion or duplication affecting the other allele and immunohistochemical staining for perlecan on frozen muscle from prior biopsy was normal. LIFR sequencing and deletion-duplication analysis was normal. Collectively, these genetic and histochemical findings do not support a diagnosis of Schwartz-Jampel syndrome. Exome sequencing, performed as part of the Canada-wide Care4Rare research consortium identified a likely pathogenic variant in one *SCN4A* allele that was confirmed with Sanger sequencing: SCN4A: NM_000334: c.2386C>G, p.Leu796Val. It was not present in either parent.

Functional Characterization of L796V Mutant Sodium Channels

Activation of L796V channels was shifted to more negative potentials

Both wild type (WT) and L796V mutant sodium channels were expressed in the plasma membrane of transiently transfected fibroblasts (HEK cells), as shown in Figure 1 by the sodium currents recorded in whole-cell voltage clamp. A plot of the peak sodium current as a function of membrane voltage (Fig. 1 C) shows the current amplitude was lower for cells expressing L796V compared to WT (-2.07 ± 0.19 nA and -3.32 ± 0.53 nA, respectively). A more accurate comparison of expression level is obtained from the maximum conductance, G_{max} , which is reflected by the slope of the current-voltage relation at voltages > 20 mV. On average, the G_{max} was 50% lower for cells expressing L796V than WT channels (37.4 ± 3.5 nS and 76.4 ± 10 nS, respectively $p <$ 0.05).

The voltage-dependence of activation is illustrated more clearly by transforming the peak current amplitude to relative conductance as a function of test potential (see Methods), as shown

in Figure 1D. The midpoint of the relative conductance curve, $V_{1/2}$, was shifted toward more negative potentials by -7.2 mV L796V channels (-25.9 ± 1.3 mV, n = 10) compared to WT channels (-18.7 ± 1.1 mV, n = 16; $p < 0.001$). The voltage dependence was slightly less steep for L796V channels (8.32 ± 0.20 mV) compared to WT (7.31 ± 0.22), but these values were not statistically different at the 0.05 level.

Fast inactivation was not altered by the L706V mutation

Several voltage-pulse protocols were used to characterize the kinetics and steady-state voltage dependence of sodium channel fast inactivation. The time constant of the sodium current decay after the early peak provides a quantitative measure of channel fast inactivation from the open state. Superposition of amplitude-normalized current traces (Fig. 2A) shows the fast inactivation time course was indistinguishable between WT and L796V channels, and the values of the time constants over the measurable range from -35 mV to + 40 mV were overlapping (Fig. 2C, circles). Recovery from fast inactivation was measured in a two-pulse protocol. First, channels were fast inactivated by a 30 msec conditioning pulse to -10 mV, then after a variable recovery interval at a hyperpolarized potential, the amount of recovery was measured as the relative current elicited by a test pulse to -10 mV. The time course of recovery at -90 mV was indistinguishable for WT and L796V channels (Fig. 2B), and the time constant for recovery was identical over the measured range from -130 mV to -80 mV (Fig. 2C, squares). The kinetics of entry to fast inactivation from closed states was measured in a two-pulse protocol for which a variable duration conditioning pulse was applied to partially inactivate channels (without opening), and then a test pulse to -10 mV was applied to measure the relative current. The time constant for the onset of close-state fast inactivation was modestly smaller for L796V over the voltage range

from -70 mV to -50 mV (Fig. 2C, inverted triangles). This difference is not predicted to be biologically significant, because the more rapid kinetics of entry to inactivation at the peak of the action potential (0 to 20 mV) and the rapid recovery at the resting potential (-80 to -95 mV) will dominate the kinetics of fast inactivation in muscle fibers. The voltage dependence of steady-state fast inactivation was measured as the relative peak current elicited at -10 mV, after a 300 msec conditioning pulse to potentials over a range from -120 mV to -40 mV. The data were indistinguishable for WT and L796V channels (Fig. 2D), as confirmed by the parameter estimates from fits to a Boltzmann function ($V_{1/2}$ -70.5 ± 0.91 mV n = 15, -72.0 ± 1.5 mV n = 10 for WT and L796V, respectively; K 5.37 ± 0.56 mV, 5.02 ± 0.40 mV for WT and L796V, respectively).

Slow inactivation was impaired by L796V

Slow inactivation of sodium channels occurs on a time scale of seconds, compared to the millisecond range for fast inactivation. Depolarization promotes both forms of inactivation, and the slow inactivated component is experimentally resolved by measuring the proportion of current that fails to recover during a brief hyperpolarization (-120 mV for 20 milliseconds). The time course for the onset of slow inactivation is shown in Figure 3A, in which repeated trials with a progressively longer duration conditioning pulse to -50 mV have been applied and the relative current decreased as a greater proportion of channels became slow inactivated. The time constant of this exponential decay is shown for various test potentials from -50 mV to -10 mV in Figure 3C (inverted triangles). The time constant decreases (faster entry rate) at more positive potentials for WT channels, whereas the time constant is voltage independent and small for L796V channels.

The time course for recovery from slow inactivation at hyperpolarized potentials was measured by monitoring the recovery of peak sodium current after a 30 second conditioning pulse

to -10 mV to maximally slow inactivate channels. Recovery at -80 mV is shown in Figure 3B. Fewer L796V channels are slow inactivated at the beginning of the recovery period (25% current already recovered at 0.020 sec compared to 10% for WT) and the time course of recovery of L796V is more rapid than for WT (left shift of recovery curve). The recovery time constant measured over a voltage range from -80 mV to -120 mV was independent of voltage for L796V channels (Fig. 3C upright red triangles), whereas for WT channels the time constant decreased (faster recovery) with hyperpolarization (Fig. 3C upright black triangles).

The voltage dependence of steady-state slow inactivation was measured as the loss of current availability (i.e. decreased peak current amplitude) measured after a 30 second conditioning pulse (Fig. 3D). The maximal extent of slow inactivation was reduced for L796V channels, as shown by the higher amplitude plateau in the availability curve at voltages more positive than -20 mV. The fitted parameter estimates for the plateau were S_0 0.11 ± 0.07, n = 5; 0.23 ± 0.02, n = 5 for WT and L796V, respectively (p = 0.01). In addition, the steepness of the voltage dependence was reduced for L796V channels (K 10.7 ± 1.0 mV, n = 5 for WT; 13.9 ± 0.4 mV, n = 5 for L796V, $p < 0.01$). There was a trend for a hyperpolarized shift in the midpoint for the voltage dependence of slow inactivation for L796V, but this difference was not distinguishable statistically ($V_{1/2}$ -59.1 ± 1.9 mV, n = 5 for WT; -67.0 ± 3.4 mV, n = 5 for L796V, p = 0.11).

At first glance, the changes in slow inactivation properties for L796V channels appear to be a mixture of gain and loss of function effects. Enhancement of slow inactivation is expected at the resting potential of -80 mV because of the reduced slope of the voltage dependence and the tendency for a left shift (Fig. 3D, reduced availability at -80 mV), as well as for a faster rate of entry over the voltage range of -50 mV to -30 mV (Fig. 3C, smaller time constants). On the other hand, impairment of slow inactivation is expected at depolarized potentials because inactivation

of L796V is less complete than WT (Fig. 3D higher plateau -20 mV to 20 mV), and the recovery from slow inactivation is faster for L796V at the resting potential (Fig. 3C smaller time constant at -80 mV). We propose the overall effect will be impaired slow inactivation for L796V channels, in the context of the slow inactivation that occurs during sustained bursts of action potentials (e.g. myotonia). The basis for this prediction is that entry to slow inactivation occurs primarily at voltages near the peak depolarization of the action potential (where the predominant change is less complete slow inaction for L796V) and trapping of channels in the slow inactivated state is primarily dependent on the rate of recovery at the resting potential of -80 mV (which is faster for L796V channels). This prediction is supported by experimental evidence showing the use-dependent reduction of sodium current is more pronounced for WT than L796V channels during repetitive stimulation at 50 Hz. Figure 4A shows a superposition of sodium currents recorded in response to the first 10 pulses to +10 mV from a holding potential of -80 mV. The initial decline in peak amplitude from the first to the second pulse is predominantly caused by incomplete recovery from fast inactivation, whereas the subsequent decline for additional pulses is due to progressive loss of channel availability from slow inactivation. The slow inactivation effect is illustrated in Fig. 4B for the entire 40 second train of 3 msec depolarizations at 50 Hz (2000 pulses). The peak amplitude for each pulse is normalized by the amplitude of the second pulse (Fig 4A, blue trace) to isolate the effect of slow inactivation, which under these conditions is about 10% less for L796V channels compared to WT.

Functional Defects of L796V Mutant Channels Cause Myotonia in a Simulated Muscle Fiber.

The functional consequences of the defects in activation and in slow inactivation for L796V mutant channels were explored in a computational model of a muscle fiber (See Supplemental

materials for details). For a simulated fiber with WT sodium channels, the resting potential was -90.3 mV and the voltage threshold to elicit an action potential was -66 mV. Susceptibility to myotonic discharges was tested by simulated injection of a 100 msec depolarizing current pulse (20 $\mu A/cm^2$). A single action potential was elicited in a simulated WT fiber (Figure 5A), followed by a small depolarization to about -80 mV that decayed back to the normal resting potential at the end of the current injection.

The model for the patient's muscle contained 50% WT sodium channels and 50% with L796V properties to emulate the heterozygous state. The derangements in the L796V channels were simulated as shown by the fitted curves in Figures 2 through 4 (See Supplemental material for details). The predominant changes for L796V mutant channels were reduced conductance, -7.2 mV left shift of activation, and altered slow inactivation (faster kinetics, reduced voltage dependence, and less complete). The resting potential was modestly depolarized in the simulated patient muscle (-86.0 mV), and more importantly the voltage threshold for an action potential was markedly hyperpolarized at a value of -79 mV. These effects are caused by the left shift in the voltage dependence of activation for L796V channels. The same 100 msec depolarizing current injection now elicited repetitive discharges that persisted beyond the duration of the stimulus (Figure 5B). The "after-discharges" are triggered by the small depolarization produced from the use-dependent accumulation of K^+ in the T-tubules. Each action potential produces an efflux of K^+ into the T-tubules, and the restricted diffusion of these long narrow tubules results in an increase in extracellular [K^+] and membrane depolarization. Normally, this small depolarization of only a few mV is insufficient to elicit action potentials, but with the left-shifted activation of L796V channels, the threshold is lower and self-sustained bursts of myotonic discharges occur.

Amongst the sodium channel gain-of-function defects known to cause myotonia, a left shift of activation is especially potent (e.g. compared to the more common cause from a slower rate of inactivation) because of the effect on action potential threshold (Yang et al., 1994; Green et al., 1998). Consequently, the trains of discharges tend to be very prolonged, lasting more than 10 sec (Figure 5C). The mechanism by which a myotonic burst ends is not completely understood, and likely depends on several events. One proposal is that use-dependent reduction of sodium channel availability, caused by the normal trapping of channels in the slow inactivated state, reduces fiber excitability and thereby terminates the myotonic burst (Hawash et al., 2017). This mechanism is impaired for L796V mutant channels because the recovery from slow inactivation is accelerated at the resting potential (Figure 4B), and the prediction is that myotonic bursts may be exceptionally prolonged. We demonstrate this effect by modifying the simulated L796V channels to include all the anomalies detected in the voltage-clamp experiments, except the kinetics of slow inactivation retained WT behavior (i.e. 3 times slower at the resting potential). Simulated muscle with this hypothetical mutant sodium channel still exhibited myotonic discharges (Figure 5D), because of the left shift of activation, but the duration of the myotonic burst was shortened. This simulation demonstrates how the addition of a slow inactivation defect can exacerbate the severity of myotonia, which heretofore has been attributed gain-of-function defects in fast gating mechanisms alone (activation and fast inactivation).

3.4 DISCUSSION

We report a patient with a de novo heterozygous *SCN4A* variant c.2386C>G; p.L796V who had congenital anomalies and early-onset myotonia. This same variant was recently been reported

in a patient with multiple congenital anomalies including hip dysplasia, scoliosis, and myopathic features who developed myotonia and episodic weakness in adolescence (Waldrop et al., 2019). Several criteria support the assignment of pathogenic mutation to L796V. From a genetic perspective, this de novo heterozygous *SCN4A* allele arose independently in two families with the probands having severe myotonic syndromes with overlapping features, and the variant was not in unaffected family members or in public databases (gnomAD_v2.1.1 or ExAC, although the Moroccan population may be under represented). The L796V missense mutation is located in a functionally important transmembrane segment (S6 of domain I) that contributes to the inner vestibule of the ion-conducting pore (Pan et al., 2018). Residue L796 is highly conserved amongst human $Na_V1.x$ isoforms and across species. Moreover, a site three residues downstream, and therefore on the same face of the S6 helix, is an established mutation (A799S) with gain-of-function changes (Simkin et al., 2011) that causes a severe myotonic phenotype with episodic laryngospasm (Lion-Francois et al., 2010). Finally, our expression studies revealed gain-of-function defects for L796V with enhanced activation and impaired slow inactivation.

The congenital onset, with secondary joint and skeletal anomalies, was notable in both L796V patients. Our patient had arthrogryposis multiplex, with the other reported L796V case having hip dysplasia and scoliosis (Waldrop et al., 2019). The etiology of these skeletal deformities remains to be established. In our patient, sonographic evidence of oligohydramnios was present just prior to delivery, but three prior ultrasounds (as late as 30 weeks gestation) revealed normal amniotic fluid levels. One possibility is a contribution from reduced mobility in utero caused by myotonia. Both L796V patients had early-onset severe myotonia, and our patient required pharmacologic intervention with sodium channel blockers to alleviate neonatal breathing difficulties. The propensity for exceptionally long-duration myotonic discharges in our model

simulation with the L796V functional defects (Fig. 5) may predispose to secondary joint defects. A monoallelic variant of HSPG2 was identified in our patient, and while we cannot exclude the possibility of a modifier effect that exacerbates myotonia from the sodium channel L796V defect, we think this is unlikely for several reasons. First, perlecan staining was normal. Second, the needle EMG at six weeks of age (supplemental video 2) showed classical myotonic runs that waxed and waned in frequency and amplitude. Conversely, in the Schwartz-Jampel syndrome (SJS) with proven biallelic mutations of HSPG2 the needle EMG shows complex repetitive discharges of constant amplitude and frequency, with abrupt discontinuation of the burst (Bauche et al., 2013). These discharges in SJS are attributed to peripheral nerve hyperexcitability, rather than myotonia from altered sarcolemmal excitability. Third, our model simulations show the functional defect of L796V alone is sufficient to cause exceptionally prolonged myotonic bursts. Congenital joint and bone deformities are not a frequent accompaniment of congenital myotonia, but have been reported. Club foot with peripheral contractures, hip dislocation, and facial dysmorphism were reported for a newborn with diffuse muscle stiffness and widespread myotonic discharges who later developed muscle hypertrophy and was found to be heterozygous for *SCN4A* c.3539A>T; p.N1180I (Fusco et al., 2015). Severe scoliosis with peripheral contractures in childhood was described for siblings with myotonic stiffness, profuse myotonic discharges, and the *SCN4A* p.P1158A mutation (Xu et al., 2018), but no details were provided about the clinical presentation at birth.

Congenital myopathy was a feature of the prior report for L796V, as manifest by polyhydramnios, fetal hypokinesia, hip dysplasia and later progression to include high arched palate and elongated face (Waldrop et al., 2019). A muscle biopsy at age 27 had myopathic features with type I fiber predominance and hypertrophy. The other case of congenital myotonia with joint

abnormalities (*SCN4A* p.N1180I) also had signs of neonatal myopathic weakness with polyhydramnios, high arched palate, and downslanting palpebral fissures (Fusco et al., 2015). These cases are distinctly different, however, from the recently described syndrome of congenital myopathy with severe fetal hypokinesia caused by biallelic mutations for *SCN4A* (Zaharieva et al., 2016; Gonorazky et al., 2017). In this latter syndrome, the core phenotype includes neonatal hypotonia, moderate to severe myopathic weakness that may be fatal, and *SCN4A* loss-of-function mutations that are asymptomatic in heterozygous parents. In contrast, the heterozygous p.L796V patients and the p.N1108I case had neonatal myotonic stiffness, only mild myopathic weakness that subsequently improved and in some progressed to muscle hypertrophy, and for p.L796V, experimentally established gain-of-function defects. Electromyographic evidence of myotonia in early infancy, as we observed at 6 weeks, is unusual and differentiates the hypotonia and weakness in our patient from the syndrome of congenital myopathy with hypotonia associated with recessive loss-of-function mutations of *SCN4A* (Zaharieva et al., 2016). Myopathic features may be a component of the dominantly inherited *SCN4A* myotonic syndromes (sodium-channel myotonia, myotonia permanens, severe neonatal episodic laryngospasm, SNEL) or the late permanent muscle weakness of periodic paralysis. In our view, however, neither a single allelic variant of *SCN4A* nor a dominant inheritance pattern has been associated with a syndrome for which congenital myopathy is the predominant feature.

We propose a new *SCN4A* syndrome, myotonic myopathy with secondary joint and bone anomalies, should be applied to the phenotype for p.L796V and p.N1108I. The core elements are congenital joint and bone anomalies with neonatal or infantile myotonic stiffness and widespread myotonic discharges. Breathing difficulties may be present, as in our patient, but stridor and respiratory compromise are not the predominant presentation. The relation of myotonic

myopathy with joint and bone anomalies to the other sodium channelopathies of skeletal muscle is illustrated in Figure 6. This new syndrome is envisioned to be positioned between SNEL and paramyotonia congenita (PMC). Overlap with SNEL may be manifest as breathing difficulties and with PMC as episodic weakness (reported for p.L796V (Waldrop et al., 2019)). We have previously shown that impairment of slow inactivation predisposes to episodes of periodic paralysis, and the slow inactivation defect observed herein for L796V may account for susceptibility to episodic weakness.

3.5 FIGURES

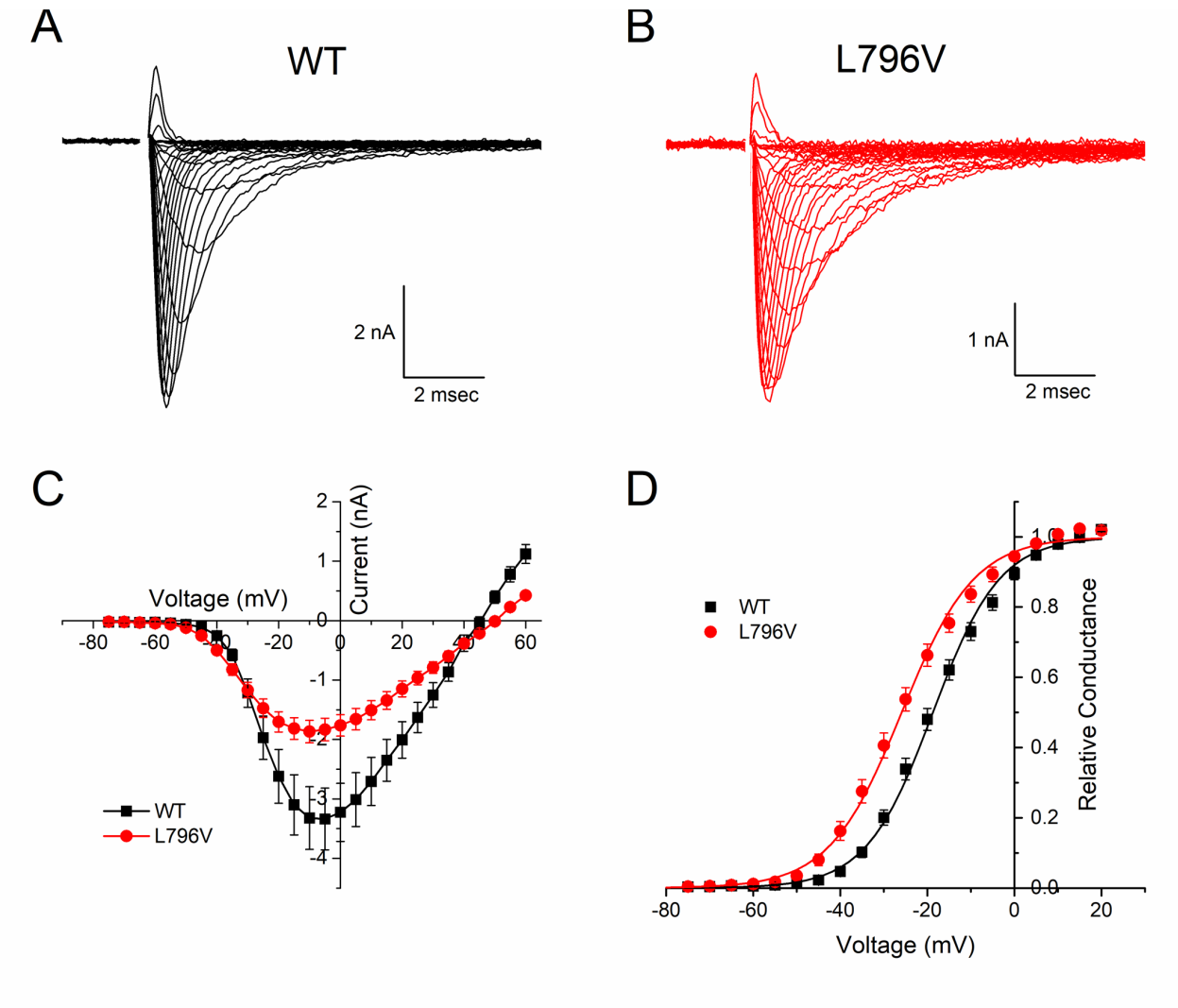

Figure3-1. Activation of L796V channels is shifted toward more negative potentials. Sodium currents were recorded from HEK cells expressing WT (**A**) and L796V (**B**) channels. Superimposed traces show currents elicited by depolarization to test potentials of -75 to +60 mV from a holding potential of -120 mV. (**C**) Peak sodium current is shown as a function of test potential and reveals a reduced amplitude for L796V compared to WT. (**D**) Transforming the peak current to relative conductance (see Methods and Materials) shows a 7.2 mV hyperpolarized shift for L796V channels. Symbols show means from n = 16 (WT) or n = 10 (L796V) cells.

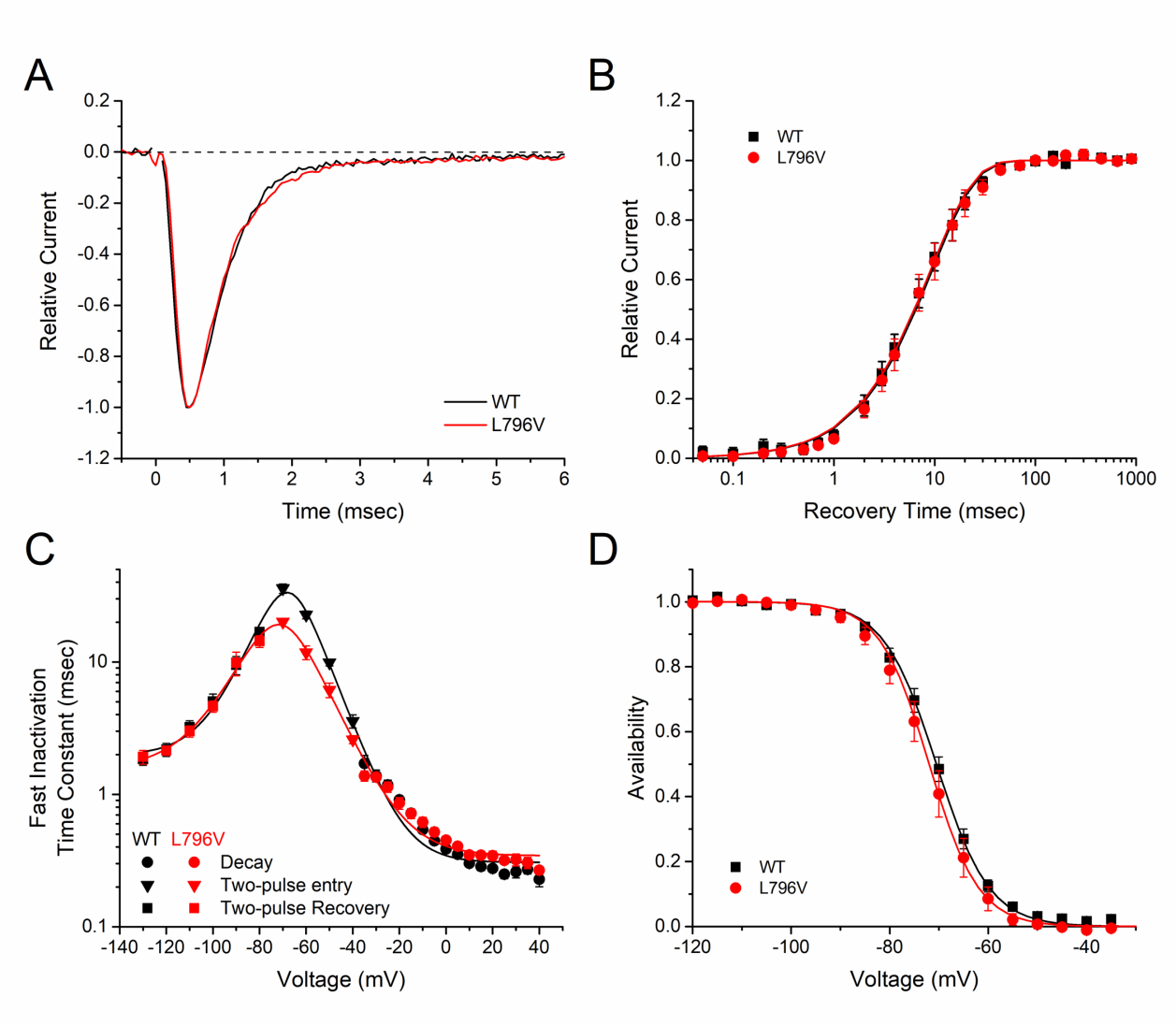

Figure3-2. Fast inactivation is not affected by the L796V mutation. (**A**) Sodium current decay kinetics are indistinguishable for WT and L796V channels. Representative current traces elicited at -10 mV have been normalized by peak amplitude. (**B**) Recovery from fast inactivation is identical for WT and L796V channels. Data show the time course for the recovery of peak current amplitude at a holding potential of -90 mV, after channels were inactivated with a conditioning pulse of 30 msec at -10 mV. Symbols show means for WT (n = 8) and L796V (n = 5). (**C**) Summary plot of the time constants for entry or recovery from fast inactivation shows identical kinetics for WT and L796V channels. Three separate protocols were used to measure inactivation kinetics, depending on the voltage range, as described in Methods and Materials. Symbols show means from WT (n = 16) and L796V (n = 10). (**D**) The steady-state voltage dependence of fast inactivation was indistinguishable for WT (n = 15) and L796V (n = 10) channels. Plot

shows relative amplitude for the peak sodium current elicited by a depolarization to -10 mV after a 300 msec conditioning pulse at the indicated voltage (abscissa).

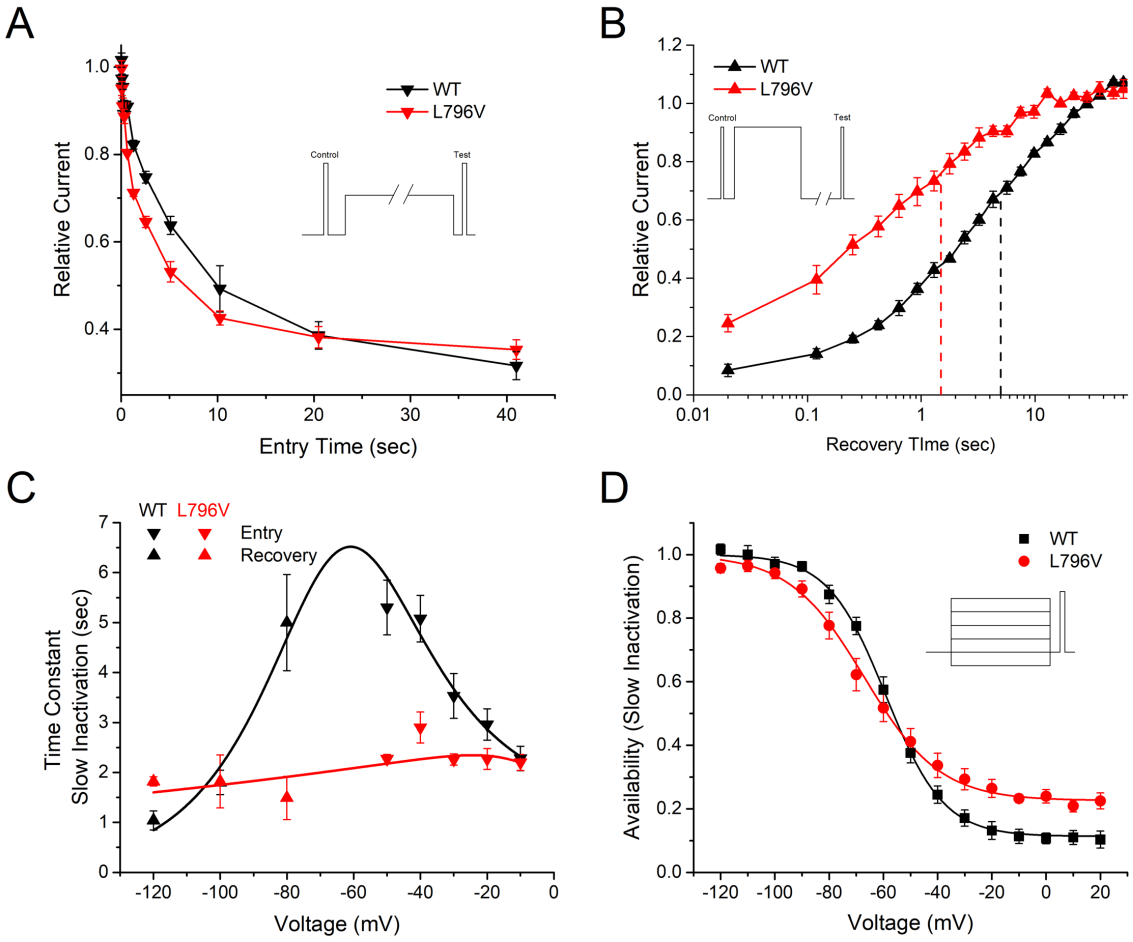

Figure3- 3. Slow inactivation is altered by the L796V mutation. (**A**) A two-pulse protocol with a variable duration condition pulse to – 50 mV (inset) shows accelerated onset of slow inactivation for L796V channels. Symbols show means for WT (n = 5) and L796V (n = 3) channels. (**B**) Recovery from slow inactivation at -80 mV is accelerated four-fold for L796V compared to WT channels. Channels were slow inactivated with a 30 sec conditioning pulse to -10 mV (inset), and then recovery from slow inactivation was measured as the relative peak current elicited by a brief pulse to -10 mV, after variable period of recovery at -80 mV. Symbols show means for WT (n = 5) and L796V (n = 4). (**C**) Summary plot for the kinetics of slow inactivation entry and recovery shows a nearly voltage-independent time constant for L796V mutant channels. Symbols show means for WT (n = 5) and L796V (n = 4) channels. (**D**) Steady-state voltage dependence of slow inactivation shows a decreased slope (-100 mV to -40 mV range) and

less complete slow inactivation (higher plateau at -20 mV to +20 mV) for L796V (n = 5) compared to WT (n = 5) channels.

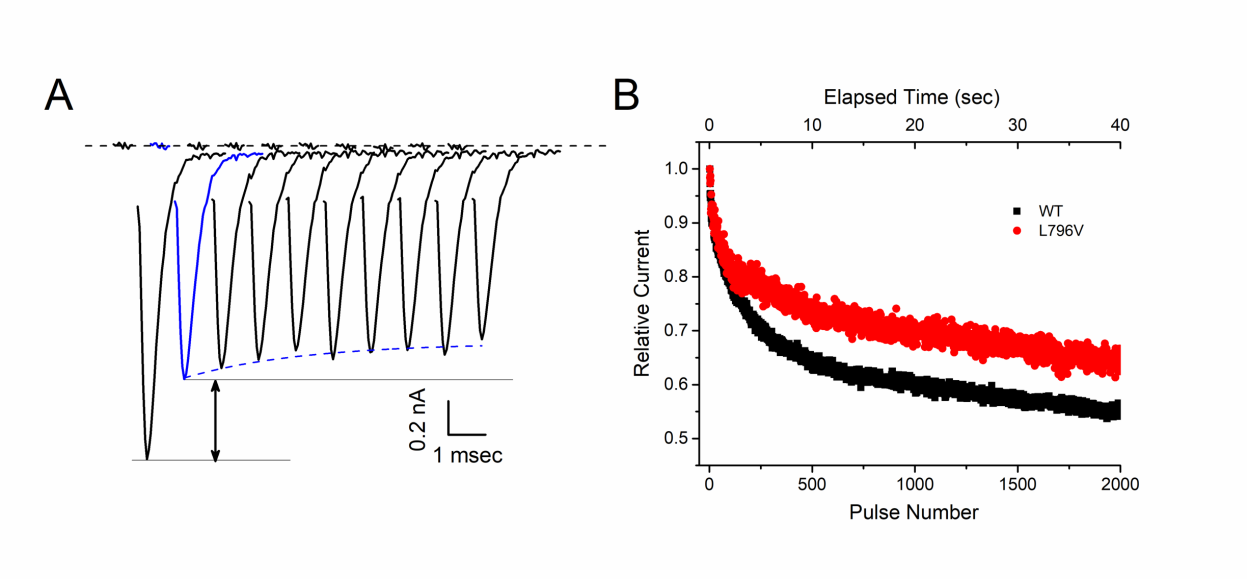

Figure3- 4 The decline of sodium current peak amplitudes during a 50 Hz train of pulses is less pronounced for L796V channels, thereby showing a gain-of-function change caused by altered slow inactivation. (A) Exemplary WT sodium currents elicited by the first 10 pulses in a 50 Hz train of 3 msec depolarizations to -10 mV are shifted in time and superimposed to illustrate the decline in peak amplitude. The holding potential between pulses was -80 mV. The large decline between the first and second pulse (black arrow) reflects trapping of channels in the fast-inactivated state. The subsequent decline starting from the second pulse (blue) is caused by loss of channels successively trapped in the slow-inactivated state. (B) The decline in peak sodium current during a prolonged 50 Hz train of 3 msec pulses is attenuated for L796V channels. Points show mean relative current for WT (n = 7) and L796V (n = 3) channels, as defined by normalization to the peak amplitude of the sodium current elicited by the second pulse (blue).

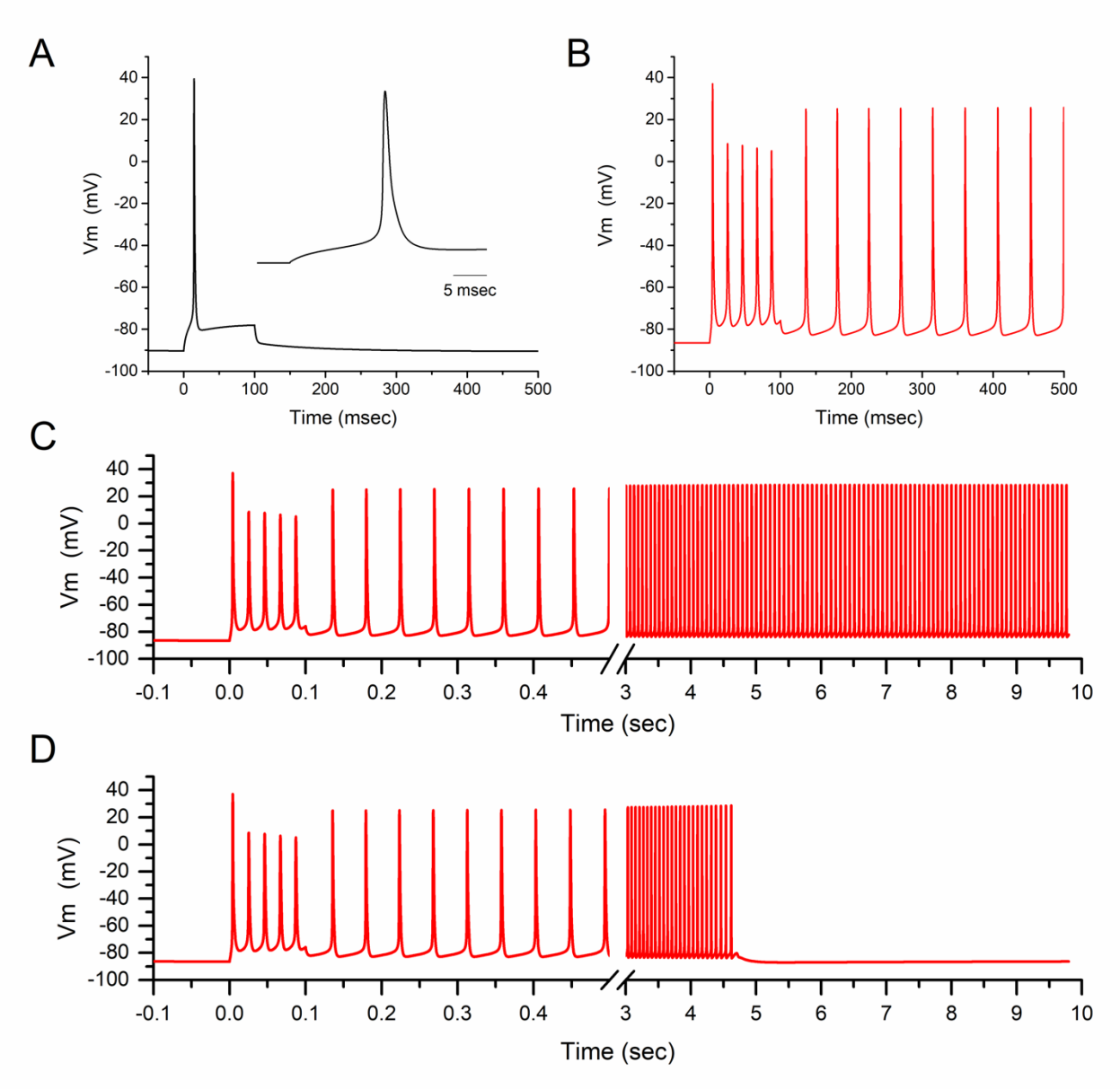

Figure3- 5. Model simulation predicts sustained busts of myotonia from the L796V channel defects. (**A**) The action potential elicited by a 20 μA/cm^2 current pulse applied for 100 msec is shown for a simulated muscle fiber with normal values for voltage-activated ion channels. Inset shows the initial 25 msec of the model simulation. (**B**) When 50% of the simulated sodium channels are modeled using parameters to emulate the altered behavior of L796V channels, then the same 100 msec current stimulus triggers a burst of myotonic discharges that persist beyond the 100 msec duration of the stimulus. (**C**) Extended simulation over time shows stable self-sustained repetitive myotonic discharges that do not cease. (**D**) When the simulated mutant channels are modified to have the slow inactivation kinetics for WT channels,

then use-dependent reduction of the sodium current is enhanced (see Fig. 5) and the myotonic burst ends after 4.5 sec.

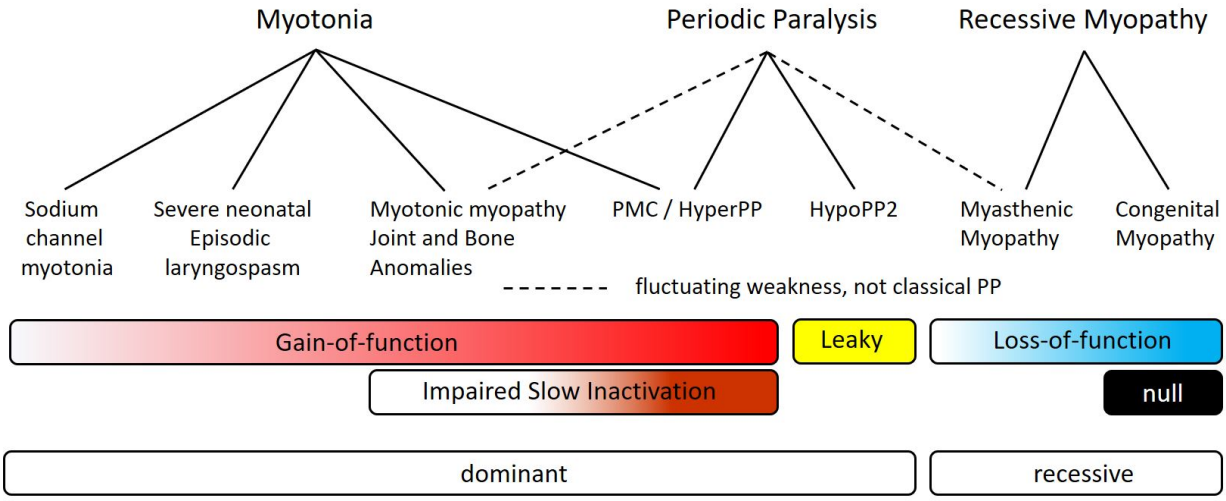

Figure3- 6 Myotonic myopathy with secondary joint and bone anomalies is a dominantly expressed allelic disorder on the spectrum of SCN4A sodium channelopathies of skeletal muscle. The top row depicts the primary clinical manifestations, which may be overlapping in specific disorders (second row). Dashed lines are used to indicate fluctuating muscle weakness for myotonic myopathy and for myasthenic myopathy, as distinct from the more clearly demarcated attacks of classical periodic paralysis that usually have well-defined trigger factors (solid lines). The bars show the overlap of different functional defects of mutant sodium channels, with the more intense color indicating more severe changes. The final row indicates the inheritance pattern for expression of symptoms.

4.6 SUPPLAMENTARY MATERIAL

Simulation of L796V sodium channel gating defects

The gating behavior for WT and L796V sodium channels was simulated with a modified version of the Hodgkin-Huxley equations. The sodium current, $I_{Na}(V,t)$, was modeled as a combination of activation, $m(V,t)$, fast inactivation, $h(V,t)$, and slow inactivation, $s(V,t)$, that collectively determined the open probability of the channel, and $i_{Na}(V)$ was the voltage dependence of current flow through an open channel.

$$I_{Na}(V,t) = m(V,t)^3 h(V,t) s(V,t) i_{Na}(V) .$$

Each of the gating terms (m, h, s) was approximated by a single transition between two states. For example, channel activation was modeled as:

$$closed\ "1 - m"\ \underset{\beta_m(V)}{\overset{\alpha_m(V)}{\rightleftarrows}}\ open\ "m"$$

such that

$$\frac{dm}{dt} = \alpha_m(1-m) - \beta_m m \quad .$$

The parameter estimates for the voltage-dependent rate constants, $\alpha_m(V)$ and $\beta_m(V)$, were obtained by fitting the voltage-clamp data for sodium currents in HEK cells. The reduced data are represented as voltage-dependent time constants, $\tau_m(V)$, and steady-state probability, $m_\infty(V)$, for which the rate constant dependencies are:

$$\tau_m = 1/(\alpha_m + \beta_m) \text{ and } m_\infty = \alpha_m/(\alpha_m + \beta_m)$$

Empirically, we fit the steady-state data to a Boltzmann equation (see Methods) and then determined the parameters for the rate constants by non-linear least-square fit (Origin 9.1, Microcal) to

$$\alpha_m = m_\infty/t_m \text{ and } \beta_m = (1-m_\infty)/\tau_m .$$

This same procedure was used to estimate the parameter values for the rate constants governing fast inactivation and slow inactivation. The rate equations were similar to those used by Hodgkin and Huxley:

$$\alpha_m = \overline{\alpha_m}(V - V_m)/(1 - e^{-(V-V_m)/k_{\alpha m}}) \qquad \beta_m = \overline{\beta_m}\, e^{-(V-V_{m)/k_{\beta m}}}$$

$$\alpha_h = \overline{\alpha_h}/(1 + e^{(V-V_{\alpha h})/k_{\alpha h}}) \qquad \beta_h =$$

$$\overline{\beta_h}/(1 + e^{-(V-V_{\beta h)/k_{\beta h}}})$$

$$\alpha_s = \overline{\alpha_s}\, e^{-V/k_{\alpha s}} \qquad \beta_s = \overline{\beta_s}/(1 + e^{-(V-V_{s)/k_{\beta s}}})$$

The estimated parameter values for WT and L796V channels are listed in Table S1. In the computer simulation of a muscle fiber (see below), the gating terms were computed from the independent fits to the voltage-dependent time constant (using $\alpha(V)$ and $\beta(V)$ as above) and to the steady-state probability (using a Boltzmann function). For example, the activation term, m, was computed as

$$\frac{dm}{dt} = \frac{m_\infty - m}{\tau_m} \ .$$

Table S1 Parameters for sodium channel gating variables: m, h, s

Gating	Parameter	Units	WT	L796V
Activation, m	$\overline{\alpha_m}$ [1]	msec^{-1}	0.28	0.28
	V_m	mV	-46	-46
	$k_{\alpha m}$	mV	10	10
	$\overline{\beta_m}$	msec^{-1}	1.4	1.4
	$k_{\beta m}$	mV	18	18
	$V_{1/2}$ [2]	mV	-46	-53.2
	k [3]	mV	4.3	4.9
Fast Inactivation, h	$\overline{\alpha_h}$	msec^{-1}	0.51	0.63
	$V_{\alpha h}$ [2]	mV	-110	-117
	$k_{\alpha h}$	mV	10	12
	$\overline{\beta_h}$	msec^{-1}	3.3	2.9
	$V_{\beta h}$ [2]	mV	-26	-26
	$k_{\beta h}$	mV	9.1	11
	$V_{1/2}$ [2]	mV	-75	-77
	k [3]	mV	5.4	5.0
Slow Inactivation, s	$\overline{\alpha_s}$	msec^{-1}	4.0 x 10^{-4}	3.7 x 10^{-4}
	$k_{\alpha s}$	mV	21	230
	$\overline{\beta_s}$	msec^{-1}	7.3 x 10^{-4}	1.3 x 10^{-4}
	$V_{\beta s}$	mV	-17	-7.4
	$k_{\beta s}$	mV	21	11
	$V_{1/2}$	mV	-59	-67
	k	mV	11	14
	s_0	-	.012	0.23

1 Values for parameters of activation kinetics ($\overline{\alpha_m}, V_m, k_{\alpha m}, \overline{\beta_m}, k_{\beta m}$) taken from Cannon et al. (1993).

2 Value for WT has a hyperpolarized shift, to account for differences between HEK cells and mammalian muscle (Fu *et al.*, 2011). Relative shift for L796V was set to the value from this study.

3 Value for WT was set to the steepness of voltage-dependence observed in mammalian muscle (Fu *et al.* , 2011). Ratio of k_{WT}/k_{L796V} was set to the value from this study.

The most impactful parameter changes between WT and L796V that contribute to sustained myotonic discharges are highlighted in blue.

Simulation of muscle fiber electrical excitability

The simulated muscle fiber is an extension of our two compartment model (Cannon *et al.* , 1993), that represents the sarcolemma and transverse tubular (T-tubule) membranes. For our simulated fiber with a radius of 40 μm, the ratio of T-tubule membrane surface area to sarcolemmal membrane surface area is γ = 4.8, separated by an access resistance of R_a= 40 Ω-cm^2. Each membrane compartment contains a voltage-dependent sodium conductance and a delayed rectifier potassium conductance as before (Cannon *et al.* , 1993). The revised model herein also includes an inward rectifier potassium conductance (Struyk and Cannon, 2008), and a voltage-activated chloride conductance (DiFranco *et al.*, 2011) replaces the "leak" conductance in the prior model. The open-channel current-voltage relation for each conductance was simulated using the GHK constant field equation (Hille, 2001). Finally, a pump current was included to simulate the electrogenic contribution from the Na/K-ATPase (Wallinga *et al.*, 1999).

The total membrane current per unit area of sarcolemma, I_m , is a combination capacitive current, ionic currents through conductances and pumps, plus the net current from the T-tubule:

$$I_m = C_m \frac{dV}{dt} + \sum I_{ionic} + I_{pump} + I_{TT}$$

where

$$\sum I_{ionic} = I_{Na} + I_{Kir} + I_{Kdr} + I_{Cl} \quad \text{and} \quad I_{TT} = \frac{V - V_{TT}}{R_a} .$$

Similarly, the total current across the T-tubule (per unit area of sarcolemmal membrane) is

$$I_{TT} = \gamma C_m \frac{dV_{TT}}{dt} + \gamma \sum I_{TT\_ionic} .$$

The concentration of K^+ in the T-tubule (an extracellular space) increases in response to the firing of action potentials (Cannon *et al.* , 1993, Wallinga *et al.* , 1999), which produce an efflux of myoplasmic K^+ during repolarization. This increase is balanced by losses from influx through the Na/K-ATPase and from equilibration with the interstitial space (passive diffusion). The net mass balance is

$$\frac{d[K]_{TT}}{dt} = \frac{\left(I_{TT_{Kir}} + I_{TT_{Kdr}} - I_{TT_{pump\,K}}\right)}{F\varsigma} - \frac{[K]_{TT} - [K]_{out}}{\tau_K}$$

where $\varsigma = 10^{-6}$ cm is the volume to surface area ratio of the T-tubule, and τ_K = 350 msec is the decay time constant for equilibration of T-tubule $[K]_{TT}$ with the interstitial $[K]_{out}$.

These coupled differential equations were solved numerically by Euler integration with an adaptive step size, Δt, such that the change in membrane potential for a single step was less than 0.05 mV. Parameter values for the voltage-dependent gating of ionic conductances were set to the values in the references cited above, and the maximum permeability for the conductances in each membrane compartment are listed in Table S2. Ion concentrations for each compartment are listed in Table S3.

Table S2. Maximum permeability (cm/sec)

channel type	sarcolemma	T-tubule
P_{Na_WT}	1.1×10^{-4}	0.88×10^{-4}
P_{Na_L796V}	0.81×10^{-4}	0.65×10^{-4}
P_{Kir}	6.4×10^{-6}	6.4×10^{-6}
P_{Kdr}	2.4×10^{-5}	2.4×10^{-5}
P_{Cl}	8.0×10^{-4}	2.4×10^{-4}

Table S3. Ion Concentrations (mM)

Ion	myoplasm	T-tubule	interstium
Na^+	15.1	140	140
K^+	152	4.0 *	4.0
Cl^-	4.0	105	105

* concentration varies with simulated fiber electrical activity

4.7 REFRENCES

1. Arnold, W.D., Feldman, D.H., Ramirez, S., He, L., Kassar, D., Quick, A., et al. (2015). Defective fast inactivation recovery of Nav 1.4 in congenital myasthenic syndrome. *Ann Neurol* 77(5)**,** 840-850. doi: 10.1002/ana.24389

.

2. Bauche, S., Boerio, D., Davoine, C.S., Bernard, V., Stum, M., Bureau, C., et al. (2013). Peripheral nerve hyperexcitability with preterminal nerve and neuromuscular junction remodeling is a hallmark of Schwartz-Jampel syndrome. *Neuromuscul Disord* 23(12)**,** 998-1009. doi: 10.1016/j.nmd.2013.07.005.

3. Caietta, E., Milh, M., Sternberg, D., Lepine, A., Boulay, C., McGonigal, A., et al. (2013). Diagnosis and outcome of SCN4A-related severe neonatal episodic laryngospasm (SNEL): 2 new cases. *Pediatrics* 132(3)**,** e784-787. doi: 10.1542/peds.2012-3065.

4. Cannon, S.C. (2015). Channelopathies of skeletal muscle excitability. *Compr Physiol* 5(2)**,** 761-790. doi: 10.1002/cphy.c140062.

5. Cannon, S.C. (2018). Sodium Channelopathies of Skeletal Muscle. *Handb Exp Pharmacol* 246**,** 309-330. doi: 10.1007/164_2017_52.

6. Cannon, S.C., Brown, R.H., Jr., and Corey, D.P. (1993). Theoretical reconstruction of myotonia and paralysis caused by incomplete inactivation of sodium channels. *Biophysical Journal* 65(1)**,** 270-288.

7. Elia, N., Palmio, J., Castaneda, M.S., Shieh, P.B., Quinonez, M., Suominen, T., et al. (2019). Myasthenic congenital myopathy from recessive mutations at a single residue in NaV1.4. *Neurology* 92(13)**,** e1405-e1415. doi: 10.1212/WNL.0000000000007185.

8. Fusco, C., Frattini, D., Salerno, G.G., Canali, E., Bernasconi, P., and Maggi, L. (2015). New phenotype and neonatal onset of sodium channel myotonia in a child with a novel mutation of SCN4A gene. *Brain Dev* 37(9)**,** 891-893. doi: 10.1016/j.braindev.2015.02.004.

9. Gonorazky, H.D., Marshall, C.R., Al-Murshed, M., Hazrati, L.N., Thor, M.G., Hanna, M.G., et al. (2017). Congenital myopathy with "corona" fibres, selective muscle atrophy, and craniosynostosis associated with novel recessive mutations in SCN4A. *Neuromuscul Disord* 27(6)**,** 574-580. doi: 10.1016/j.nmd.2017.02.001.

10. Green, D., George, A., and Cannon, S. (1998). Human sodium channel gating defects caused by missense mutations in S6 segments associated with myotonia: S804F and V1293I. *Journal of Physiology* 510**,** 685-694.

11. Habbout, K., Poulin, H., Rivier, F., Giuliano, S., Sternberg, D., Fontaine, B., et al. (2016). A recessive Nav1.4 mutation underlies congenital myasthenic syndrome with periodic paralysis. *Neurology* 86(2)**,** 161-169. doi: 10.1212/WNL.0000000000002264.

12. Hawash, A.A., Voss, A.A., and Rich, M.M. (2017). Inhibiting persistent inward sodium currents prevents myotonia. *Ann Neurol* 82(3)**,** 385-395. doi: 10.1002/ana.25017.

13. Hayward, L.J., Brown, R.H., Jr., and Cannon, S.C. (1996). Inactivation defects caused by myotonia-associated mutations in the sodium channel III-IV linker. *Journal of General Physiology* 107(5)**,** 559-576.

14. Lion-Francois, L., Mignot, C., Vicart, S., Manel, V., Sternberg, D., Landrieu, P., et al. (2010). Severe neonatal episodic laryngospasm due to de novo SCN4A mutations: a new treatable disorder. *Neurology* 75(7)**,** 641-645. doi: 10.1212/WNL.0b013e3181ed9e96.

15. Matthews, E., Manzur, A.Y., Sud, R., Muntoni, F., and Hanna, M.G. (2011). Stridor as a neonatal presentation of skeletal muscle sodium channelopathy. *Arch Neurol* 68(1)**,** 127-129. doi: 10.1001/archneurol.2010.347.

16. Palmio, J., Sandell, S., Hanna, M.G., Mannikko, R., Penttila, S., and Udd, B. (2017). Predominantly myalgic phenotype caused by the c.3466G>A p.A1156T mutation in SCN4A gene. *Neurology* 88(16)**,** 1520-1527. doi: 10.1212/WNL.0000000000003846.

17. Pan, X., Li, Z., Zhou, Q., Shen, H., Wu, K., Huang, X., et al. (2018). Structure of the human voltage-gated sodium channel Nav1.4 in complex with beta1. *Science* 362(6412). doi: 10.1126/science.aau2486.

18. Portaro, S., Rodolico, C., Sinicropi, S., Musumeci, O., Valenzise, M., and Toscano, A. (2016). Flecainide-Responsive Myotonia Permanens With SNEL Onset: A New Case and Literature Review. *Pediatrics* 137(4). doi: 10.1542/peds.2015-3289.

19. Simkin, D., Lena, I., Landrieu, P., Lion-Francois, L., Sternberg, D., Fontaine, B., et al. (2011). Mechanisms underlying a life-threatening skeletal muscle Na+ channel disorder. *The Journal of physiology* 589(Pt 13)**,** 3115-3124.

20. Singh, R.R., Tan, S.V., Hanna, M.G., Robb, S.A., Clarke, A., and Jungbluth, H. (2014). Mutations in SCN4A: a rare but treatable cause of recurrent life-threatening laryngospasm. *Pediatrics* 134(5)**,** e1447-1450. doi: 10.1542/peds.2013-3727.

21. Tsujino, A., Maertens, C., Ohno, K., Shen, X.M., Fukuda, T., Harper, C.M., et al. (2003). Myasthenic syndrome caused by mutation of the SCN4A sodium channel. *Proc Natl Acad Sci U S A* 100(12)**,** 7377-7382.

22. Waldrop, M., Amornvit, J., Pierson, C.R., Boue, D.R., and Sahenk, Z. (2019). A Novel De Novo Heterozygous SCN4a Mutation Causing Congenital Myopathy, Myotonia and Multiple Congenital Anomalies. *J Neuromuscul Dis* 6**,** 467-473. doi: 10.3233/JND-190425.

23. Xu, Y.Q., Liu, X.L., Huang, X.J., Tian, W.T., Tang, H.D., and Cao, L. (2018). Novel Mutations in SCN4A Gene Cause Myotonia Congenita with Scoliosis. *Chin Med J (Engl)* 131(4)**,** 477-479. doi: 10.4103/0366-6999.225061.

24. Yang, N., Ji, S., Zhou, M., Ptacek, L.J., Barchi, R.L., Horn, R., et al. (1994). Sodium channel mutations in paramyotonia congenita exhibit similar biophysical phenotypes in vitro. *Proceedings of the National Academy of Sciences of the United States of America* 91(26)**,** 12785-12789.

25. Yoshinaga, H., Sakoda, S., Shibata, T., Akiyama, T., Oka, M., Yuan, J.H., et al. (2015). Phenotypic variability in childhood of skeletal muscle sodium channelopathies. *Pediatr Neurol* 52(5)**,** 504-508. doi: 10.1016/j.pediatrneurol.2015.01.014.

26. Zaharieva, I.T., Thor, M.G., Oates, E.C., van Karnebeek, C., Hendson, G., Blom, E., et al. (2016). Loss-of-function mutations in SCN4A cause severe foetal hypokinesia or 'classical' congenital myopathy. *Brain* 139(Pt 3)**,** 674-691. doi: 10.1093/brain/awv352.

27. Cannon SC, Brown RH, Jr., Corey DP. Theoretical reconstruction of myotonia and paralysis caused by incomplete inactivation of sodium channels. Biophys J. 1993;65(1):270-88.

28. DiFranco M, Herrera A, Vergara JL. Chloride currents from the transverse tubular system in adult mammalian skeletal muscle fibers. J Gen Physiol. 2011 Jan;137(1):21-41.

29. Fu Y, Struyk A, Markin V, Cannon S. Gating behaviour of sodium currents in adult mouse muscle recorded with an improved two-electrode voltage clamp. J Physiol. 2011 Feb 1;589(Pt 3):525-46.

30. Hille B. Ion Channels of Excitable Membranes. 3rd ed. Sunderland, MA: Sinauer; 2001.

31. Struyk AF, Cannon SC. Paradoxical depolarization of Ba^{2+}- treated muscle exposed to low extracellular K^{+}: insights into resting potential abnormalities in hypokalemic paralysis. Muscle Nerve. 2008 Mar;37(3):326-37.

32. Wallinga W, Meijer SL, Alberink MJ, Vliek M, Wienk ED, Ypey DL. Modelling action potentials and membrane currents of mammalian skeletal muscle fibres in coherence with potassium concentration changes in the T-tubular system. Eur Biophys J. 1999;28(4):317-29.